Journal of Manufacturing Processes

Experimental Investigation into the Effect of Magnetorheological Fluid Damper on Vibration and Chatter in Straight Turning Process

--Manuscript accepted--

Mohsen Emami[*1], Vahid Hasan Nasab[2], Samet Akar[3] and Andre Batako[4]

[1] Department of Mechanical Engineering, Behbahan Khatam Alanbia University of Technology, Behbahan, Iran.

* P.O.B. 63616-47189 Behbahan, Iran, Dr.emami@bkatu.ac.ir

[2] MSc in Manufacturing Engineering, n.hasannasab@yahoo.com

[3] Department of Mechanical Engineering, Çankaya University, Ankara, Türkiye, samet.akar@cankaya.edu.tr

[4] General Engineering Research Institute, Liverpool Jhon Moores University, Merseyside L3 5UX, UK, a.d.batako@ljmu.ac.uk

Abstract:

Magneto-Rheological (MR) dampers have received a great deal of attention in recent years due to the potential of offering semi-active control. MR dampers have been successfully applied in the vibration control of several machining processes. However, the effect of the material of the damper's fluid chamber on its magnetic properties has not been studied much. In this study, an MR damper has been designed to control the chatter vibration of the straight turning operation. The magnetic properties of the MR damper are simulated in the FEM software COMSOL Multiphysics with two types of steel AISI 410 and AISI 1018, and the material with the best performance for constructing the fluid chamber is determined. Then, the MR damper with an assembly to hold the cutting tool was fabricated and experimentally tested during straight turning operation and its effect on the tool vibration, and work surface roughness was analyzed. From the result, it was observed that the MR damper reduced tool vibration and chatter effectively. The results obtained in this research confirm that the application of the MR damper in the straight-turning process can either suppress the chatter or greatly reduce the frequency amplitude of the chatter. The reduction of the tool's acceleration amplitude with the MR damper was more intense in the condition of chatter suppression and reached up to 89.42%. Moreover, the MR damper reduced the roughness of the machining surface. This reduction was higher in cases where the chatter was suppressed and it was observed up to 29%.

Keywords: Turning Process; Chatter Suppression; Magneto-Rheological (MR) Fluid Damper, Tool's Acceleration, Surface Roughness

Nomenclature

MR	Magneto-Rheological	F_r(N)	Radial force
FFT	Fast Fourier Transform	$G(\omega)$	Real components of the FRF
B(A/m)	Magnetic flux density	$H(\omega)$	Imaginary components of the FRF
H(A/m)	Intensity of the magnetic field	ζ	Damping ratio
J(A/m^2)	Current density	k(N/μm)	Stiffness
μ_0(T. m/A)	Permeability of free space	d(mm)	Damper distance from the tooltip
μ_r(T. m/A)	Relative permeability of the material	f_n(Hz)	Natural frequency
∅(mm)	Diameter of workpiece	r	Frequency ratio
L(mm)	Length of workpiece	M	Mean
a(mm)	Depth of cut	σ	Standard deviation
f(mm/rev)	Feed rate	R_a (μm)	Arithmetical mean roughness
n(rpm)	Spindle speed	K	Constant
F_c(N)	Cutting force	β	Constant
F_f(N)	Feed force		

1. Introduction

In turning operations the cutting tool is subjected to a dynamic excitation due to the deformation of work material during the cutting operation. In some cases, the metal cutting system is accompanied by intense relative movements between the tool and the workpiece, which considerably inhibits the production rate.The identification of tool vibration as a limitation for machining was initially found by Taylor [1]. The regeneration of waves on the workpiece was identified by Arnold [2] as a potential cause of chatter in turning. The modulated chip thickness due to vibration affects cutting forces dynamically, which increases vibration amplitudes and induces a process known as self-excited chatter. There are two well-known mechanisms of self-excited chatter: mode coupling and regeneration [3]. The mode-coupling chatter occurs when there is no interaction between the system's vibration and the workpiece's undulated surface. Whereas, the regenerative chatter results from phase differences between the inner and outer waves left on both sides of the chip. This occurs earlier than the mode-coupling chatter in most machining cases [3]. Therefore, regenerative chatter is considered the most significant mode of chatter vibration. Most of the research has been carried out on analyzing and detecting the regenerative self-excited chatter phenomenon [4, 5]. This paper refers to the "regenerative self-excited chatter" as chatter.

Chatter is a destructive phenomenon in machining processes. It not only confines machining productivity but also causes poor surface finish and reduced dimensional accuracy, increases the rate of tool wear, results in a noisy workplace, and reduces the life of a machine tool. Therefore, over recent years, many research works have been performed on chatter suppression as well as vibration suppression in machining operations. Techniques such as tunable vibration absorber (passive), and spindle speed variation (active) have been applied widely to suppress chatter in machine tools [6, 7]. In the active technique, the chatter vibrations are dynamically suppressed by continuous monitoring and diagnosis of the turning process, and by implementing necessary changes in the process. Some researchers employed techniques to disrupt the regenerative effect by actively varying process parameters like speed, feed rate, and depth of cut. Lin and Hu [8] varied the feed rate

and the spindle speed to suppress chatter in the turning process. Mei et al. [9] performed theoretical and experimental investigations into active chatter suppression by online variation of the cutting tool rake and clearance angles. However, these techniques have some limitations. Most of the active chatter control systems are limited to low spindle speeds. They require more complex hardware and software and are more expensive compared to passive systems. Additionally, active techniques require a certain amount of energy to drive the actuators to accomplish the control objective. That's why active chatter control methods are associated with high costs and high energy consumption. On the contrary, the passive techniques are more cheap and simple in application. Passive techniques suppress the chatter by changing the system's behavior. The system's behavior can be changed by improving the design of the machine tool or by using additional devices that can absorb extra energy or disrupt the regenerative effect [10]. These additional devices typically have lower rigidity and can dampen and control the chatter phenomena. Dynamic vibration absorbers, friction dampers, impact dampers, and tuned dampers are some of the most usual apparatuses added to the machine for passive chatter suppression [4]. Though in many applications, passive systems have been implemented, this technology lacks the adaptability to ever-changing loading conditions. Semi-active control is another approach that offers the reliability of passive systems while maintaining the adaptability and versatility of active systems. Magnetorheological (MR) dampers, variable orifice dampers, tuned liquid dampers, and controllable friction dampers are examples of semi-active devices. According to dynamic response, the semi-active device changes the structural properties of structures by using variable stiffness or variable damping system. In the semi-active system, control devices are driven by small power resources. A semi-active control system does not add energy to the structure and its properties can be varied dynamically. In addition, semi-active systems do not destabilize the structure and can also be utilized in the passive mode. Due to the reasons given above, in recent years semi-active control devices attract lots of interest [11]. Semi-active chatter suppression not only has better damping effectiveness than the passive mode but also has lower power and cost requirements than active suppression [12].

Magnetic fluids are prepared by incorporating soft iron particles into a nonmagnetic carrier oil such as mineral oils, synthetic oils, and aqueous fluids [13]. In the absence of a magnetic field, MR fluids behave similarly to Newtonian fluids, while under an external magnetic field, these fluids show non-Newtonian behavior, and some of the rheological properties of these fluids (yield stress and apparent viscosity) can be quickly controlled. Due to this property, these fluids have wide applications in automotive, aerospace, civil engineering, hydraulics, brakes, shock absorbers, and dampers [14].

The MR dampers are promising devices that have enabled effective semi-active control in several real-world applications such as vibration isolation under harmonic loading, civil structural vibration reduction, and vibration control in washing machines and automobiles. In essence, they are equivalent in construction to conventional hydraulic dampers except that their fluids dynamics change by applying currents-induced magnetic fields. Compared with the Electro-rheological (ER) damper, which is its analogy, the MR damper [15] requires a lower voltage which is very attractive for safety and practical reasons. The MR dampers are quite attractive for applications in machine tools because of their simplicity, low power consumption, scalability, and ability to achieve short-time responses [16].

Sathianarayanan et al. [17] investigated the effects of an MR damper on tool vibration in boring operation and found that the use of this damper can reduce the possibility of chatter and improves the stability of the machining process. Mohan and Natarajan [18] applied an MR damper in the boring process and experimentally

measured the tool vibration and workpiece surface roughness. They concluded that the MR damper significantly reduces the tool vibration and the work surface roughness. Paul et al. [19] investigated the influence of MR fluid on tool vibration during the end milling process. Their results showed that by using MR fluid damper milling tool vibrations, surface roughness, machining forces, and tool wear are reduced. Puma-Araujo et al. [20] designed a semi-active magnetorheological damper device to suppress chatter conditions during the milling operations of thin-floor components. They found that with the application of MR damper, the chatter stability boundaries shift toward higher critical axial depth of cut values, which substantially enhances stable cutting conditions. Ma et al. [21] designed an MR damping fixture to suppress machining vibration in thin-walled workpiece milling. Their results showed that with the MR fixture, the vibration response is reduced by 30 to almost 70% and the machined surface is effectively improved.

Orra and Choudhury [22] investigated the effectiveness of magneto-rheological (MR) damper in reducing the vibration and coefficient of friction and tool wear when micro-textured tools are used in the turning process. Analysis of results has revealed a maximum percentage decrease in acceleration ratio of about 66%, cutting force of about 30.07% coefficient of friction of about 16.15%, and tool wear of about 73.21%.

Emami et al. [23] designed and fabricated an MR fluid damper to suppress the chatter vibrations during the cut-off turning process. In the experiments, the tool vibration in damped and non-damped modes was evaluated and compared by measuring the tool acceleration signals. The obtained results showed that by using the MR fluid damper, the tool vibrations are significantly reduced, especially in the case of chatter occurrence.

It should be noted that different turning operations such as cut-off, straight turning, boring, etc., are different In terms of tool geometry, machining parameters, and machining forces. Hence, it is necessary to conduct more research on the design and use of MR dampers in various turning operations .

Referring to the literature, most of the applied MR dampers in machining processes have been utilized in boring operations. While in other machining operations such as straight turning, slotting, threading, etc., the chatter phenomena can take place. Therefore further research, especially on the effects of MR dampers on tool vibration and machining surface integrity, is needed. On the other hand, in previous research, the effect of design components on the intensity of the magnetic flux density generated in the damper has not been investigated. Hence, In this research, an MR damper is first modeled in CAD software. The magnetic properties of the MR damper are simulated in the FEM software COMSOL Multiphysics with two types of steel AISI 410 and AISI 1018, and the material with the best performance for constructing the fluid chamber is selected. Then, the MR damper is manufactured, and its effect on chatter suppression in the straight turning process (Fig. 1) is studied experimentally. Here, the machining properties of the workpiece are compared in two states of damper “off” and “on”, using metrics such as tool acceleration signal, the standard deviation of tool acceleration data, fast Fourier transform (FFT) plot, and work surface roughness.

2. Theory

2.1. Magnetic field

When an electric current passes through a coil, a magnetic field is induced around it. Using Maxwell-Ampere's law, the intensity of the magnetic field $H(\mathrm{A/m})$ is defined by Eq. (1):

$$\nabla \times H = J \tag{1}$$

Where $J(\mathrm{A/m^2})$ is the current density. Also, the magnetic flux density $B(\mathrm{A/m})$ can be obtained from the following equation:

$$B = \mu_0 \mu_r H \tag{2}$$

In Eq. (2), μ_0 is the permeability of free space and μ_r is the relative permeability of material and expresses the influence of the material on the wave resulting from its magnetic properties. If the field passes through a medium, the relative permeability coefficient of that medium affects the magnetic flux density.

By plotting the values of magnetic flux density (B) in terms of field intensity (H), a set of curves can be produced, which are known as magnetization curves or $B - H$ curves. This curve shows how the magnetic permeability of material changes with the flux density.

3. Design and manufacture of MR fluid damper

3.1. Parts modeling

In Fig. 2 (a) the 2D assembly drawing and Fig. 2 (b) the 3D exploded view of the damper with the part number are shown. The MR fluid damper parts are given in Table 1 with the corresponding number, description, material, and manufacturing method. Moreover, Fig. 2(c) shows MR fluid flow through the piston orifices. The fluid chamber (cylinder) of the damper is filled with a constant volume of MR fluid. A piston is embedded in the fluid chamber, which is connected to the shaft using a bolt. As the shaft moves up and down, the MR fluid flows through the piston orifices. Hence, the volume of the piston rod is compensated during the piston movement. The magnetic field is induced by a coil winded around the fluid chamber. The coil wire thickness in terms of standard wire gauge (SWG) is 0.813mm. By applying the magnetic field, the particles get a magnetic polarization, their movement is limited, and the yield stress of the MR fluid increases. Since the shaft is attached to the cutting tool, the damper can absorb the vibration energy of the tool. As mentioned in the introduction, FEM simulation is applied here to determine the suitable material for the damper's fluid chamber. It is important to notice that the material properties of the fluid chamber have a great influence on the magnetic flux density passing through the chamber and consequently on the damping coefficient of the MR damper. The other parts of the damper are made of 7075 aluminum alloy or polymer to reduce its total weight. The damper is designed to be easily mounted beneath the cutting tool on the lathe support table. Therefore, the height of the damper's plunger is determined according to its installation location. Damper parts are assembled after fabrication, then the damper is installed under the tool. The damper is attached to the tool also done by Technofix special glue. Since the cutting force (Fig. 1) is the main force applied to the tool in the straight turning process, the damper is designed and installed in such a way that it can reduce the vibrations of the tool to the maximum extent in line with the cutting force. Here, the MR fluid damper is installed under the tool holder close to the turning insert to increase the tool stiffness in the cutting area and reduce or dampen the vibrations caused by the cutting force. However, it is possible to design and install another damper for the feed force direction.

3.2. Magnetic fluid

Magneto-Rheological fluids are smart materials because their properties can be controlled by applying a magnetic field. These fluids are composed of ferromagnetic spherical particles dispersed in a hydrocarbon, silicone, or aqueous carrier fluid [24]. The ferrous particles are randomly dispersed in the medium when there is no magnetic field. The apparent viscosity and yield stress of the suspensions can be controlled by the power of an applied magnetic field. Upon application of the magnetic field (on-state), the particles acquire a magnetic polarization and attract each other along lines of magnetic flux, forming linear chains parallel to the applied field. The schematic of the magnetic fluid suspension before and after applying the magnetic field is illustrated in Fig. 3. As the applied magnetic field is increased, the yield stress of the fluid increases until the magnetization saturation Ms of the particles is reached. Once magnetic saturation Ms is reached, the yield stress no longer increases with increasing magnetic flux density and remains constant [25]. The magnetic saturation (Ms value) of an MR fluid can be measured using a vibrating sample magnetometer (VSM test).

The liquid-particle suspension of the MR fluid has viscous properties before applying the magnetic field while in the presence of the field, it becomes a semi-solid state with an extremely high change in viscosity (105–106 times) [26]. This phenomenon restricts the movement and increases the yield stress of the MR fluid. The field-dependent yield stress of MR fluids relies on several factors including the size, geometry, composition, and volume fraction of the particles, and the strength of the applied magnetic field. Since the property changes occur instantly, MR fluids are attractive for real-time control applications. MR fluids technology has been proven in many industrial applications like dampers (shock absorbers), actuators, brakes, clutches, prosthetic devices, polishing and grinding devices, etc [27].

Here, MRF-132DG produced by Lord Corporation was used in the MR damper. MRF-132DG fluid is a suspension of micron-sized, magnetizable particles in a carrier fluid. It is formulated for general use in controllable, energy-dissipating applications such as shocks, dampers, and brakes [28]. Table 2 shows the properties of MRF-132DG [29].

3.3. Simulation

COMSOL Multiphysics® is a general-purpose software platform, based on advanced numerical methods, for modeling and simulating physics-based problems. In the present investigation, COMSOL software is used to simulate the electromagnetic fields in the MR damper. Here, FEM simulation is used to obtain an insight into the magnetic field flux behavior inside the damper's fluid chamber. Simulations have the advantage of allowing modification of the design of the damper before actual manufacture, and the damping characteristics can be improved with manufacturing cost savings. On the one hand, it is possible to ensure the optimal distribution and intensity of the magnetic field flux in the damper's fluid chamber by carrying out simulation and modifying its design if needed. On the other hand, the material selection for the construction of the fluid chamber can affect the flux density of the magnetic field generated in the damper and overshadow its damping properties. Simulation of MR damper for machining application and the optimal selection of material for its construction is required to be more investigated and has not been sufficiently highlighted by the existing literature.

In this simulation, the magnetic properties of the materials used for the MR fluid, internal casing, and plunger were accounted for in the software. In the reviewed articles [17, 18] an annealed AISI 410 stainless steel material has been used to fabricate the damper's fluid chamber. It is necessary to simulate the effect of the fluid chamber material on the magnetic field flux density of the damper to quantify the damping capacities as a function of the flux of the magnetic field passing through the fluid chamber.

In this study, annealed low carbon steel of grade AISI 1018 is proposed for fabricating the damper's fluid chamber due to its high magnetic permeability. The boundary conditions used include a coil with 120 turns, magnetic insulation considering the environment outside the damper, and zero magnetic fields as the initial value. In addition to determining the boundary conditions of the damper, it is necessary to consider the magnetic permeability coefficients of the material of the inner chamber and the fluid used in the simulation. Here, two types of annealed steel, namely 1- AISI 410 stainless steel and 2- AISI 1018 low carbon steel, are compared in the simulation of the damper's fluid chamber. The relative permeability (μ_r) of the materials mentioned above, as well as field-dependent yield stress of MR fluid, can be extracted by fitting a function to any of the B-H curves shown in Fig. 4. After fitting the B-H curve for the MRF-132DG (Fig. 4a), the field-dependent yield stress for MRF-132DG (Fig. 4b), and the B-H curve for the AISI 410 and AISI 1018 steels (Fig. 4c) and solving the Maxwell-Ampere law (Eqs. (1) & (2)) the magnetic field distribution in the fluid chamber was obtained from the Magnetic Fields module of the software. Figs. 5 and 6 respectively illustrate the results obtained from the FEM-based simulation of the magnetic flux density of the MR damper for both AISI 410 stainless steel and AISI 1018 low carbon steel when the coil current was 9 A. Figs. 5a and 5b respectively show the 2D and 3D views of the magnetic flux density in the MR damper's fluid chamber designed with AISI 410. The 2D and 3D views of the magnetic flux density in the MR damper's fluid chamber designed with AISI 1018 are shown in Figs. 6a and b, respectively. Here the red color represents the areas with the highest and the blue color shows the areas with the lowest magnetic flux density. Figs. 5a,b show that the magnetic flux density in the fluid chamber designed with AISI 410 stainless steel reaches the maximum value of 0.28 T. While according to Figs. 6a,b the maximum magnetic flux density in the fluid chamber designed with AISI 1018 low carbon steel reaches 0.7 T. This means that AISI 1018 low carbon steel leads to a higher magnetic flux density in the damping fluid chamber compared to AISI 410 stainless steel. Here, the saturation point of the MR fluid is obtained from the B-H and Yield stress-H curves as shown in Figs. 4a and 4b. From Fig. 4b, when the magnetic field intensity H reaches about 290 kA/m, the yield stress does not increase rapidly and the saturation condition is achieved. This point (H=290 kA/m) in the curve of Fig. 4a corresponds to the magnetic induction of B=1.27 T. Since the maximum magnetic flux density in the fluid chamber designed with AISI 1018 low carbon steel is lower than the magnetic saturation point (1.27 T), the design requirement is satisfied.

Therefore, due to its high magnetic permeability properties and the ability to pass the maximum magnetic field, AISI 1018 annealed steel was chosen as the material of the inner chamber of the MR damper. From Figs.5 and 6, the area inside the fluid chamber has the highest magnetic flux density. The result of this simulation confirms that the distribution of the magnetic flux density inside the damper's fluid chamber is suitable and thus the MR fluid can be well polarized. It is worth noting that with the polarization of the MR fluid along the direction of the magnetic field, its yield stress increases and enhances its damping energy. Overall, these simulation results confirm the MR damper design requirements.

4. Experimental tests

The experimental setup of this investigation is shown in Fig. 7(a-c). The machining tests were performed using a TOS SN 50 universal lathe in dry conditions. The test specimens were cylindrical in shape with a diameter of $\emptyset = 35$mm and a length of L=15mm which were prepared by cutting several equidistant grooves on a solid rod as shown in Fig. 7c. Each machining experiment was done on the prepared 15mm length of the work material in the straight turning mode.

The metal cutting parameters include depth of cut (a), feed rate (f), and spindle speed (n). Since the feed rate (f) has less effect on the chatter stability than the other two parameters (i.e. spindle speed (n) and depth of cut (a)) [5], it was kept constant in all the tests. The cutting parameters were determined as the depths of cut 0.25-4 mm, and spindle speeds of 500, 710, and 1000 rpm. However, since the feed rate has not had a considerable effect on chatter it was kept constant at 0.08 mm/rev. The MR damper was attached beneath the tool holder at two different horizontal distances of 80 mm and 35 mm from the tooltip to the center of the damper. These two distances were tested to investigate the effects of the damper position on the chatter stability. Also, all the experiments were performed in two states of damper "on" and "off". During the 'damper on' condition, the magnitude of the DC current input was 9 A. The experimental settings are summarized in Table 3. The surface roughness of work samples was measured along the feed direction by a portable Mahr (Mar Surf PS1) stylus profilometer. Surface roughness measurements (Ra & Rz) were carried out four times at a cut-off length of 5.6 mm each, and a mean value was recorded as Ra and Rz values. Tool holder type S16R SCLCR-09 of diameter 16 mm with tool insert CCMT-MP-09T304 was used to perform the turning operation. An ICP impact hammer model PCB 086C01 with a weight of 0.1 kg and a sensitivity of 2.11 mV/N, along with a piezo accelerometer sensor (PCB Piezotronics) was used during the machining tests to perform modal analysis and record the tool's vibration. The acceleration data was recorded using the data acquisition system NI USB-4431 with a data acquisition rate of 5260 Hz.

5. Results

The experimental results of this investigation including the FRF, acceleration, and FFT graphs, as well as surface roughness measurements, are presented as follows.

5.1. FRF graphs

The frequency response function (FRF) expresses the structural response to an applied force as a function of frequency. Here, the force is exerted on the tool and measured via the modal test hammer, and the response is received by the accelerometer as shown in Fig. 7b. The hammer impact is applied on top of the tool holder near the cutting insert. Also, the accelerometer is attached beneath the tool holder using a special wax. The FRFs obtained from the experimental modal analysis of the tool-damper structure for two damper positions, $d = 80$ mm and $d = 35$ mm, are shown in Figs. 8 and 9, respectively. As can be observed in these figures, each FRF graph consists of two parts: the real and the imaginary part. The equations of real $(G(\omega))$ and imaginary $(H(\omega))$ components of the FRF are as follows [5]:

$$G(\omega) = \frac{1 - r^2}{k[(1 - r^2)^2 + (2\zeta r)^2]} \tag{3}$$

$$H(\omega) = \frac{-2\zeta r}{k[(1 - r^2)^2 + (2\zeta r)^2]} \tag{4}$$

Where r is the frequency ratio (the excitation to natural frequency ratio $(r = \omega/\omega_n)$), ζ is the damping ratio, and k is the stiffness. At zero frequency crossing $(\omega = 0)$, the real part is equal to the static flexibility $(G(0) = 1/k)$. As the excitation frequency approaches the natural frequency (i.e., $\omega = \omega_n$ or r = 1), the real part becomes equal to zero $(G(\omega_n) = 0)$, the system resonates, and the amplitude of the vibrations becomes maximum. The stiffness and natural frequency of the tool-MR damper structure for two damper positions $d = 80$ mm and $d = 35$ mm were calculated from the real and imaginary graphs data and shown in Table 4. As can be seen in this table, the stiffness of the tool-MR damper structure for $d = 80$ mm is $k = 2.2$ N/μm, whereas for $d = 35$ mm increases to $k = 11.11$ N/μm. Moreover, the natural frequency of the tool-MR damper structure for two damper positions $d = 80$ mm and $d = 35$ mm are respectively around 660 and 530 Hz. The results of past research have shown that the stability of the turning process increases with the increase in tool stiffness [30].

5.2. Acceleration, FFT graphs, and Standard deviation of acceleration data

In this section, the results of the acceleration signal measurements, the extracted FFT spectrums, and the standard deviation (STDV) of the acceleration signals are shown and discussed. Figs. 10-17 depict the acceleration signal and the corresponding FFT graphs of tests No. 1-16 planned in Table 3. Each figure shows two experiments with the damper in the "off" and "on" states. The cutting parameters in the aforementioned tests include depths of cut a =0.25, 0.5, 0.75, 1, 1.5, 2, 2.25, 2.5, 3mm, feed rate f =0.08 mm/rev, and spindle speed $n = 500$ rpm. Also, the damper distance from the tooltip (d) is 80 mm. The test conditions including the cutting parameters, and the distance between the damper and the tooltip, as well as the damper status "off" or "on" are labeled on each figure. A visual examination of the acceleration signals in Figs. 10-17 shows that generally when the damper is off-state, the vibration amplitude of the tool is higher than when the damper is in on-state. Also, when the damper is “on” the fluctuation of acceleration signals is less than when it is “off”. Remarkably, this amount of amplitude reduction in tool acceleration varies depending on the machining conditions. Moreover, the comparison of FFT graphs in Figs. 10-17 shows that at the cutting depths of a = 0.25 − 2 mm, the amplitude values of the frequency spectrums are very low (less than 0.2). This means that the chatter phenomenon has not occurred at the mentioned depths of cut.

However, the FFT plots (b) and (d) in Fig. 16 show that when the damper is turned off, the frequency amplitude increases sharply to a magnitude of 9.09 at a frequency of 661.5 Hz (a frequency close to the natural frequency of the system). In other words, the machining at a cutting depth of 2.25 mm is accompanied by chatter, while when the damper is turned on, the chatter amplitude decreases considerably and reaches a magnitude of 3.67 at a frequency of 653.2 Hz. In addition, as can be seen in Fig. 17, the comparison of plots (b) and (d) shows that when the damper is turned off, the intensity of the chatter frequency reaches 11.25 at around 661 Hz, while when the damper is turned on its intensity decreases to 3.85 at almost the same frequency. Figs. 16 and 17 show that the chatter has occurred at the cutting depths of 2.25 and 2.5 mm, respectively. But the noteworthy point is that the damper in the “on” state reduces the frequency amplitude of the chatter to a significant extent. These results show that using the MR damper in the straight turning process can drastically reduce the frequency amplitude of chatter and provide more stable cutting conditions.

To quantify and better compare the amplitude of the vibration signals, the standard deviation function is used. It is noteworthy that the standard deviation function (σ) can be directly used as a characteristic parameter to evaluate the acceleration signal [31, 32]. Eqs. (5) and (6) respectively show how to calculate the mean and

standard deviation of a signal.

$$M = \frac{1}{N}\sum_{i=0}^{N-1} x_i \qquad (5)$$

$$\sigma^2 = \frac{1}{N-1}\sum_{i=0}^{N-1}(x_i - M)^2 \qquad (6)$$

Where, M is the mean, σ is the standard deviation, N is the number of signal data, and x_i is the value of each data. Here, the standard deviation of acceleration signals is used as a criterion in the evaluation of tool vibrations. The smaller the standard deviation of the acceleration signal, the more the tool vibration is damped. In Fig. 18, the standard deviation values of acceleration data obtained from the machining tests conducted with $a = 0.25 - 2.5$ mm, $n = 500$ rpm, $f = 0.08$ mm/rev , and $d = 80$ mm, are extracted and plotted in a column chart. This chart is divided into two ranges including "No chatter" (cutting depths 0.25 to 2 mm) and "chatter" (cutting depths 2.25 and 2.5 mm). It is clear that the relative difference between the standard deviation values in the "on" and "off" states of the MR damper has increased in chatter conditions. It can be concluded that the MR damper has significantly reduced the values of the standard deviation of the tool acceleration, especially at higher values of the cutting depth. The percentage reduction of the standard deviation of the acceleration signal when the damper is on compared to when it is off is shown in Table 5. This measure shows the decrease in amplitude of the tool's acceleration signal under damping conditions. Table 5 shows that this percentage reduction is 59.80% and 59.05% for the cutting depth of 2.25 and 2.5 mm, respectively. In addition, the average value of the percentage reduction of the standard deviation of the amplitude of the acceleration signal is 25.36%. This result shows that the MR damper can significantly reduce the tool vibration amplitude, especially in chatter conditions.

Tests No. 17 - 32 were performed respectively with the parameters a =0.25, 0.5, 0.75, 1, 1.5, 2, 2.5, 3, 3.5, and 4 mm, n =710 rpm, f =0.08 mm/rev, and d =35 mm as shown in Table 3. The acceleration and FFT results of this series of experiments are shown only around the range where the chatter occurred to reduce the number of graphs in the paper (Figs. 19-21). Here, chattering vibrations were observed at the depth of cut of 3.5 mm and more, while no chatter was observed during machining at the depth of cut of less than 3.5 mm. Comparing plots (a) and (c) in Figs. 19-21 shows that the amplitude as well as the fluctuation of the acceleration signals when using the damper in the on-state is much less than in the off-state. Remarkably, this amount of amplitude reduction of tool acceleration varies depending on the machining conditions. The FFT plots (b) and (d) in Fig. 19 show that no peak with considerable intensive amplitude is observed around the natural frequency of the system. In other words, no chatter has occurred here in the cutting depth of 3 mm. However, the intensity of frequencies obtained in the FFT plot (d) is lower than the plot (b). Plot (a) in Fig. 20 shows that for a cutting depth of 3.5 mm with the damper off, the amplitude of the acceleration signal and its fluctuations are significantly large. Also, plot (b) in this figure indicates that a peak of magnitude 2.3 is observed at the frequency of 504.5 Hz, which corresponds to the chatter frequency at the cutting depth of 3.5

mm. While plot (c) in Fig. 20 shows that with the damper on, the amplitude of the acceleration signal and its fluctuations are significantly reduced. Also, plot (d) in this figure shows that there is no chatter frequency at the cutting depth of 3.5 mm with the damper on.

Plots (a-d) in Fig. 21 also show that with the cutting depth of 4 mm and the damper off, the amplitude of the acceleration signal increases sharply, and chattering occurs at a frequency of 479 Hz with an intensity value of 12.7. While with the damper on, the amplitude of the acceleration signal has decreased significantly, no chatter frequency is observed and the machining has reached a stable condition.

In Fig. 22, the standard deviation values of acceleration data obtained from the machining tests conducted with $a = 0.5 - 4$ mm, $n = 710$ rpm, $f = 0.08$ mm/rev, and $d = 35$ mm are extracted and plotted in a column chart. It can be concluded that the MR damper has significantly reduced the values of the standard deviation of the tool acceleration, especially at higher values of the cutting depth. This chart is divided into two ranges including "No chatter" (cutting depths less than 3.5 mm) and "chatter" (cutting depths 3.5 and 4 mm). It is clear that the difference between the standard deviation values in the "on" and "off" states of the MR damper has increased in chatter conditions. From the comparison of Figs. 18 and 22, it can be concluded that by increasing the spindle speed from 500 rpm to 710 rpm and decreasing the distance between the MR damper and the tooltip from 80 mm to 35 mm, the critical depth of cut (the cutting depth at which chatter occurred) increases, or the stability of machining increases. In Table 6, the percent reduction of acceleration standard deviation for this series of tests is shown. These percentage reductions reach 69.56% and 82.41% for the depth of cuts of 3.5 and 4 mm, respectively. In addition, here the average percentage reduction of the standard deviation of the amplitude of the acceleration signal is 37.53%. This result shows that the MR damper is significantly effective in reducing the tool vibration amplitude, especially in chatter conditions.

The tests No. 33 - 48 were performed respectively with the parameters a =0.5, 1, 1.5, 2, 2.5, 3, 3.5, and 4 mm, n =1000 rpm, f =0.08 mm/rev and d =35 mm as shown in Table 3. The acceleration and FFT results of this series of experiments are shown only around the range where the chatter occurred to reduce the total number of graphs in the paper (Figs. 23-25).

Here, similar to the results obtained for n =710 rpm, the chattering vibrations were observed at the depth of cut of 3.5 mm and more, while no chatter was observed during machining at the depth of cut of less than 3.5 mm. As can be seen in plots (a) and (c) of Figs. 23-25, the amplitude and the fluctuation of the acceleration signals in the "on" state are much less than in the "off" state of the damper. These results depict that the amount of amplitude reduction of tool acceleration varies depending on the depths of cut. The FFT plots (b) and (d) in Fig. 23 show that no peak with considerable intensive amplitude is observed around the natural frequency of the system. In other words, no chatter has occurred here in the cutting depth of 3 mm. However, the intensity of frequencies obtained in the FFT plot (d) is lower than the plot (b). Plot (a) in Fig. 24 shows that for a cutting depth of 3.5 mm with the damper off, the amplitude of the acceleration signal and its fluctuations are significantly large. Also, plot (b) in this figure indicates that a peak of magnitude 17 is observed at the frequency of 529 Hz, which corresponds to the chatter frequency at the cutting depth of 3.5 mm. While plot (c) in Fig. 24 shows that with the damper on, the amplitude of the acceleration signal and its fluctuations are significantly reduced. Also, plot (d) in this figure shows that there is no chatter frequency in the cutting depth of 3.5 mm with the damper on.

Plots (a-d) in Fig. 25 also show that with the cutting depth of 4 mm and the damper off, the amplitude of the acceleration signal increases sharply, and chattering occurs at a frequency of 494 Hz with an intensity value of 20.2. While with the damper on, the amplitude of the acceleration signal has decreased significantly, no chatter frequency is observed and the machining has reached a stable condition.

The standard deviation values of acceleration data obtained from the machining tests conducted with $n = 1000$ rpm, $f = 0.08$ mm/rev, and $d = 35$ mm are extracted and plotted in a column chart in Fig. 26. Here it can also be concluded that the MR damper has significantly reduced the values of the standard deviation of the tool acceleration, especially at higher values of the cutting depth. This chart is divided into two ranges including "No chatter" (cutting depths less than 3.5 mm) and "chatter" (cutting depths 3.5 and 4 mm). It is clear that the relative difference between the standard deviation values in the "on" and "off" states of the MR damper has increased in chatter conditions. From the comparison of Figs. 22 and 26, it can be concluded that by increasing the spindle speed from 710 rpm to 1000 rpm, the critical depth of cut hasn't changed. The percent reduction of the standard deviation of the acceleration amplitude for this series of tests is shown In Table 7. The reduction of the standard deviation of the amplitude of the acceleration signal (vibration amplitude) for the cutting depths of 3.5 and 4 mm (chatter conditions) reaches 74.46% and 82.49%, respectively. Also, the average percentage reduction of the standard deviation of the acceleration amplitude is 38.87%. This result shows the effectiveness of the MR damper in reducing the tool's vibration amplitude, especially in chatter conditions. Because by applying the magnetic field (on-state), the particles in the MR fluid acquire a magnetic polarization and attract each other along the magnetic flux lines and form linear chains parallel to the applied field. The MR fluid particle suspension has viscous properties before applying the magnetic field, while it turns into a semi-solid state in the presence of the field. This phenomenon increases the yield stress of the MR fluid and increases the damping power of the damper in absorbing vibrations in turning operations

5.2. Surface roughness

In this section, the results of the arithmetical mean roughness (Ra) of the machined work material are shown in Figs. 27 and 28. Fig. 27 shows the graph obtained from work surface roughness values Ra of the machining test conducted with $n = 500$ rpm, and $d = 80$ mm and Fig. 28 shows the graph obtained from Ra values of the machining test conducted with $n = 1000$ rpm, and $d = 35$ mm. The relative reduction percentage of surface roughness for each experiment is calculated and shown on the graphs. It can be seen in Figs. 27 and 28 that the MR damper in the on-state gives a lower surface roughness than in the off-state. But considering that the chatter is not completely suppressed in the test with n =500 rpm and $d = 80$ mm, it can be seen in Fig. 27 that the surface roughness does not decrease much in the cutting depths of 2.25 and 2.5 mm. However, since the chatter vibration is completely suppressed in the experiments conducted with $n = 1000$ rpm, and $d = 35$ mm, the surface roughness at the cutting depths of 3.5 and 4 mm is significantly reduced and shows a 17% and 29% reduction respectively. Here, the average reduction of Ra surface roughness in Figs. 27 and 28 are 9% and 13.29% respectively.

6. Conclusion

In this study, an MR damper was designed to control the chatter vibration of the straight turning operation. The magnetic properties of the MR damper were simulated in the FEM software COMSOL Multiphysics with

two types of steel AISI 410 and AISI 1018. The results show that AISI 1018 low carbon steel leads to a higher magnetic flux density in the damping fluid chamber compared to AISI 410 stainless steel. It is worth mentioning that the effective design can improve the magnetic flux density of the MR damper and increase its damping capacity. In addition, the results of the modal test show that the stiffness of the tool-MR damper structure for $d = 80$ mm is $k = 2.2$ N/μm, while it increases to $k = 11.11$ N/μm for $d = 35$ mm. This means that reducing the distance between the damper and the tool increases the rigidity of the structure and hence the stability of the turning process. In general, the comparison of tool acceleration signals in two states "damper off" and "damper on" for different machining conditions shows that the presence of the MR damper is effective in reducing the intensity of chatter frequency or suppressing the chatter. More precisely, with a spindle speed of n =500 rpm and $d = 80$ mm, the use of the MR damper reduces the intensity of chatter frequency, without removing the chatter. While at the speeds of n =710 and 1000 rpm and $d = 35$ mm, the chatter frequency is completely suppressed. Therefore, more stable cutting conditions are achieved with the MR damper at higher spindle speeds and less distance between the damper and the tool. The average percentage reduction of the standard deviation of the acceleration signals in the experiments with a spindle speed of n =500 rpm and $d =$ 80 mm, is 25.36%. Whereas this value reaches 37.53% in the experiments with n =710 and $d = 35$ and reaches 38.87% in the experiments with n =1000 and $d = 35$ mm. The results show that the percent reduction of the standard deviation of the acceleration amplitude increases in chatter conditions. For example, this value reaches 82.49% for a depth of cut 4 mm in the experiments with n =1000 and d =35 mm. These results are compatible with the results obtained from [22] regarding the significant reduction of the acceleration ratio with the MR damper in the turning process. The results of the surface roughness measurement in the experiments show that in the conditions of suppressing the chatter with the MR damper, the roughness of the machining surface is significantly reduced and therefore the quality of the work surface is improved.

The results obtained in this research confirm that the application of the MR damper in the straight-turning process can either suppress the chatter or greatly reduce the frequency amplitude of the chatter. However, to achieve more stable cutting conditions for machining at lower spindle speeds, it is suggested to add another MR damper and install it in line with the feed forces of the tool.

For future work, the design and manufacture of MR damper for milling operations of thin-walled components are suggested. Also, the authors are currently designing MR dampers for the car suspension system and the car engine

Acknowledgments

The authors are indebted to the mechanical engineering department of Atilim University, Turkey, for the facilities needed for performing the experimental tests.

References

[1] Taylor FW. On the art of cutting metals. American society of mechanical engineers; 1906.

[2] Arnold R. Cutting tools research: report of subcommittee on carbide tools: the mechanism of tool vibration in the cutting of steel. Proceedings of the institution of mechanical engineers 1946;154(1):261-84. https://doi.org/10.1243/PIME_PROC_1946_154_037_02.

[3] Gulizia S. Novel titanium additive manufacturing technologies–from powder to product. 3 rd International congress on 3D printing technologies and digital industry 2018.

[4] Siddhpura M, Paurobally R. A review of chatter vibration research in turning. Int J Mach Tools Manuf 2012;61:27-47. https://doi.org/10.1016/j.ijmachtools.2012.05.007.

[5] Altintas Y, Ber A. Manufacturing automation: metal cutting mechanics, machine tool vibrations, and CNC design. Appl Mech Rev 2001;54(5):B84-B. https://doi.org/10.1115/1.1399383.

[6] Pratt J, Nayfeh A, Pratt J, Nayfeh A, editors. Active vibration control for chatter suppression. 38th Structures, Structural Dynamics, and Materials Conference 1997. https://doi.org/10.2514/6.1997-1210.

[7] Tarng Y, Kao J, Lee E. Chatter suppression in turning operations with a tuned vibration absorber. J Mater Process Technol 2000;105(1-2):55-60. https://doi.org/10.1016/S0924-0136(00)00585-9.

[8] Lin S, Hu M. Low vibration control system in turning. Int J Mach Tools Manuf 1992;32(5):629-40. https://doi.org/10.1016/0890-6955(92)90018-C.

[9] Mei Z, Yang S, Shi H, Chang S, Ehmann K. Active chatter suppression by on-line variation of the rake and clearance angles in turning—principles and experimental investigations. Int J Mach Tools Manuf 1994;34(7):981-90. https://doi.org/10.1016/0890-6955(94)90029-9.

[10] Quintana G, Ciurana J. Chatter in machining processes: A review. Int J Mach Tools Manuf 2011;51(5):363-76. https://doi.org/10.1016/j.ijmachtools.2011.01.001.

[11] Bankar VK, Aradhye A. A review on active, semi-active and passive vibration damping. Int J Curr Eng Technol 2016;6:2187-91.

[12] Lam HF, Liao W-H. Semi-active control of automotive suspension systems with magnetorheological dampers, Proc. SPIE 4327, Smart Structures and Materials 2001: Smart Structures and Integrated Systems, (16 August 2001); https://doi.org/10.1117/12.436523.

[13] Sutrisno J, Purwanto A, Mazlan SA. Recent progress on magnetorheological solids: materials, fabrication, testing, and applications. Adv Eng Mater 2015;17(5):563-97. https://doi.org/10.1002/adem.201400258.

[14] Kumar S, Sehgal R, Wani M, Sharma MD. Stabilization and tribological properties of magnetorheological (MR) fluids: A review. J Magn Magn 2021;538:168295. https://doi.org/10.1016/j.jmmm.2021.168295.

[15] Nguyen M, Dalvand H, Yu Y-H, Ha Q, editors. Seismic responses of civil structures under magnetorheological-device direct control. ISARC 2008-Proceedings from the 25th International Symposium on Automation and Robotics in Construction; 2008.

[16] Milecki A. Investigation and control of magneto–rheological fluid dampers. Int J Mach Tools Manuf 2001;41(3):379-91. https://doi.org/10.1016/S0890-6955(00)00085-7.

[17] Sathianarayanan D, Karunamoorthy L, Srinivasan J, Kandasami G, Palanikumar K. Chatter suppression in boring operation using magnetorheological fluid damper. Mater Manuf Process 2008;23(4):329-35. https://doi.org/10.1080/10426910701860897.

[18] Mohan E, Natarajan U. Experimental investigation on boring tool vibration control using MR fluid damper. J Adv Manuf Syst 2016;15(01):13-25. https://doi.org/10.1142/S0219686716500025.

[19] Paul PS, Shobhan Kumar C, Joshua M, Vignesh S, Saravanan S, Varadarajan A. Study on the influence of magnetorheological fluid on tool vibration during end milling process. Int J Dyn Control 2017;5(3):696-703. https://doi.org/10.1007/s40435-015-0214-x.

[20] Puma-Araujo SD, Olvera-Trejo D, Martínez-Romero O, Urbikain G, Elías-Zúñiga A, López de Lacalle LN. Semi-active magnetorheological damper device for chatter mitigation during milling of thin-floor components. Appl Sci 2020;10(15):5313. https://doi.org/10.3390/app10155313.

[21] Ma J, Li Y, Zhang D, Zhao B, Pang X. Dynamic characteristic reconfiguration of a fixture-workpiece system for vibration suppression in milling of thin-walled workpieces based on MR damping fixture. Int J Adv Manuf Technol 2022;122(9-10):3751-68. https://doi.org/10.1007/s00170-022-10143-0.

[22] Orra K, Choudhury SK. Experimental investigation of machining process by micro-textured cutting insert together with magneto-rheological damper. Wear. 2021 Jul 15;476:203731. https://doi.org/10.1016/j.wear.2021.203731.

[23] Emami M, Hasan Nasab V. Experimental Investigation of the Effects of Magneto-Rheological (MR) Fluid Damper on Tool Vibrations in Cut-off Operation. Iranian Journal of Manufacturing Engineering. 2020;7(12):24-36.

[24] Klingenberg DJ. Magnetorheology: Applications and challenges. American Institute of Chemical Engineers. AIChE Journal. 2001;47(2):246. https://doi.org/10.1002/aic.690470202.

[25] Ginder JM, Davis L, Elie L. Rheology of magnetorheological fluids: models and measurements. Int J Mod Phys B 1996;10(23n24):3293-303. https://doi.org/10.1142/S0217979296001744.

[26] Genç S, Phulé PP. Rheological properties of magnetorheological fluids. Smart Mater Struct 2002;11(1):140. https://doi.org/10.1088/0964-1726/11/1/316.

[27] Truong D, Ahn K. MR fluid damper and its application to force sensorless damping control system. Smart Actuation and Sensing Systems-Recent Advances and Future Challenges. 2012:383-425. https://doi.org/10.5772/51391.

[28] 'MRF-132DG Magntorheological Fluid,'LORDCorporation, Cary NC, USA, 2011.

[29] Hasannasab V, Bazargan-Lari Y. Design and Manufacture of a Magnetorheological Brake System Applicable for Wheelchair Manipulations. J Test Eval 2019;49(3):1586-98. DOI: 10.1520/JTE20180926.

[30] Siddhpura M, Siddhpura A, Paurobally R. Chatter stability prediction for a flexible tool-workpiece system in a turning process. Int J Adv Manuf Technol. 2017;92(1):881-96. https://doi.org/10.1007/s00170-017-0208-2

[31] Yeh L, Lai G. A study of the monitoring and suppression system for turning slender workpieces. Proceedings of the Institution of Mechanical Engineers, Part B: Journal of Engineering Manufacture. 1995;209(3):227-36.

[32] Liu H, Chen Q, Li B, Mao X, Mao K, Peng F. On-line chatter detection using servo motor current signal in turning. Sci China Technol Sci 2011;54(12):3119-29. https://doi.org/10.1007/s11431-011-4595-6.

[33] Purandare S, Zambare H, Razban A. Analysis of magnetic flux in magneto-rheological damper. J Phys Commun 2019;3(7):075012. **DOI** 10.1088/2399-6528/ab33d7.

[34] Multiphysics C, Module C. COMSOL multiphysics user's guide. Version: COMSOL Multiphysics. 2014;3.

Table 1. MR fluid damper parts.

Part Number	Part Name	Description	Material	Manufacturing Method
1	External casing	External cover and retainer of internal parts	Polymer	Machining-Turning & Drilling
2	Flange	To close and seal the bottom of the fluid chamber	Stainless steel 316L	Machining-Turning & Drilling
3	Coil	Conductor of DC electric current to generate the magnetic field	Copper	Winding
4	Piston	MR fluid compressor to create damping force	Al 7075	Machining-Turning & Drilling
5	Cylinder	The fluid chamber in which the piston moves back and forth	AISI 1018	Machining-Turning
6, 9	Sealing washer	To seal and prevent fluid from escaping around the piston shaft	Polymer	Standard
7, 10	Circlip	Retaining ring of the sealing washer	Low alloy steel	Standard
8	Shaft guide and cap	Preventing the deviation of the piston shaft during reciprocating movement - top cap	Stainless steel 316L	Machining-Turning & Drilling
11	Shaft	The rod connecting the tool holder to the piston	Al 7075	Machining-Turning & Drilling

Table 2. MRF-132DG characteristics [29].

Base fluid	**Operating temperature**	**Density**	**Viscosity @ 40°C (no magnetic field applied)**	**K**	***β***
Hydrocarbon	-40 to 130° C	3.09 g/cc	0.09 (±0.02) Pa.s	0.269 Pa.m/A	1

Table 3. Experimental Design.

			Damper parameters	
Test No.	**Depth of cut a (mm)**	**Spindle speed n (rpm)**	**Damper distance from tooltip d (mm)**	**Damper's magnet condition**
1	0.25	500	80	Off
2	0.25	500	80	On
3	0.5	500	80	Off
4	0.5	500	80	On
5	0.75	500	80	Off
6	0.75	500	80	On
7	1	500	80	Off
8	1	500	80	On
9	1.5	500	80	Off
10	1.5	500	80	On
11	2	500	80	Off
12	2	500	80	On
13	2.25	500	80	Off
14	2.25	500	80	On
15	2.5	500	80	Off
16	2.5	500	80	On
17	0.5	710	35	Off
18	0.5	710	35	On
19	1	710	35	Off
20	1	710	35	On
21	1.5	710	35	Off
22	1.5	710	35	On
23	2	710	35	Off
24	2	710	35	On
25	2.5	710	35	Off
26	2.5	710	35	On
27	3	710	35	Off
28	3	710	35	On
29	3.5	710	35	Off
30	3.5	710	35	On
31	4	710	35	Off
32	4	710	35	On
33	0.5	1000	35	Off
34	0.5	1000	35	On
35	1	1000	35	Off
36	1	1000	35	On
37	1.5	1000	35	Off
38	1.5	1000	35	On
39	2	1000	35	Off
40	2	1000	35	On
41	2.5	1000	35	Off
42	2.5	1000	35	On
43	3	1000	35	Off
44	3	1000	35	On
45	3.5	1000	35	Off
46	3.5	1000	35	On
47	4	1000	35	Off
48	4	1000	35	On

Table 4. Comparison of stiffness and natural frequency of the tool-MR damper structure in two damper positions of "$d = 80$ mm" and "$d = 35$ mm".

Damper distance from the tooltip d (mm)	$\boldsymbol{G(0)}$	**Stiffness** $\boldsymbol{k}(\mathrm{N}/\boldsymbol{\mu m})$	**Natural Frequency** $\boldsymbol{f_n}(\mathbf{Hz})$
80	0.45	2.22	660
35	0.09	11.11	530

Table 5 Percentage reduction of the standard deviation of the tool's acceleration signal with $n = 500$ rpm, $f = 0.08 \frac{\text{mm}}{\text{rev}}$, and $d = 80$ mm.

Depth of cut	**0.25mm**	**0.5mm**	**0.75mm**	**1mm**	**1.5mm**	**2mm**	**2.25mm**	**2.5mm**
Percentage reduction of σ_a(vibration amplitude)	10%	15.79%	4.17%	5.71%	13.04%	35.33%	59.80%	59.05%

Table 6 Percentage reduction of the standard deviation of the tool's acceleration signal with $n = 710$ rpm, $f = 0.08 \frac{\text{mm}}{\text{rev}}$, and $d = 35$ mm.

Depth of cut (mm)	**0.5**	**1**	**1.5**	**2**	**2.5**	**3**	**3.5**	**4**
Percentage reduction of σ_a(vibration amplitude)	0	18.5%	7.14%	28.57%	30.08%	64%	69.56%	82.41%

Table 7 Percentage reduction of the standard deviation of the tool's acceleration signal with $n = 1000$ rpm, $f = 0.08 \frac{\text{mm}}{\text{rev}}$, and $d = 35$ mm

Depth of cut	**1mm**	**1.5mm**	**2mm**	**2.5mm**	**3mm**	**3.5mm**	**4mm**
Percentage reduction of σ_a(vibration amplitude)	6.67%	14.81%	0	29.03%	64.66%	74.46%	82.49%

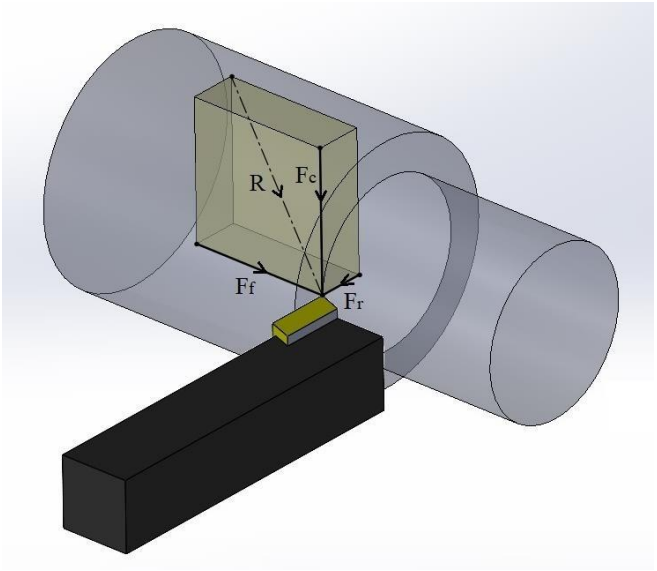

Fig. 1. Schematic of the straight turning process, F_c, F_f, F_r, and R are cutting, feed, radial, and resultant forces, respectively [23].

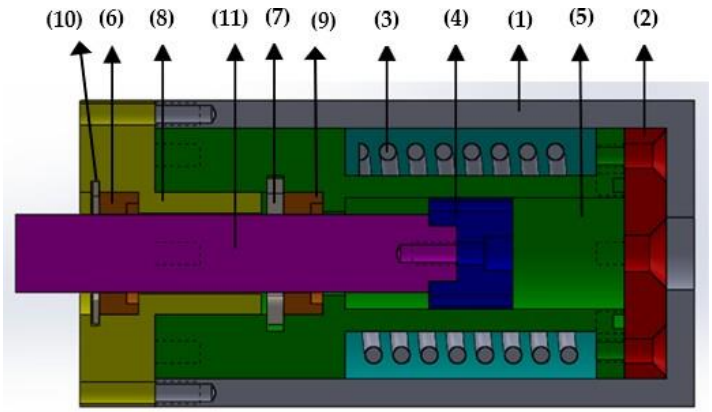

(a)

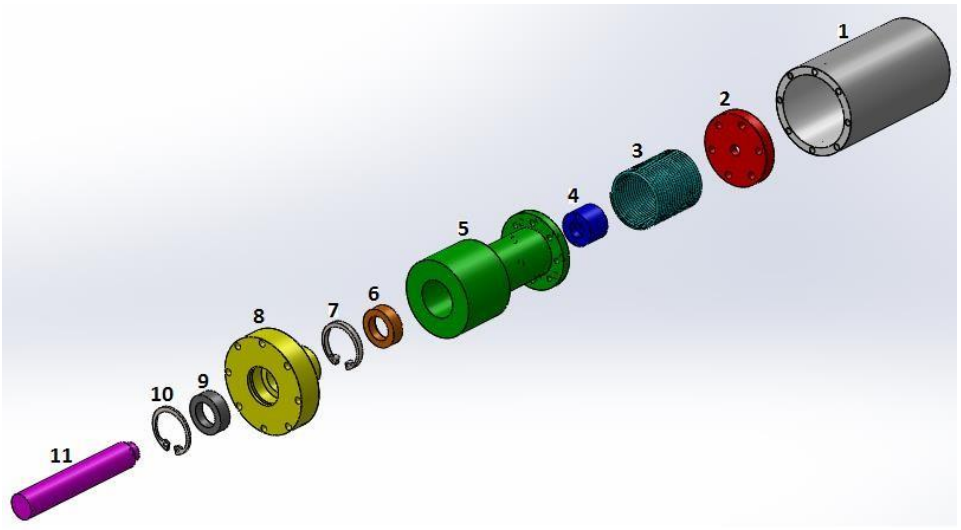

(b)

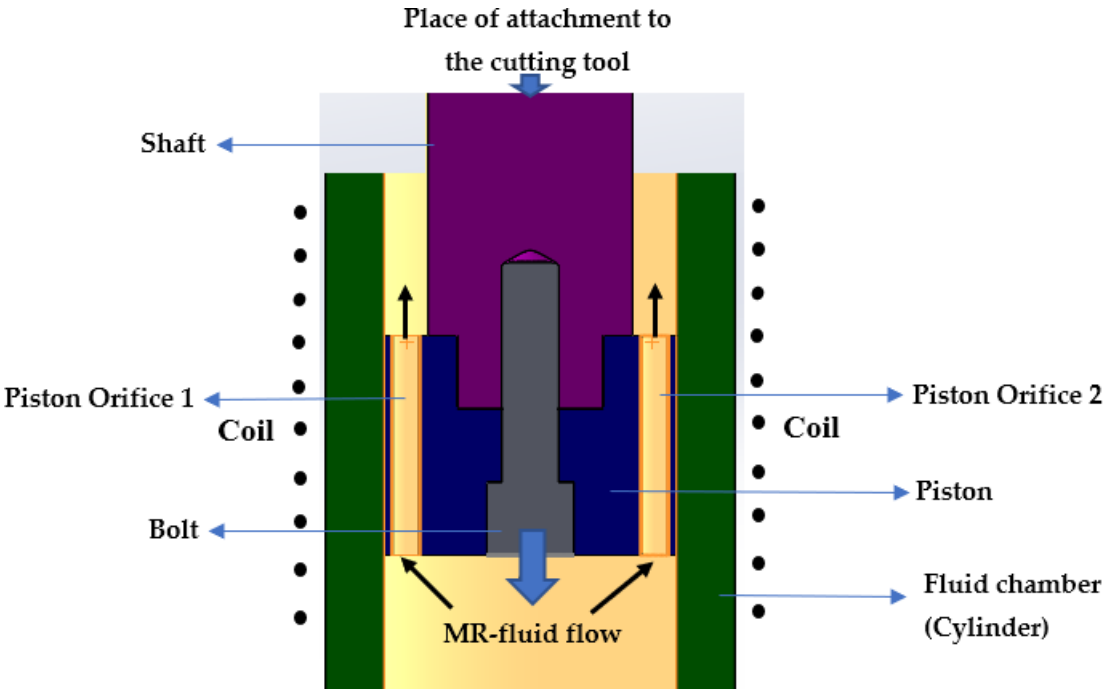

(c)

Fig. 2. (a) 2D assembly view and (b) 3D explosive model of the designed damper with part number [23], (c) MR fluid flow through the piston orifices.

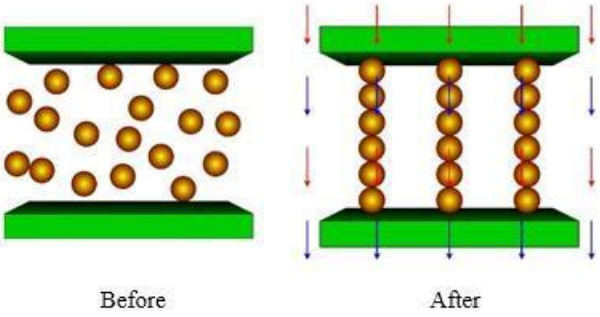

Fig. 3. Schematic of magnetic fluid suspension before and after application of magnetic field [27].

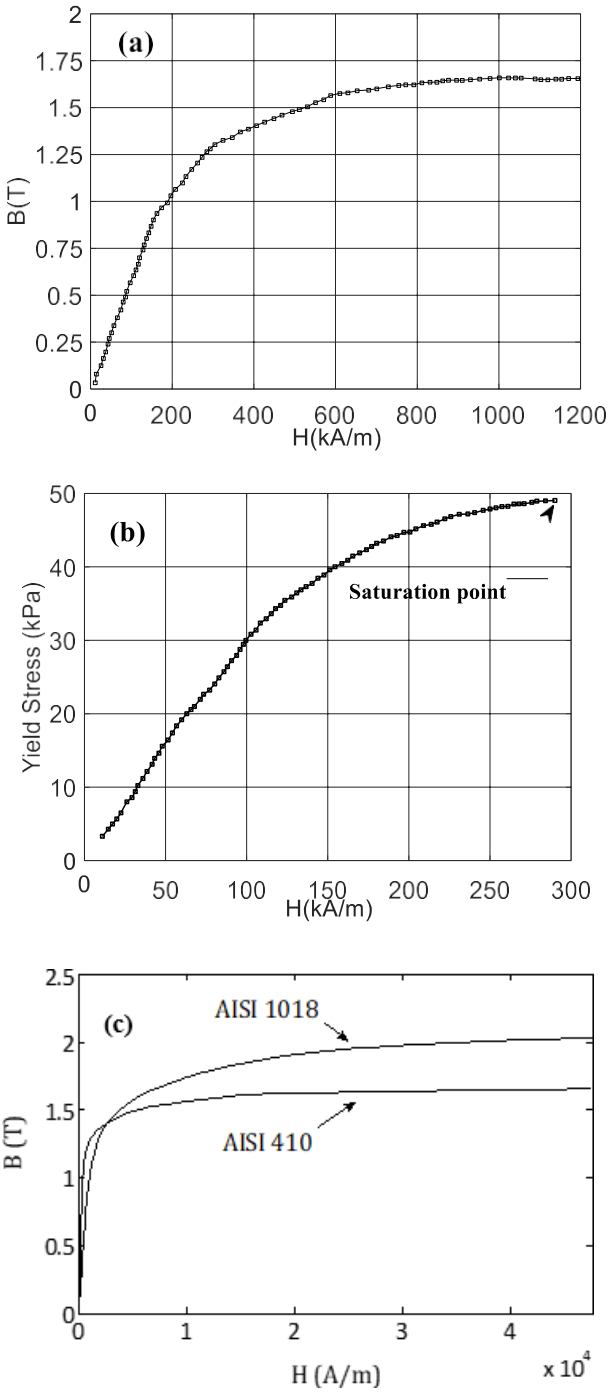

Fig. 4. (a) $B - H$ curve for MRF-132DG [29], **(b)** field-dependent yield stress for MRF-132DG [33], **(c)** $B - H$ curve for AISI 1018 and AISI 410 steels [34], [23].

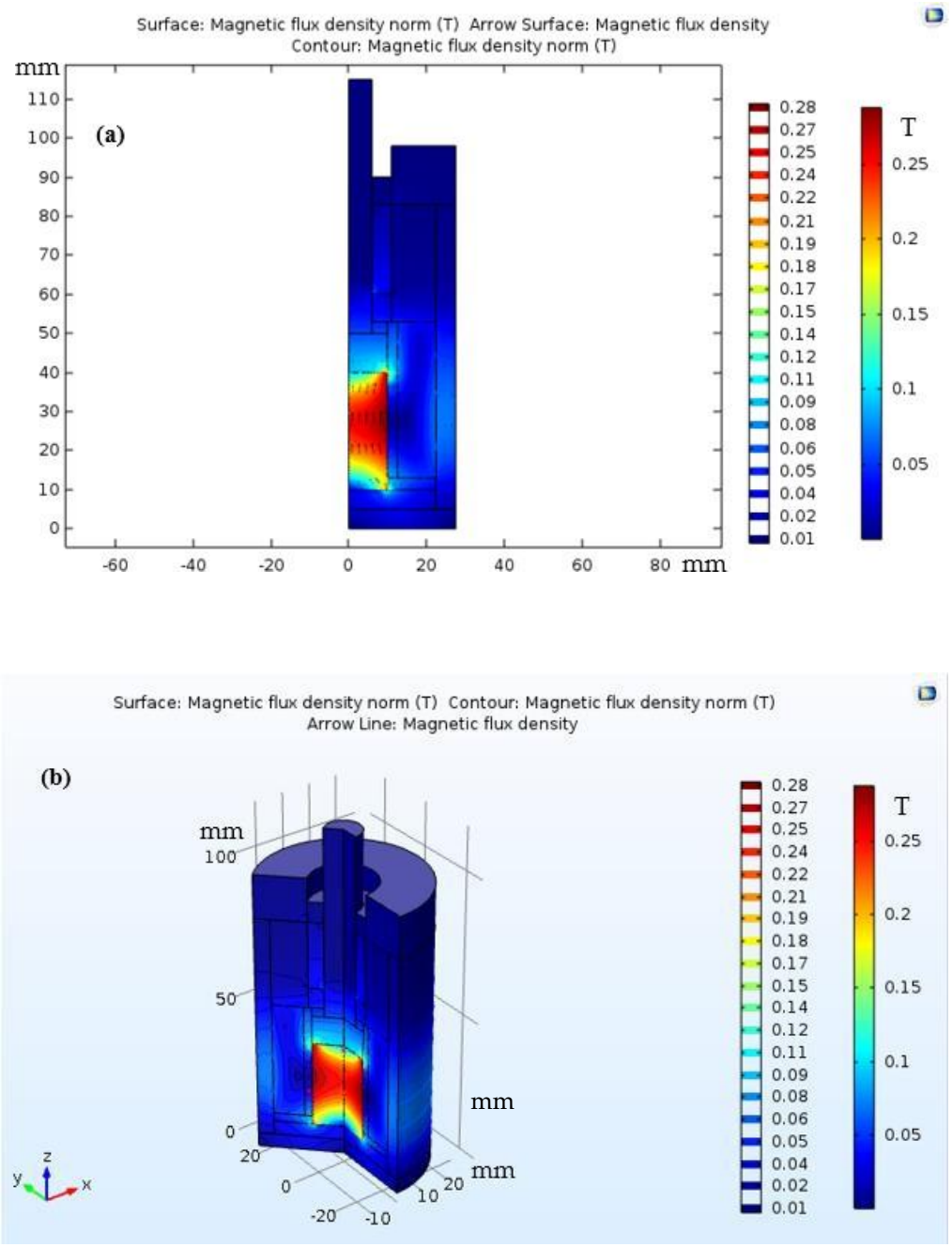

Fig. 5. Magnetic flux density distribution in the fluid chamber of the MR damper for AISI 410 **(a)** 2D view [23], **(b)** 3D view.

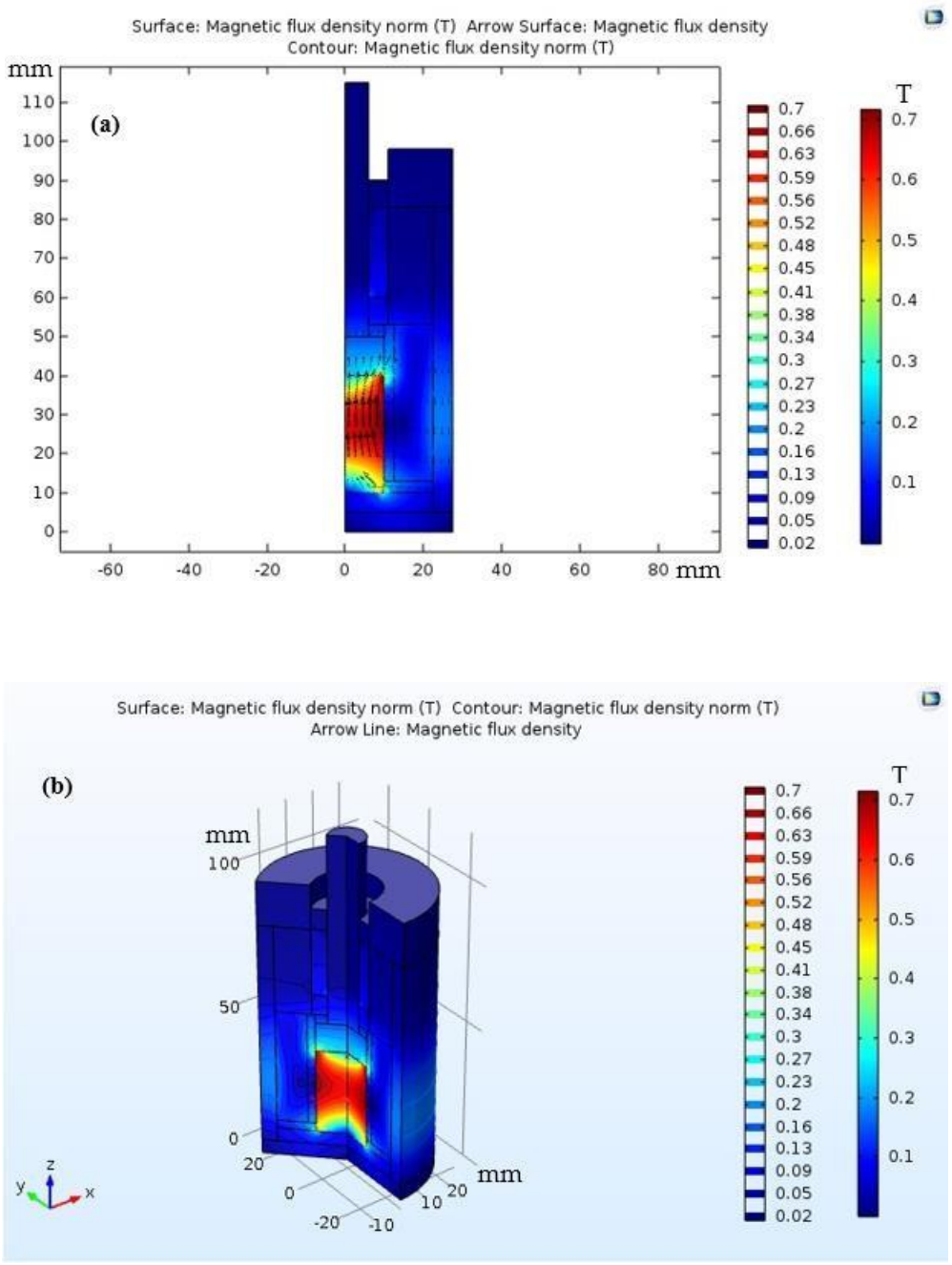

Fig. 6. Magnetic flux density distribution in the fluid chamber of the MR damper for AISI 1018 **(a)** 2D view [23], **(b)** 3D view.

(a)

(b)

(c)

Fig. 7. Experimental setup including the turning machine, workpiece, tool, modal test hammer, accelerometer, MR damper, and power supply.

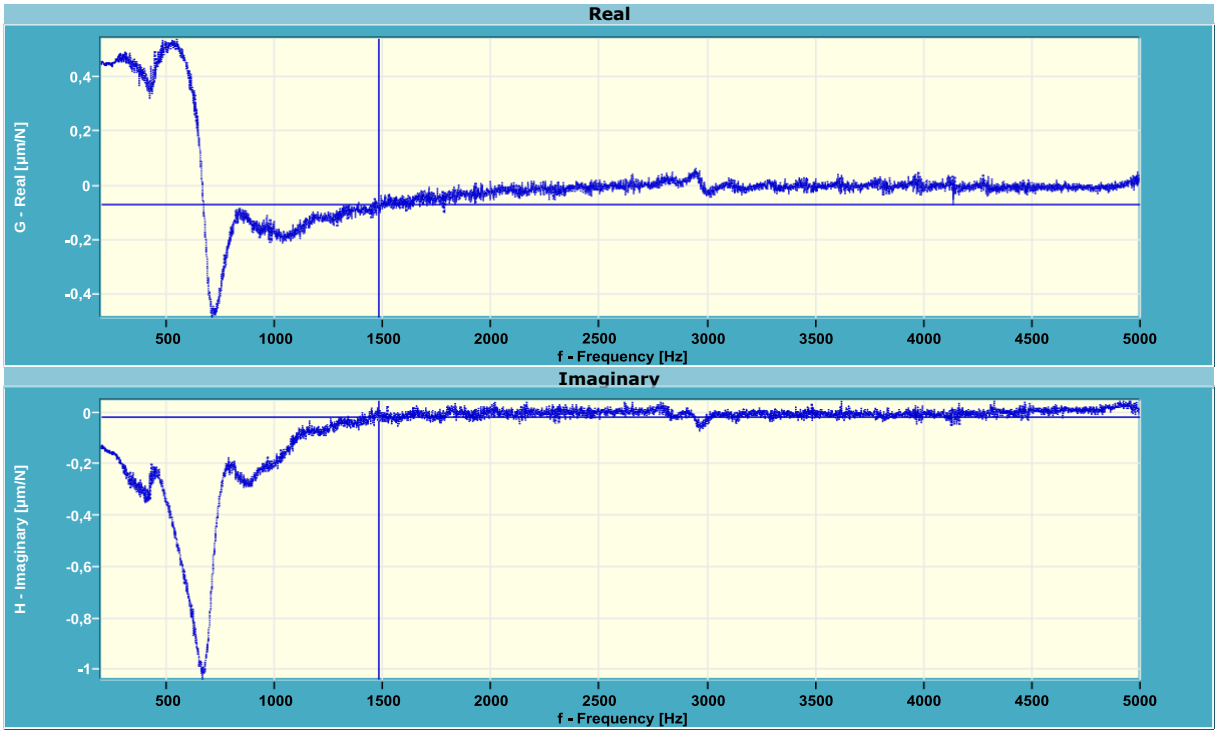

Fig. 8. The FRF obtained from the experimental modal analysis of the tool-damper structure with $d = 80$ mm.

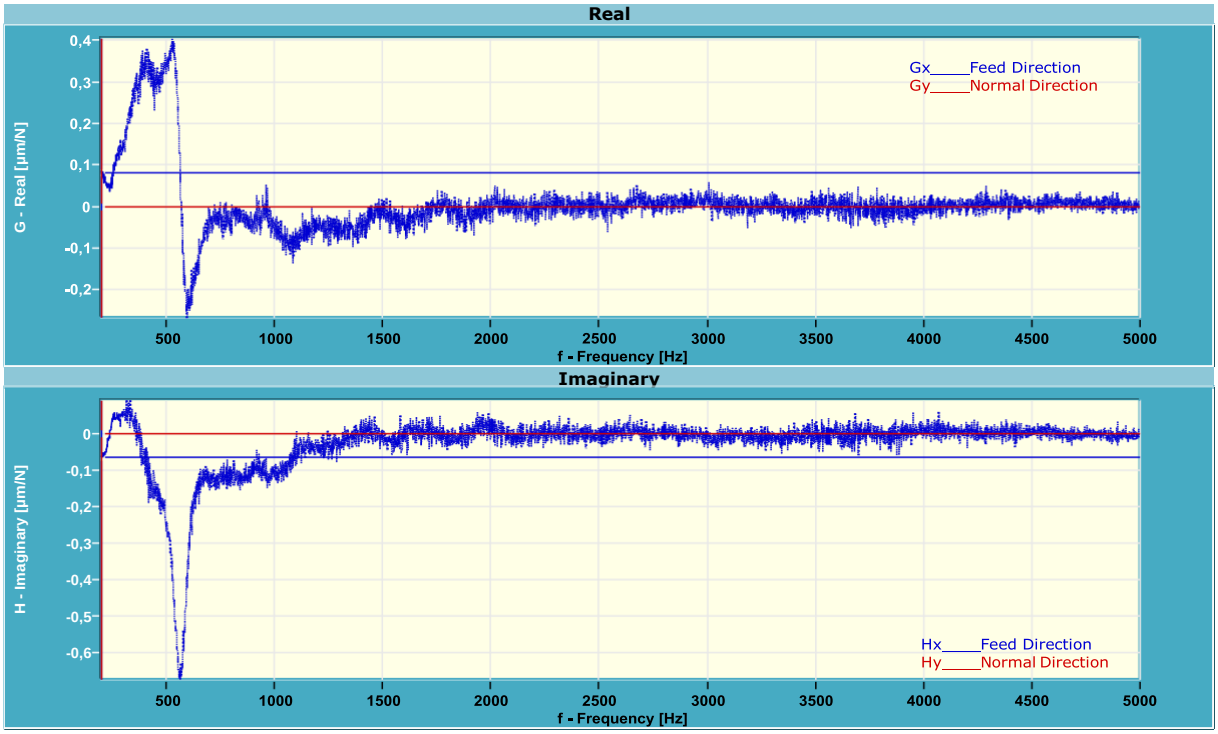

Fig. 9. The FRF obtained from the experimental modal analysis of the tool-damper structure with $d = 35$ mm.

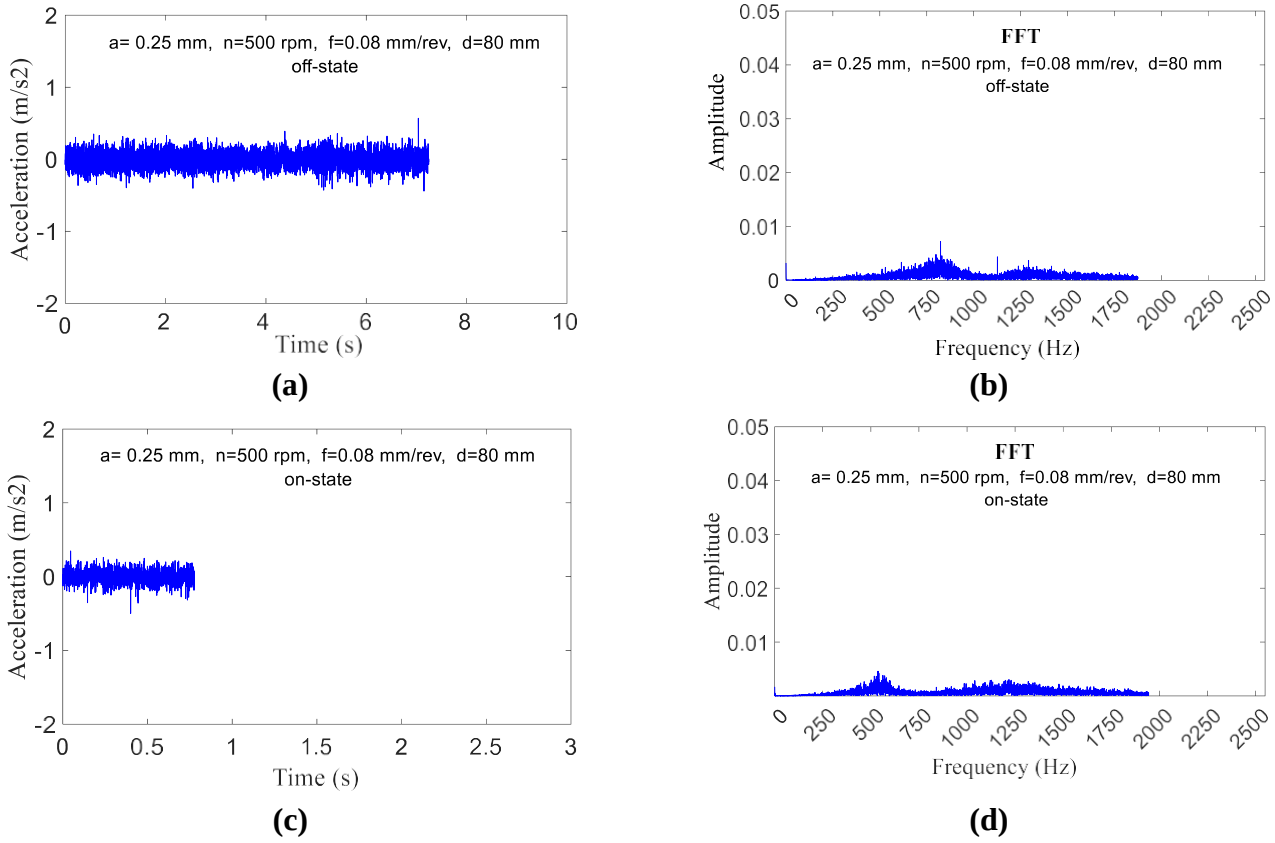

Fig. 10. Comparison of the tool acceleration signals and their corresponding FFT graphs obtained for two modes ” damper off” and “damper on”- (machining parameters a=0.25mm, n=500 rpm, f= 0.08 mm/rev, d=80 mm).

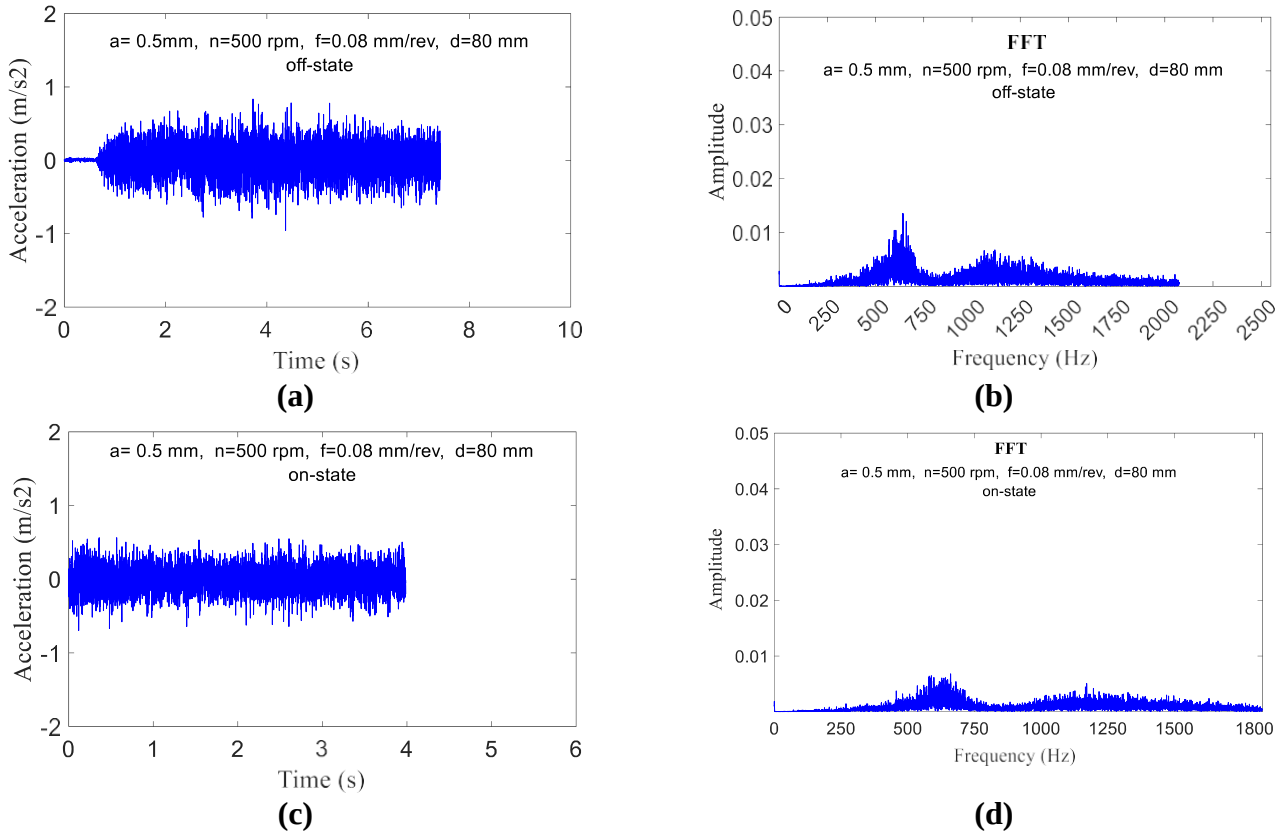

Fig. 11. Comparison of the tool acceleration signals and their corresponding FFT graphs obtained for two modes ” damper off” and “damper on”- (machining parameters a=0.5 mm, n=500 rpm, f= 0.08 mm/rev, d=80 mm).

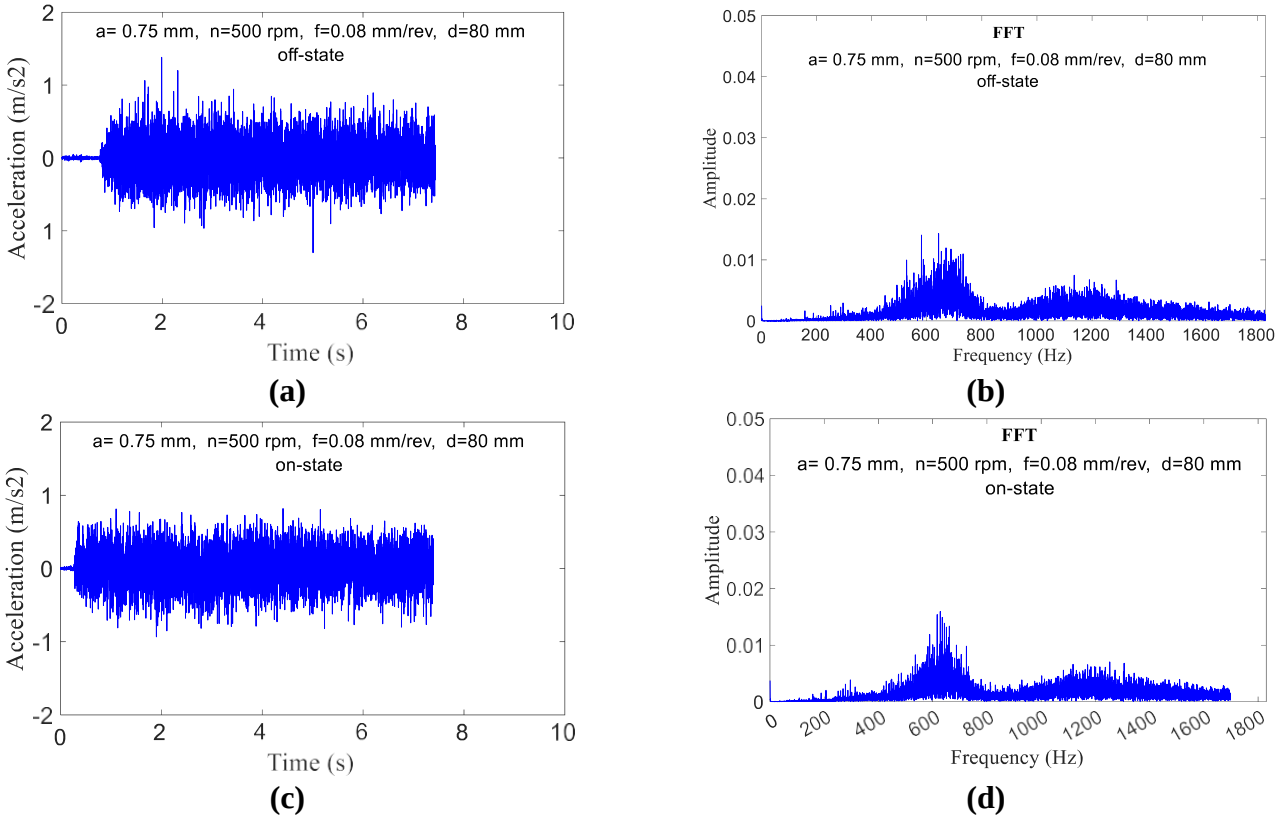

Fig. 12. Comparison of the tool acceleration signals and their corresponding FFT graphs obtained for two modes ” damper off” and “damper on”- (machining parameters a=0.75 mm, n=500 rpm, f= 0.08 mm/rev, d=80 mm).

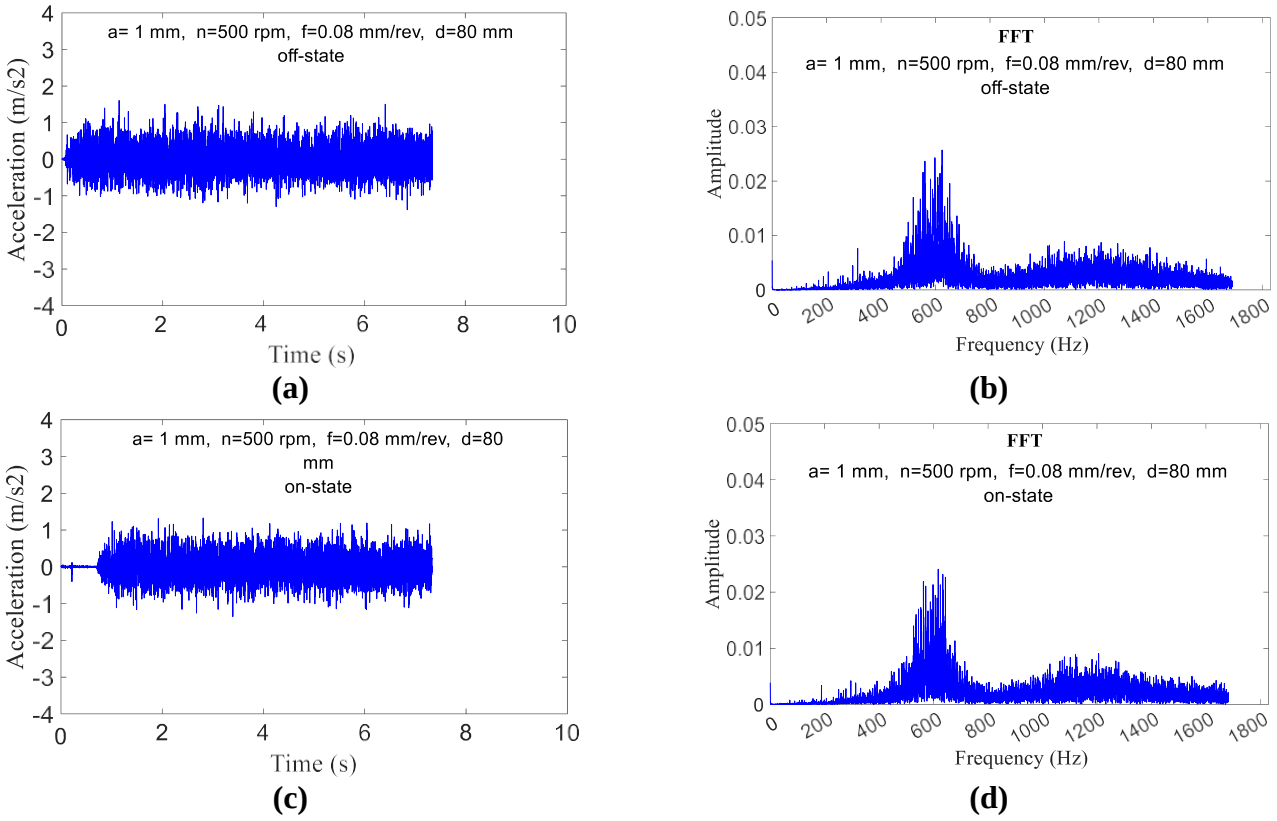

Fig. 13. Comparison of the tool acceleration signals and their corresponding FFT graphs obtained for two modes ” damper off” and “damper on”- (machining parameters a=1 mm, n=500 rpm, f= 0.08 mm/rev, d=80 mm).

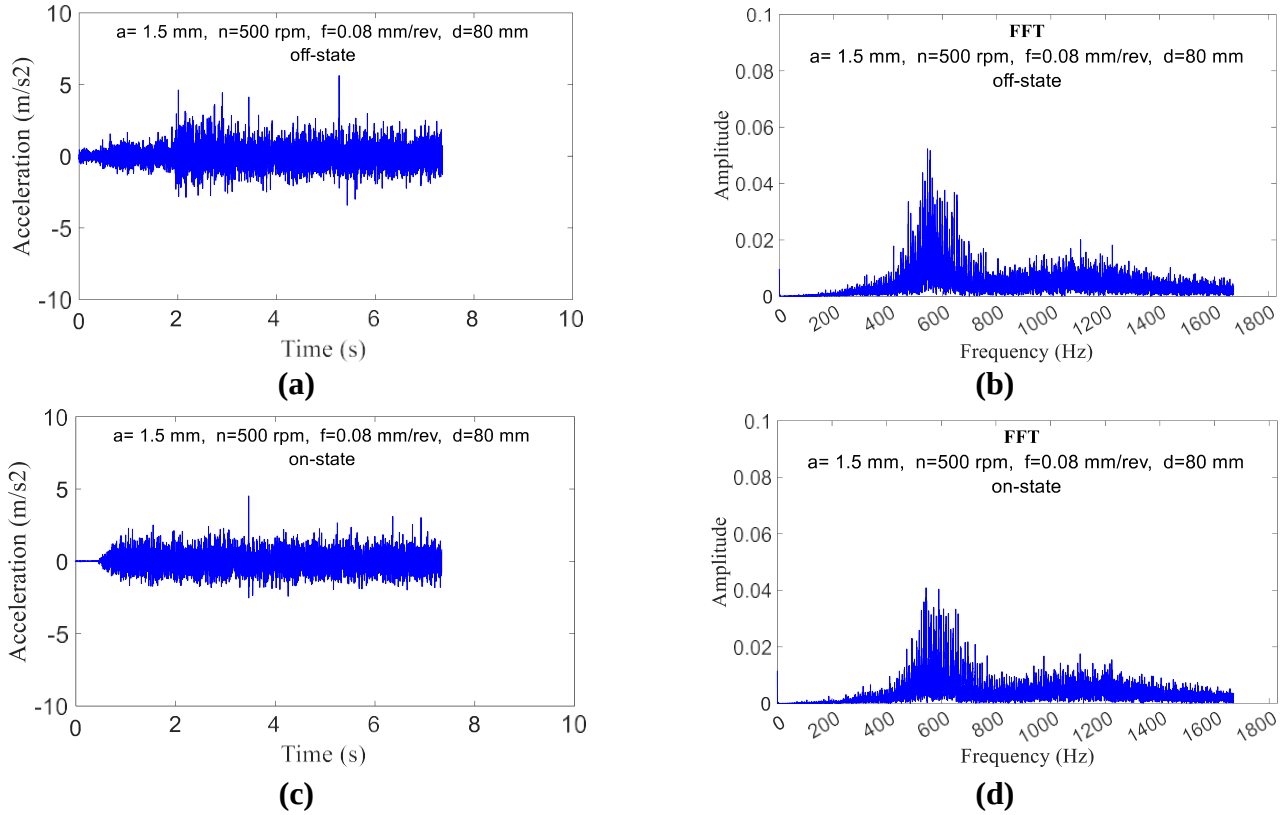

Fig. 14. Comparison of the tool acceleration signals and their corresponding FFT graphs obtained for two modes ” damper off” and “damper on”- (machining parameters a=1.5 mm, n=500 rpm, f= 0.08 mm/rev, d=80 mm).

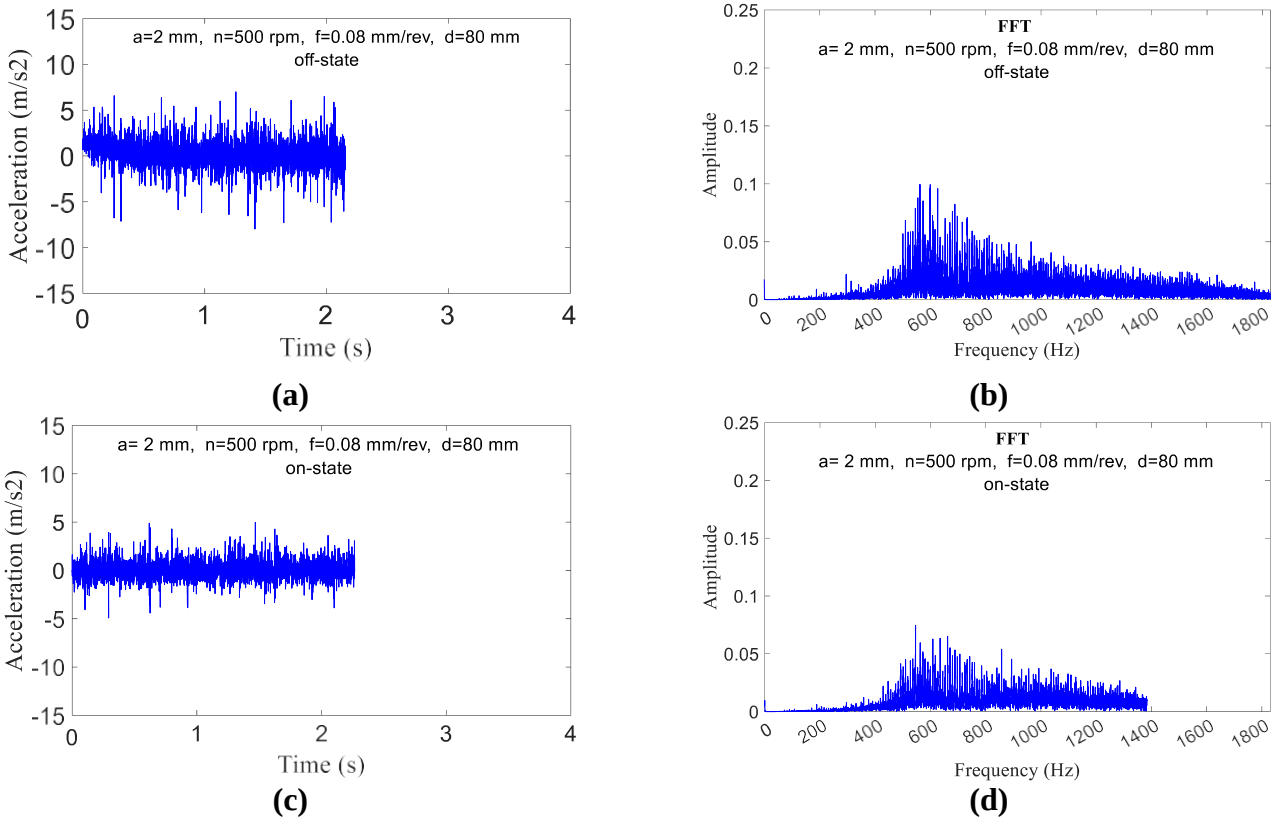

Fig. 15. Comparison of the tool acceleration signals and their corresponding FFT graphs obtained for two modes ” damper off” and “damper on”- (machining parameters a=2 mm, n=500 rpm, f= 0.08 mm/rev, d=80 mm).

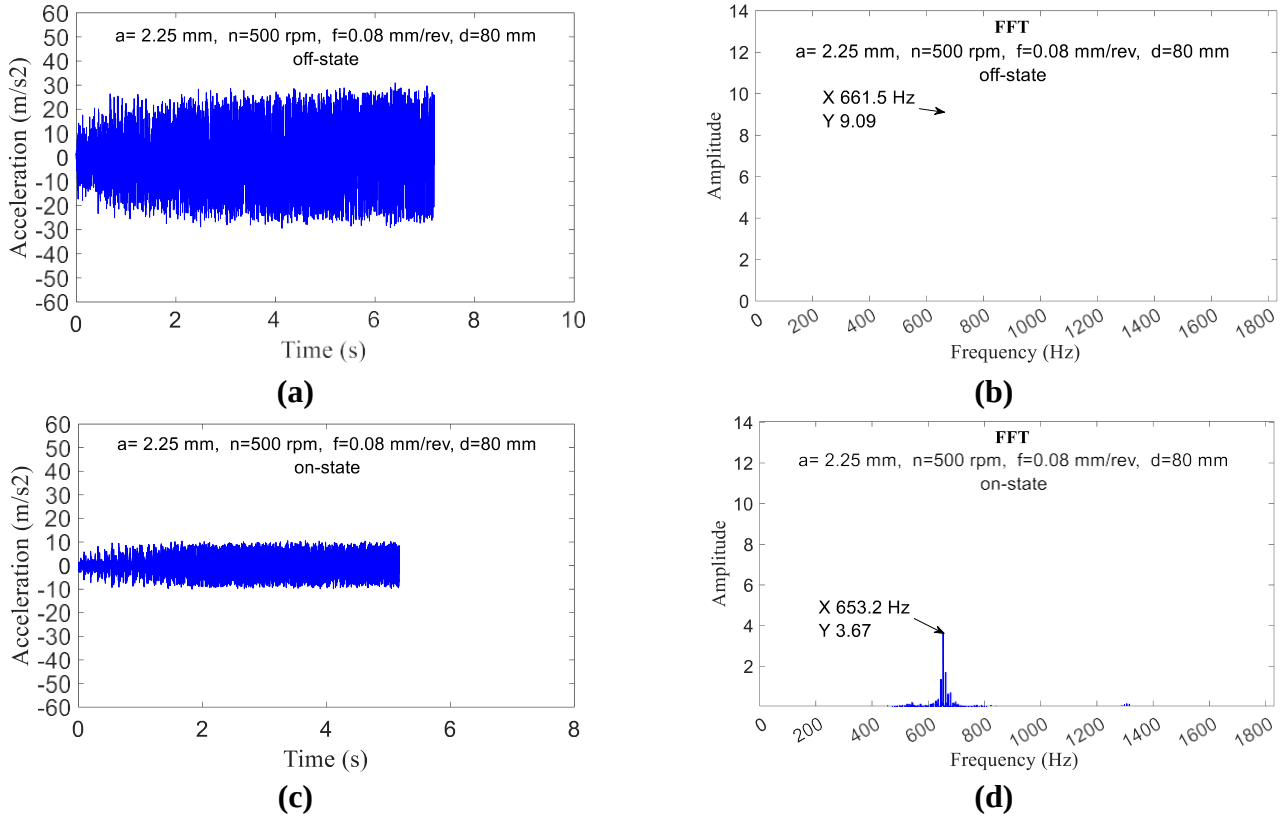

Fig. 16. Comparison of the tool acceleration signals and their corresponding FFT graphs obtained for two modes ” damper off” and “damper on”- (machining parameters a=2.25 mm, n=500 rpm, f= 0.08 mm/rev, d=80 mm).

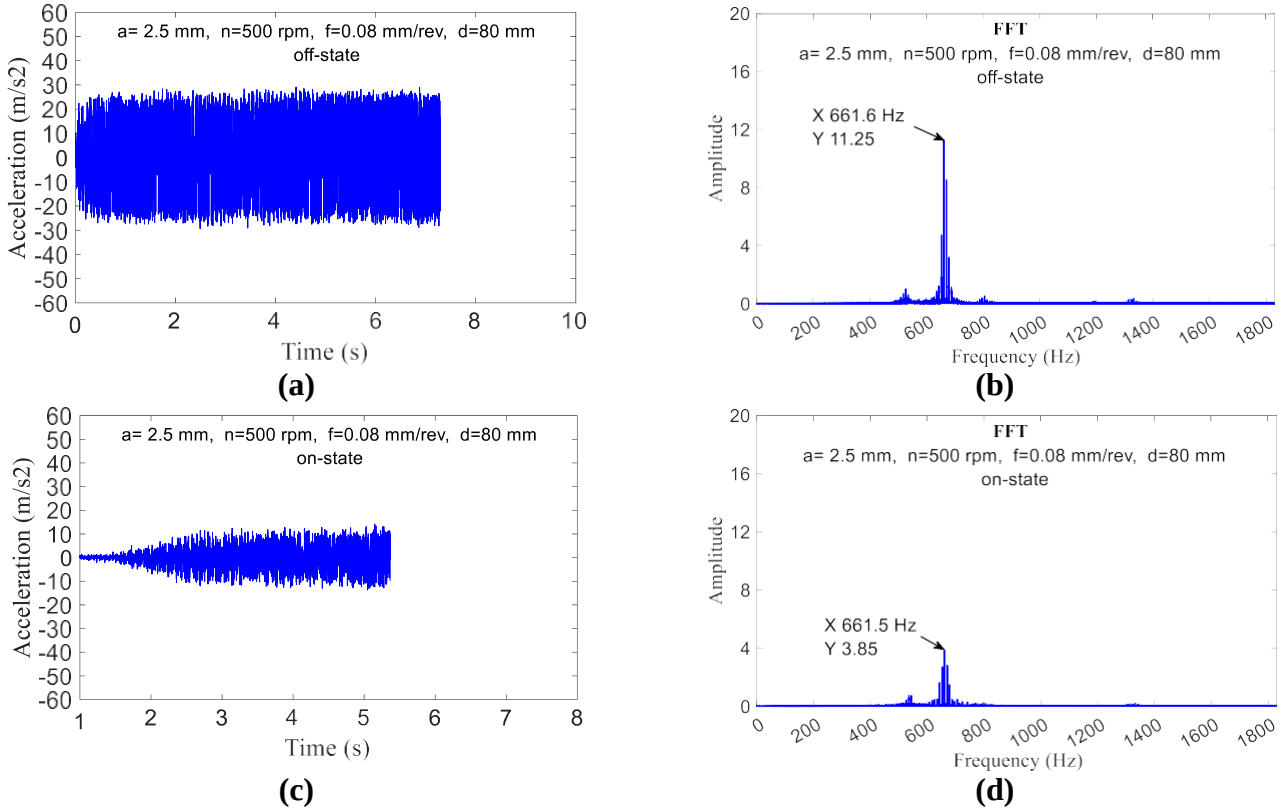

Fig. 17. Comparison of the tool acceleration signals and their corresponding FFT graphs obtained for two ” damper off” and “damper on”- (machining parameters a=2.5 mm, n=500 rpm, f= 0.08 mm/rev, d=80 mm).

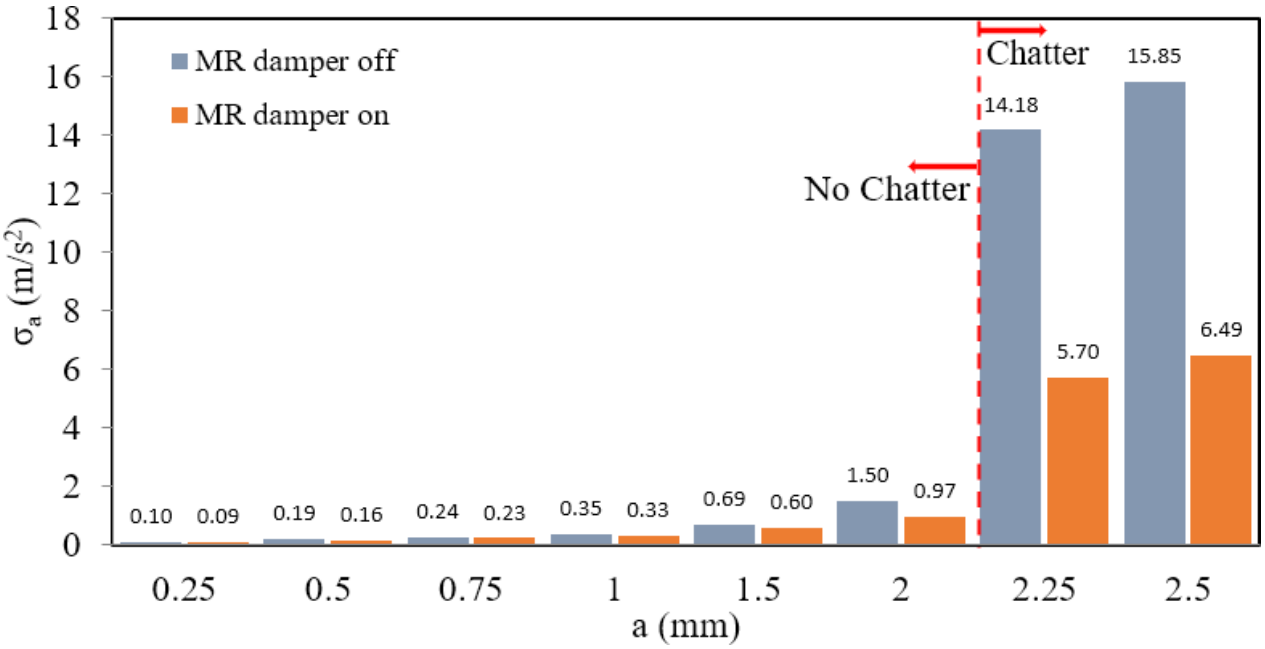

Fig. 18. Standard deviation values of the tool's acceleration data obtained from the machining test conducted with $n = 500$ rpm, $f = 0.08 \frac{\text{mm}}{\text{rev}}$, and $d = 80$ mm.

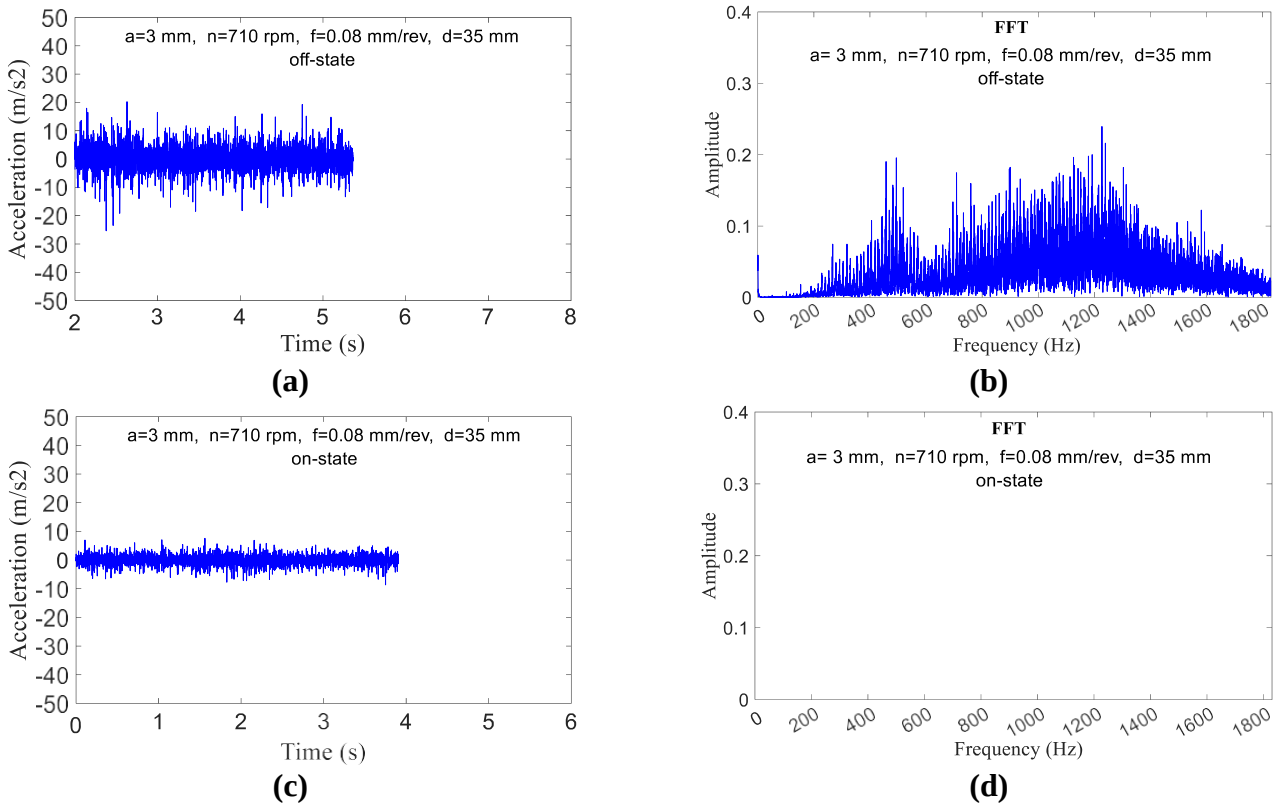

Fig. 19. Comparison of the tool acceleration signals and their corresponding FFT graphs obtained for two modes ”damper off” and “damper on”- (machining parameters a=3 mm, n=710 rpm, f= 0.08 mm/rev, d=35 mm).

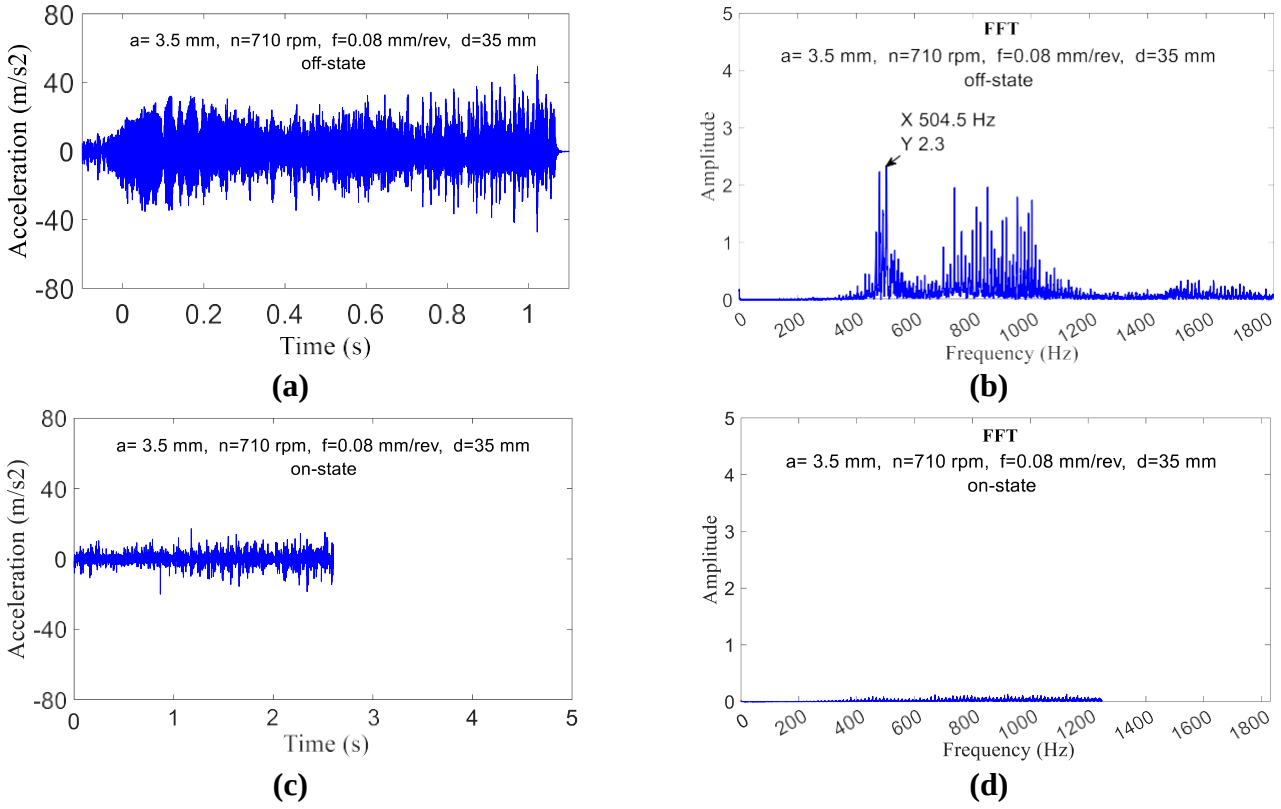

Fig. 20. Comparison of the tool acceleration signals and their corresponding FFT graphs obtained for two ”damper off” and “damper on”- (machining parameters a=3.5 mm, n=710 rpm, f= 0.08 mm/rev, d=35 mm).

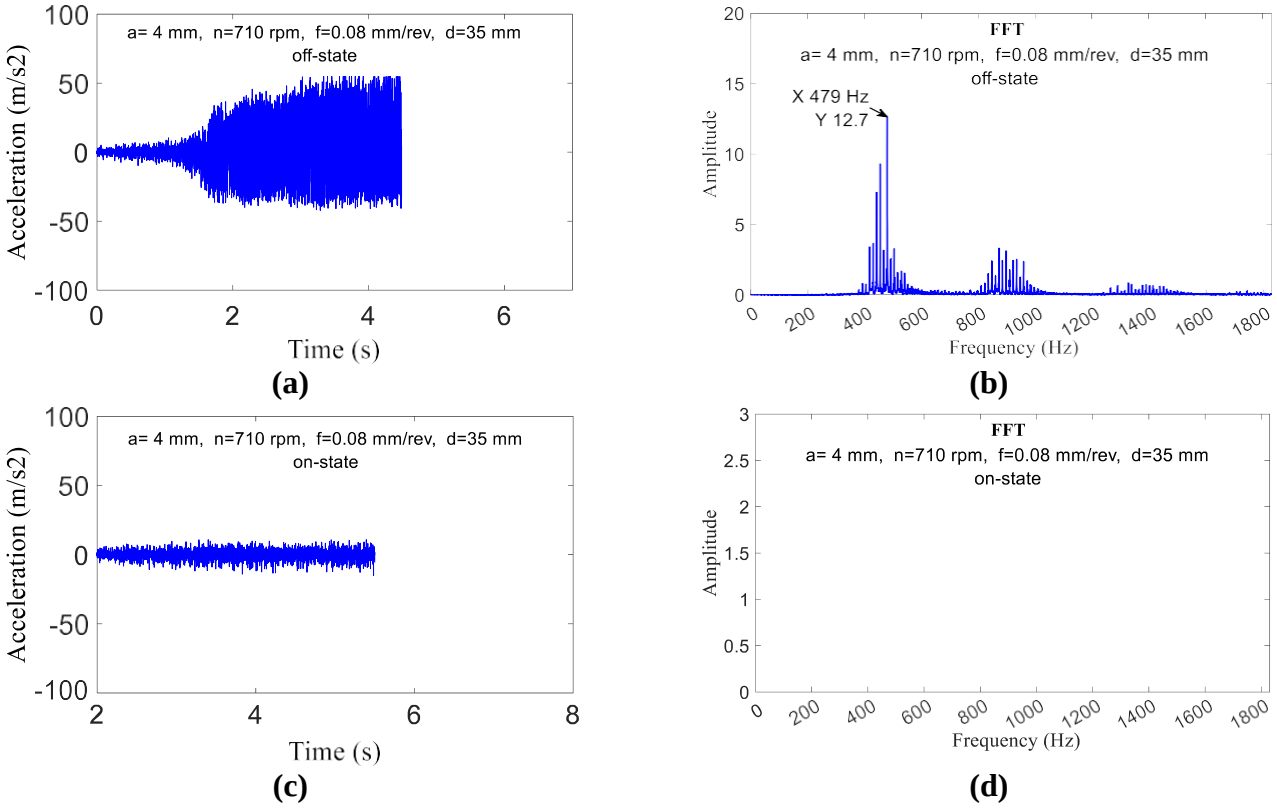

Fig. 21. Comparison of the tool acceleration signals and their corresponding FFT graphs obtained for two ”damper off” and “damper on”- (machining parameters a=4 mm, n=710 rpm, f= 0.08 mm/rev, d=35 mm).

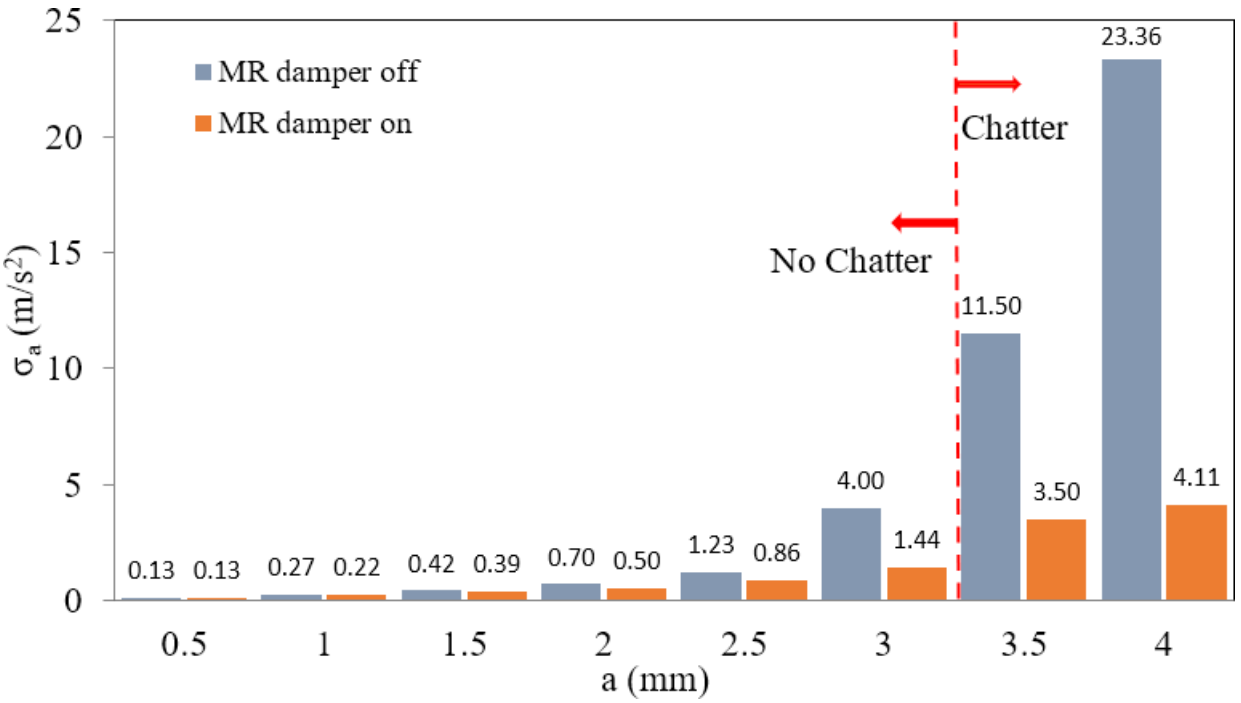

Fig. 22. Standard deviation values of the acceleration data obtained from the machining test conducted with $n = 710$ rpm, $f = 0.08 \frac{\text{mm}}{\text{rev}}$, and $d = 35$ mm.

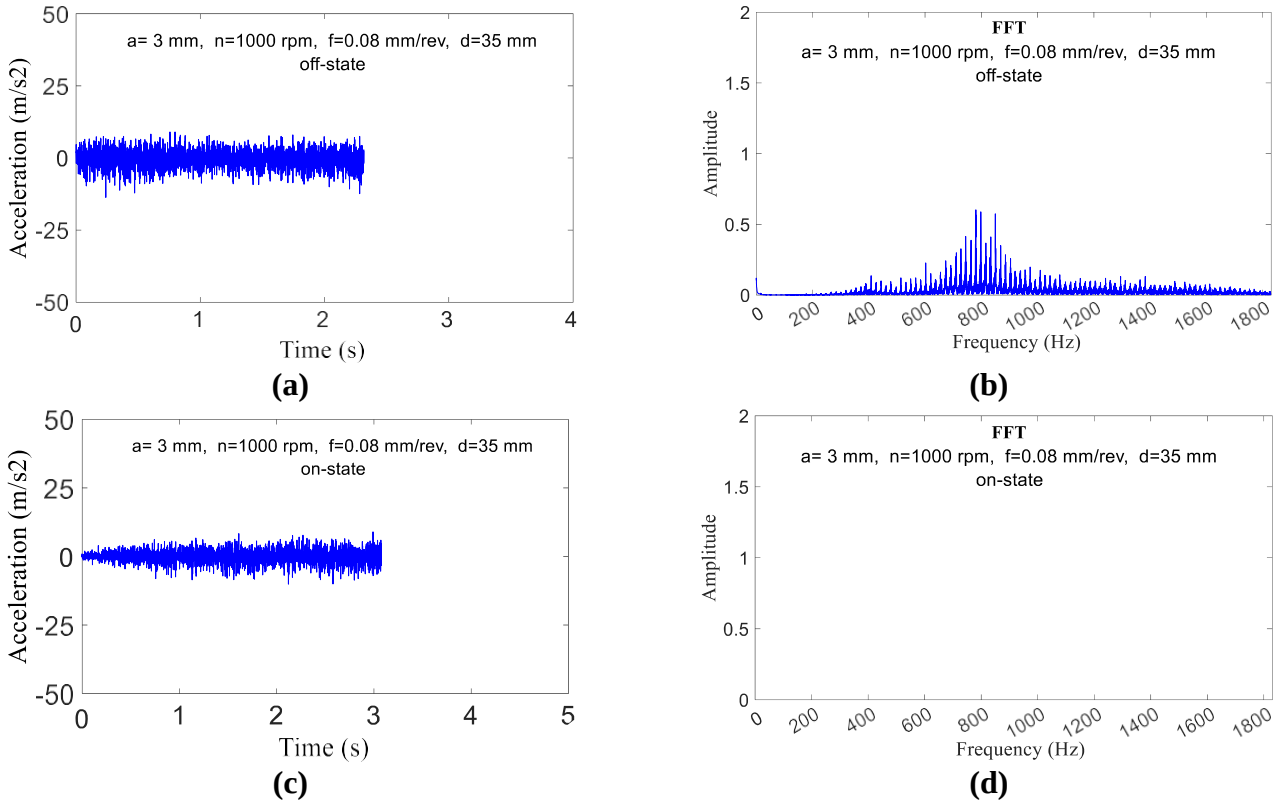

Fig. 23. Comparison of the tool acceleration signals and their corresponding FFT graphs obtained for two modes ”damper off” and “damper on”- (machining parameters a=3 mm, n=1000 rpm, f= 0.08 mm/rev, d=35 mm).

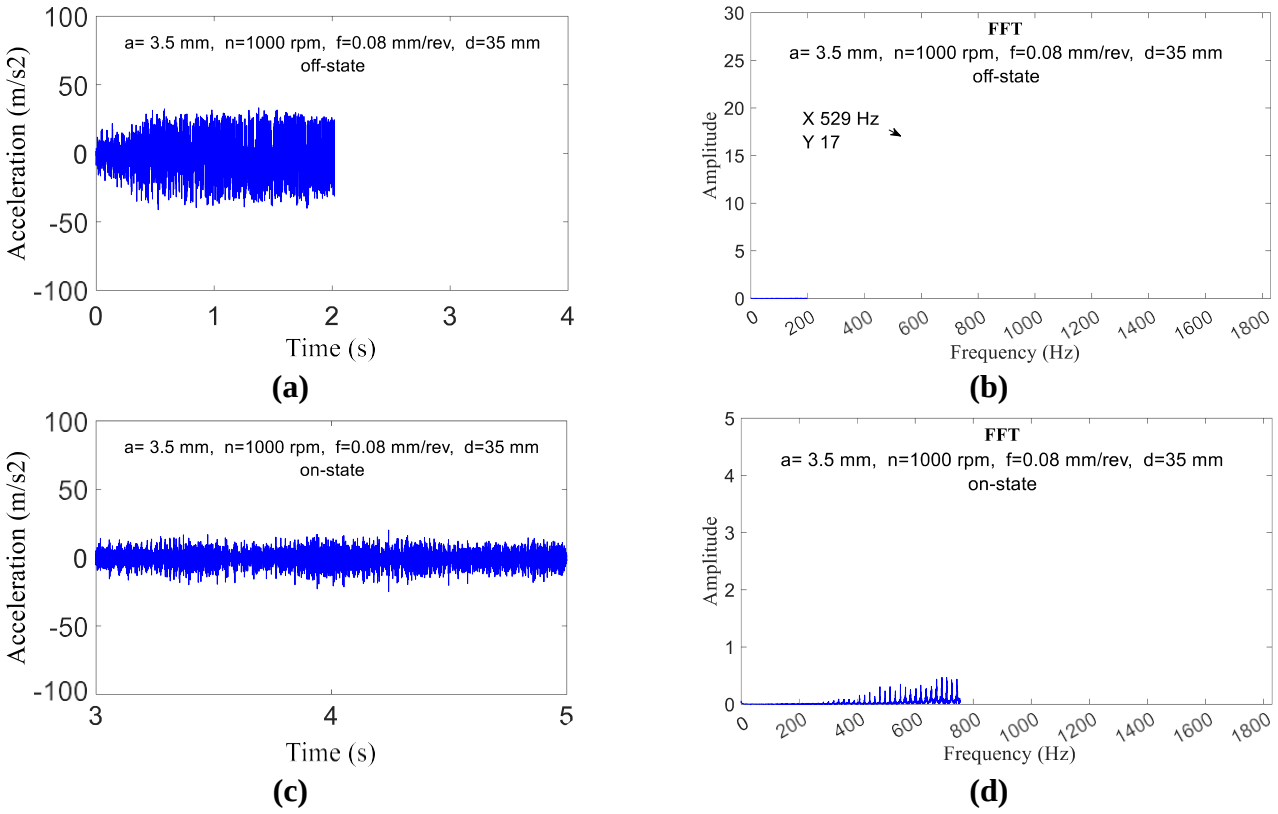

Fig. 24. Comparison of the tool acceleration signals and their corresponding FFT graphs obtained for two modes ”damper off” and “damper on”- (machining parameters a=3.5 mm, n=1000 rpm, f= 0.08 mm/rev, d=35 mm).

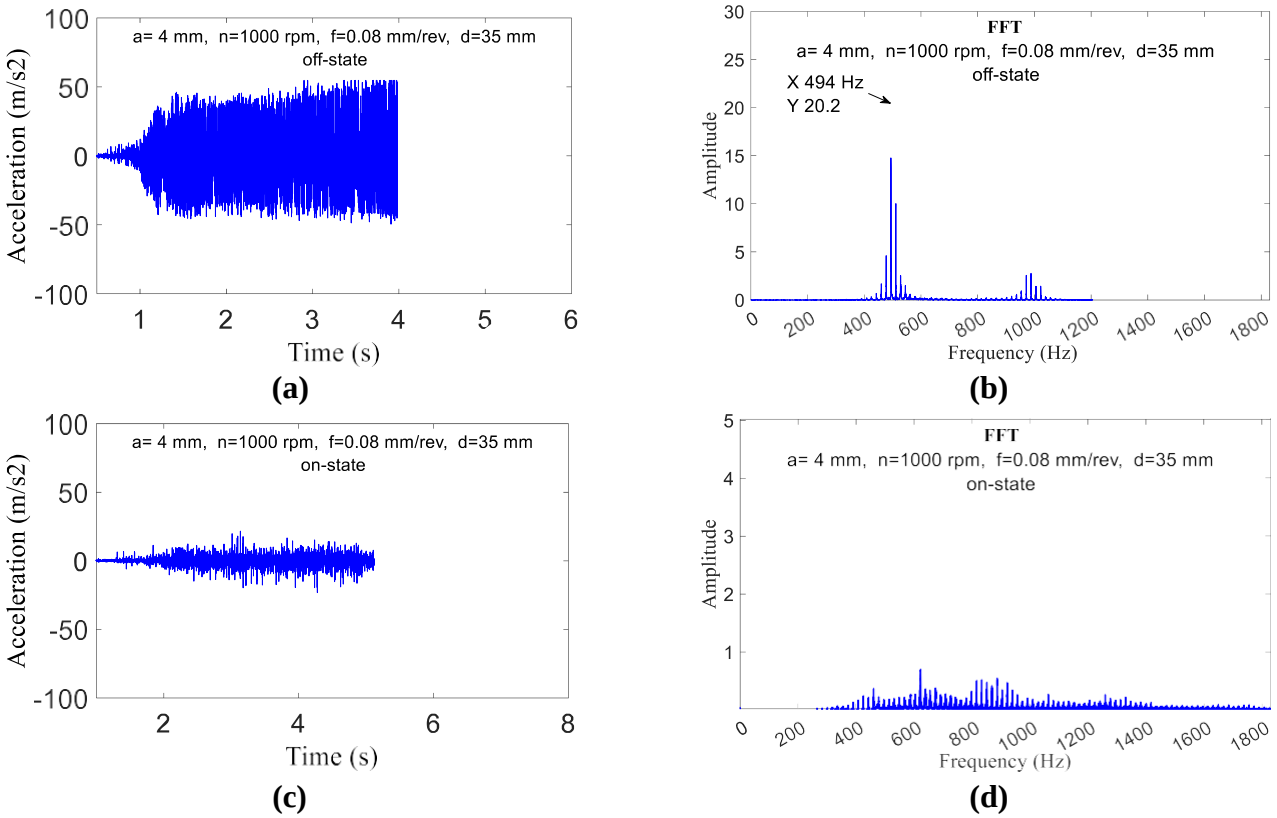

Fig. 25. Comparison of the tool acceleration signals and their corresponding FFT graphs obtained for two modes ”damper off” and “damper on”- (machining parameters a=4 mm, n=1000 rpm, f= 0.08 mm/rev, d=35 mm).

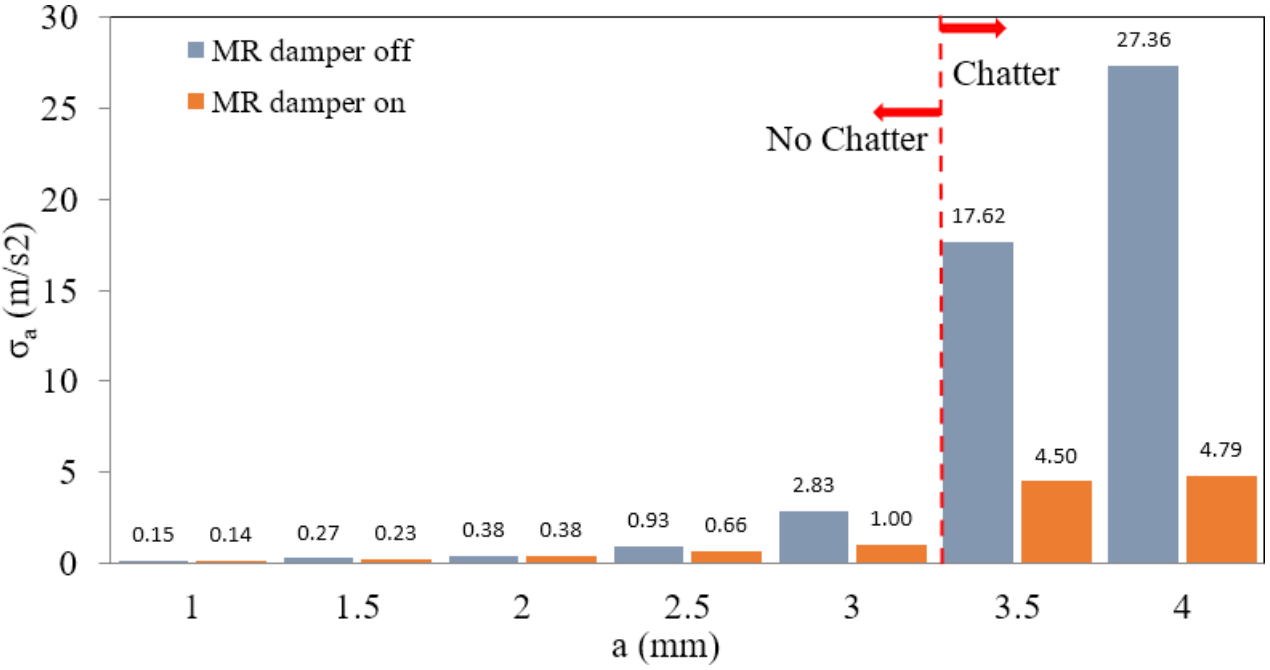

Fig. 26. STDV values of acceleration data obtained from the machining test conducted with $n = 1000$ rpm, $f = 0.08 \frac{\text{mm}}{\text{rev}}$, and $d = 35$ mm.

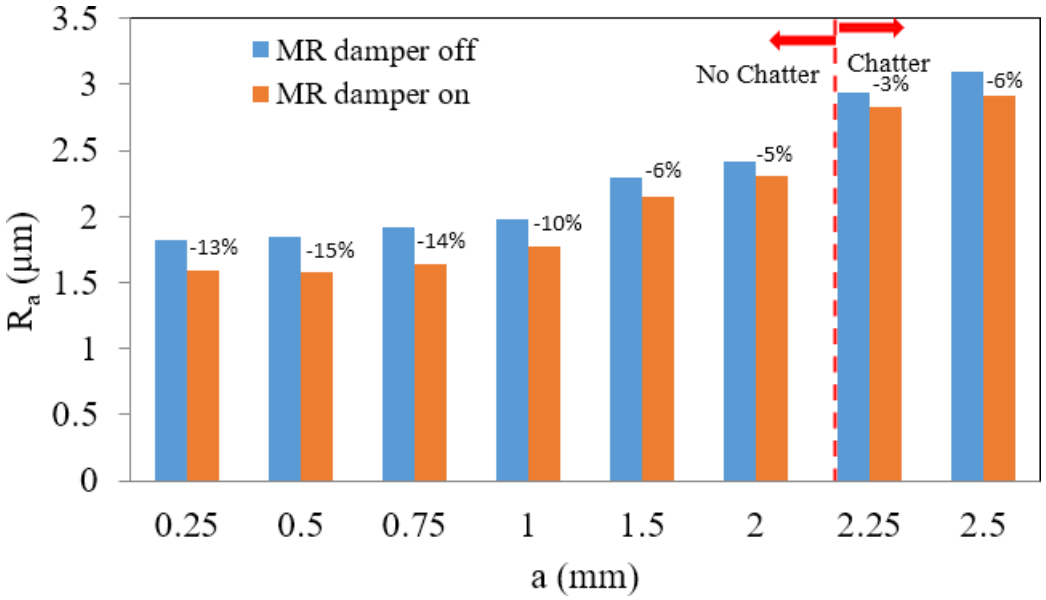

Fig. 27. Work Surface roughness values Ra obtained from the machining test conducted with $n = 500$ rpm, $f = 0.08 \frac{\text{mm}}{\text{rev}}$, and $d = 80$ mm.

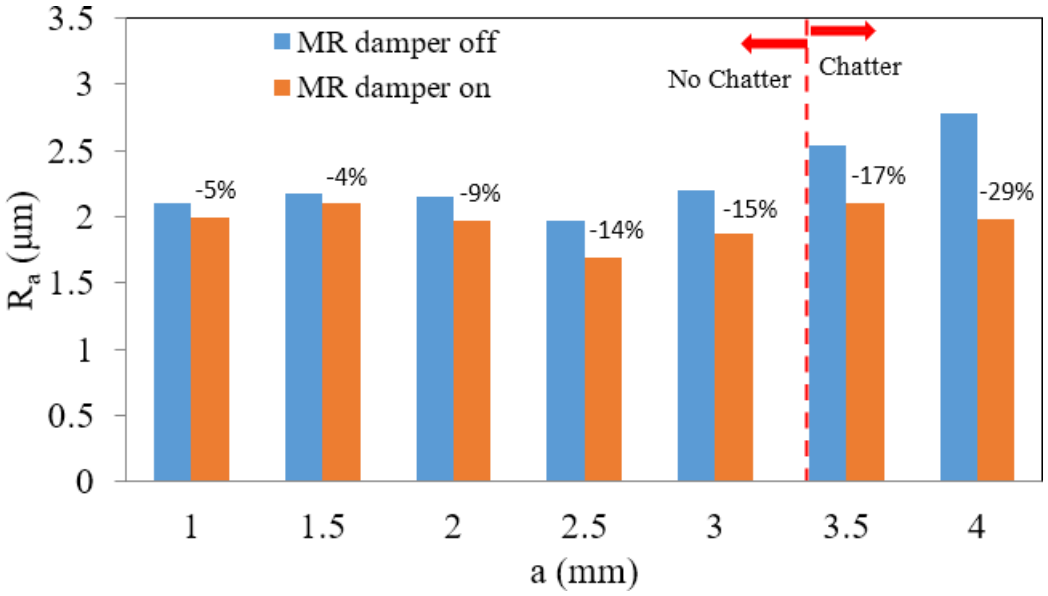

Fig. 28. Work Surface roughness values Ra obtained from the machining test conducted with $n = 1000$ rpm, $f = 0.08 \frac{\text{mm}}{\text{rev}}$, and $d = 35$ mm.

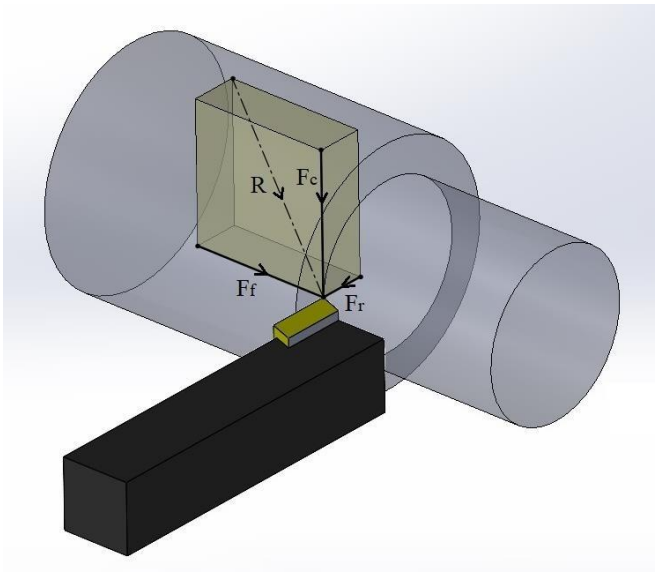

Fig. 1. Schematic of the straight turning process, F_c, F_f, F_r, and R are cutting, feed, radial, and resultant forces, respectively [23].

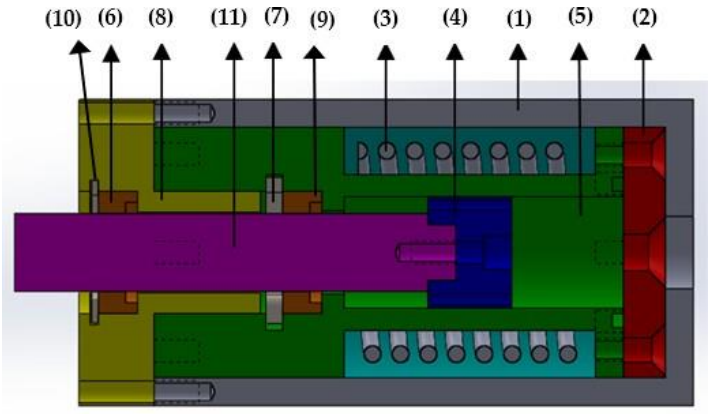

(a)

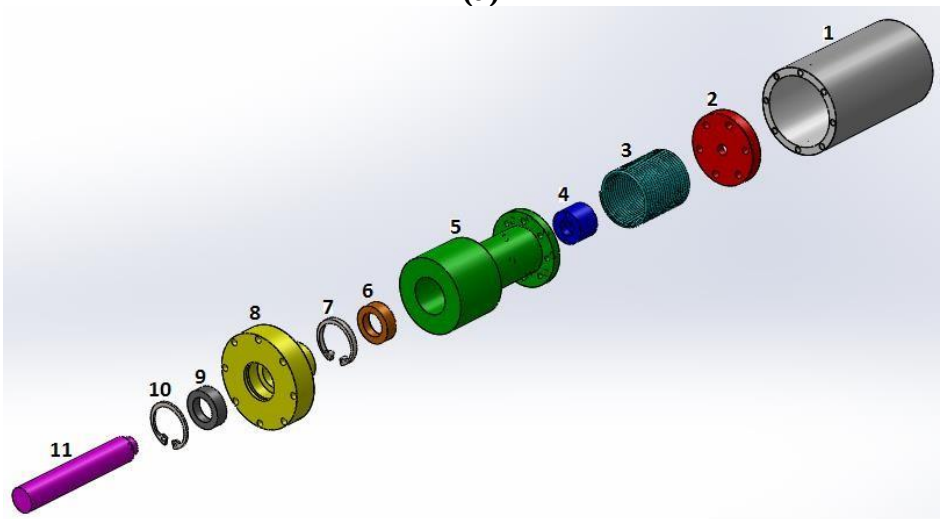

(b)

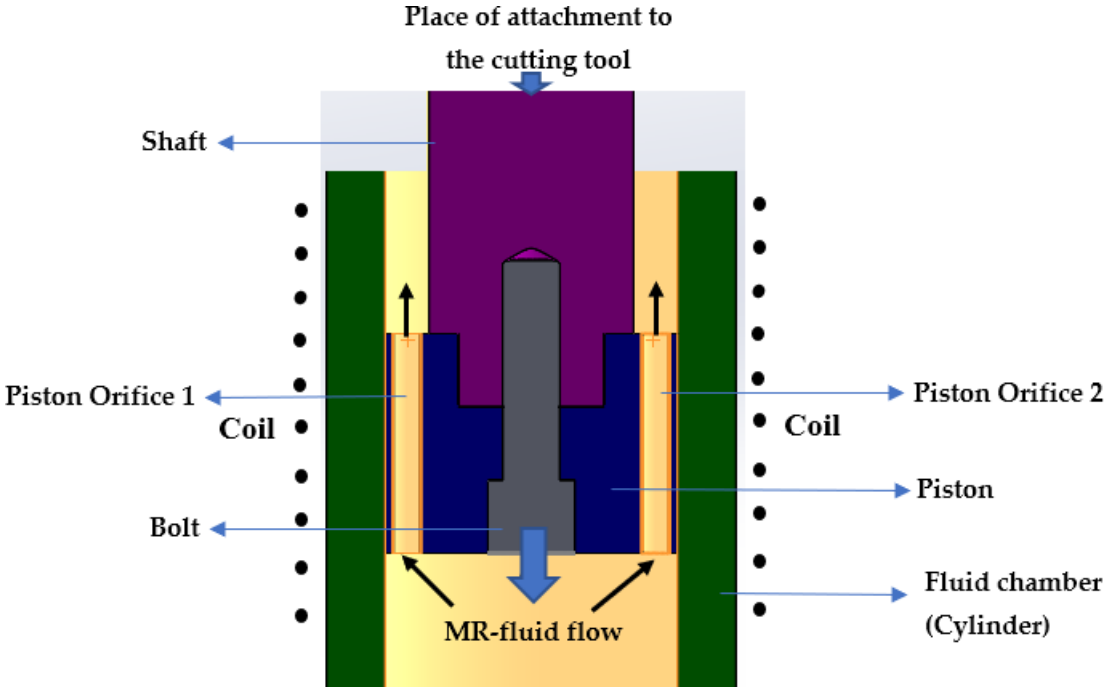

(c)

Fig. 2. (a) 2D assembly view and (b) 3D explosive model of the designed damper with part number [23], (c) MR fluid flow through the piston orifices.

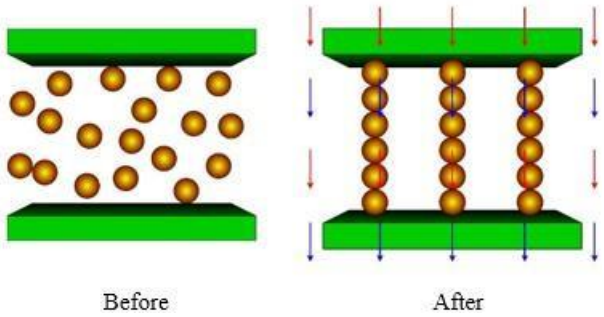

Fig. 3. Schematic of magnetic fluid suspension before and after application of magnetic field [27].

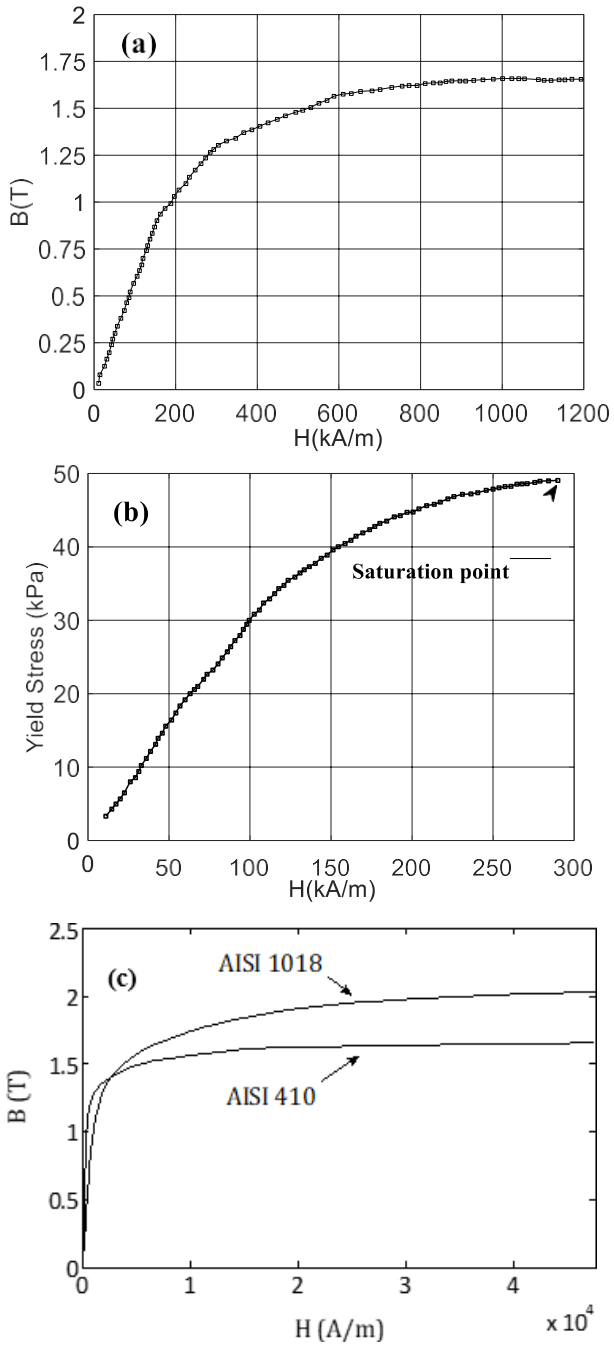

Fig. 4. (a) $B-H$ curve for MRF-132DG [29], **(b)** field-dependent yield stress for MRF-132DG [33], **(c)** $B-H$ curve for AISI 1018 and AISI 410 steels [34], [23].

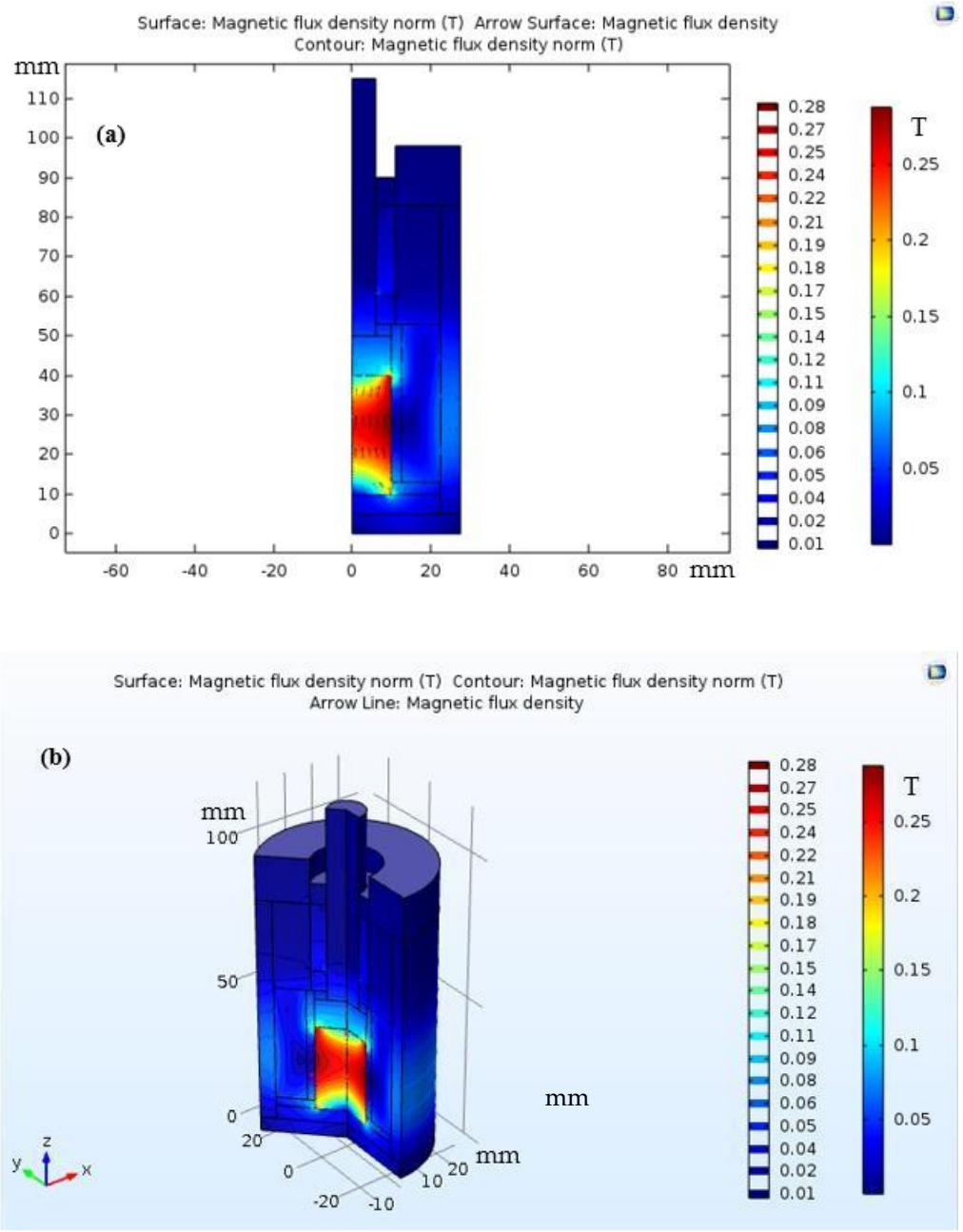

Fig. 5. Magnetic flux density distribution in the fluid chamber of the MR damper for AISI 410 **(a)** 2D view [23], **(b)** 3D view.

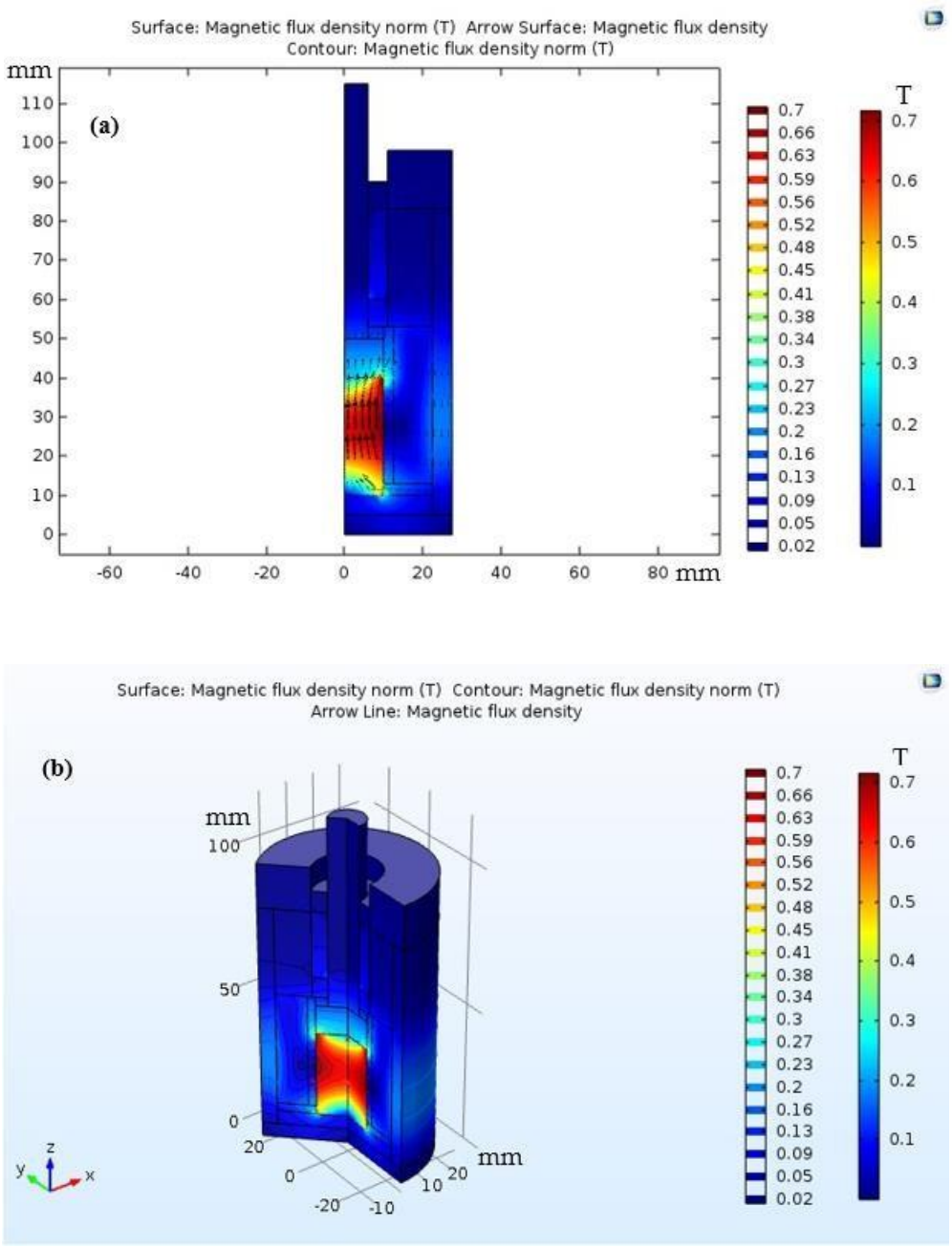

Fig. 6. Magnetic flux density distribution in the fluid chamber of the MR damper for AISI 1018 **(a)** 2D view [23], **(b)** 3D view.

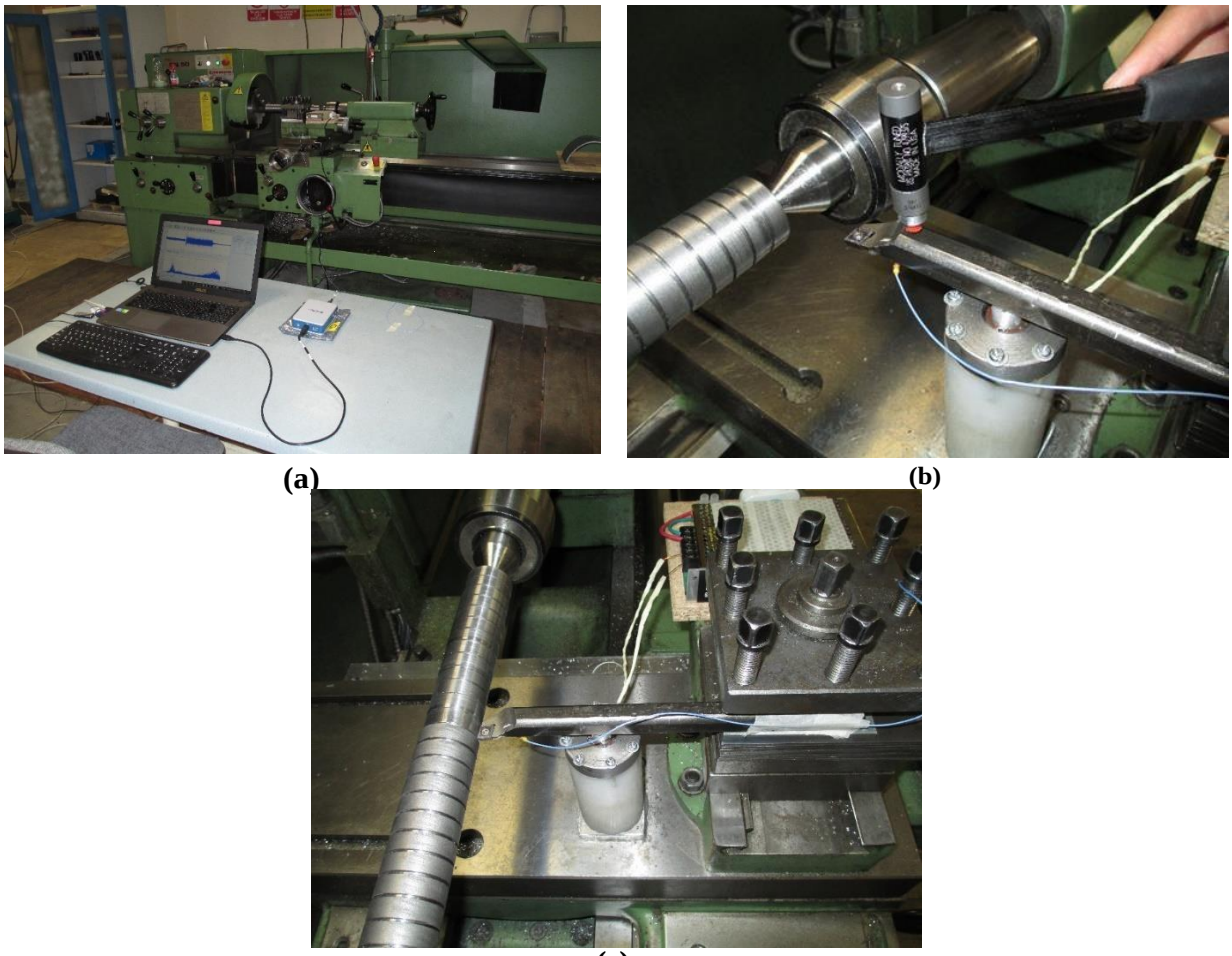

Fig. 7. Experimental setup including the turning machine, workpiece, tool, modal test hammer, accelerometer, MR damper, and power supply.

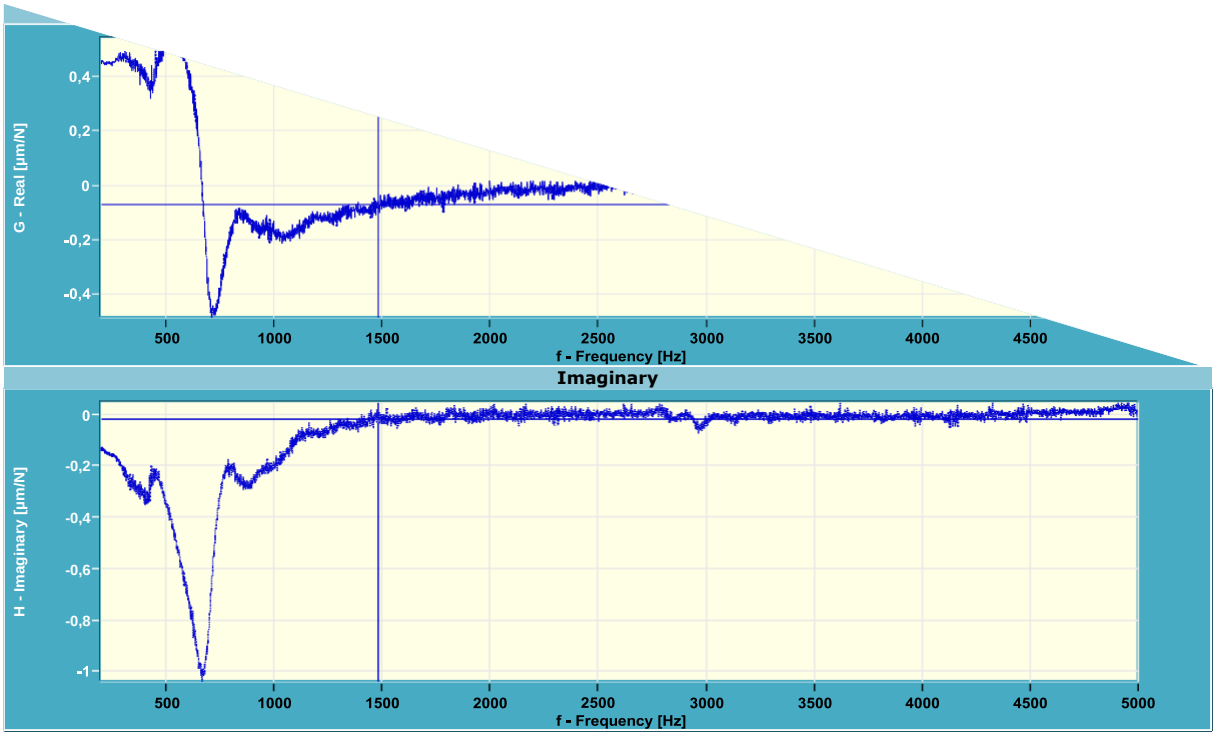

Fig. 8. The FRF obtained from the experimental modal analysis of the tool-damper structure with $d = 80$ mm.

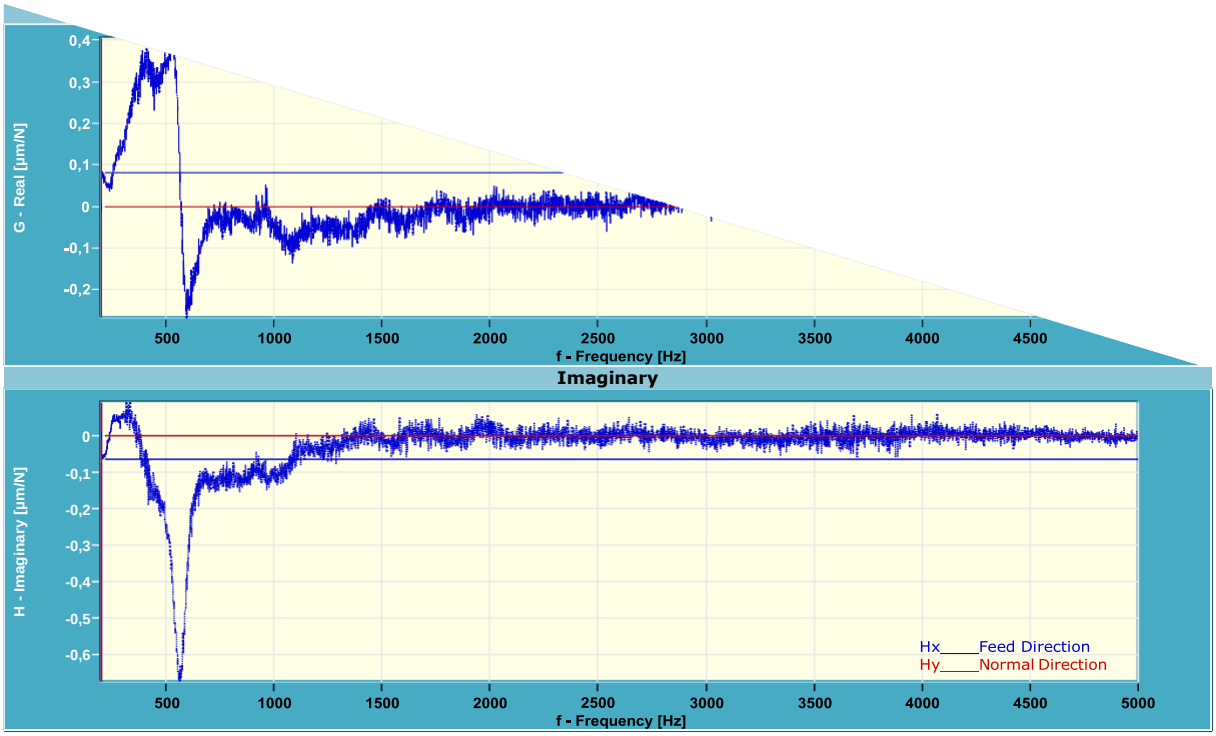

Fig. 9. The FRF obtained from the experimental modal analysis of the tool-damper structure with $d = 35$ mm.

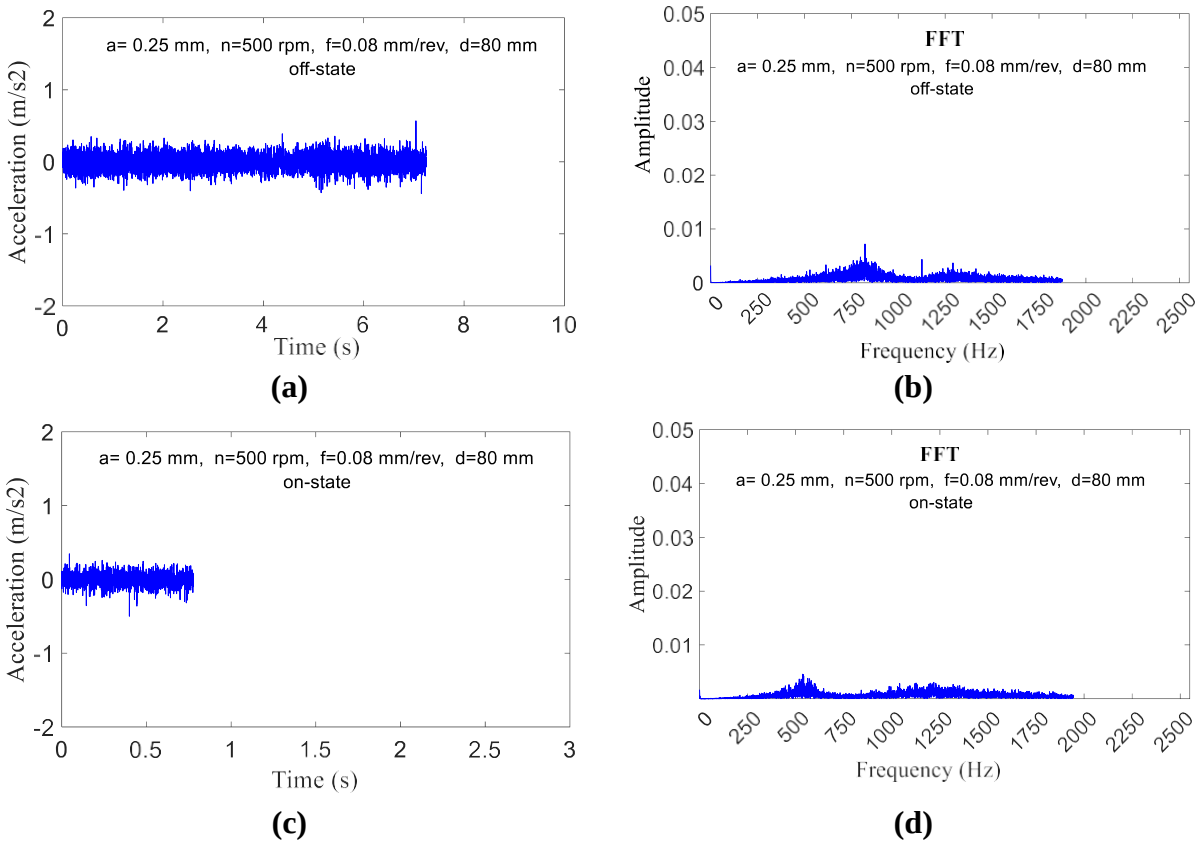

Fig. 10. Comparison of the tool acceleration signals and their corresponding FFT graphs obtained for two modes ”damper off” and “damper on”- (machining parameters a=0.25mm, n=500 rpm, f= 0.08 mm/rev, d=80 mm).

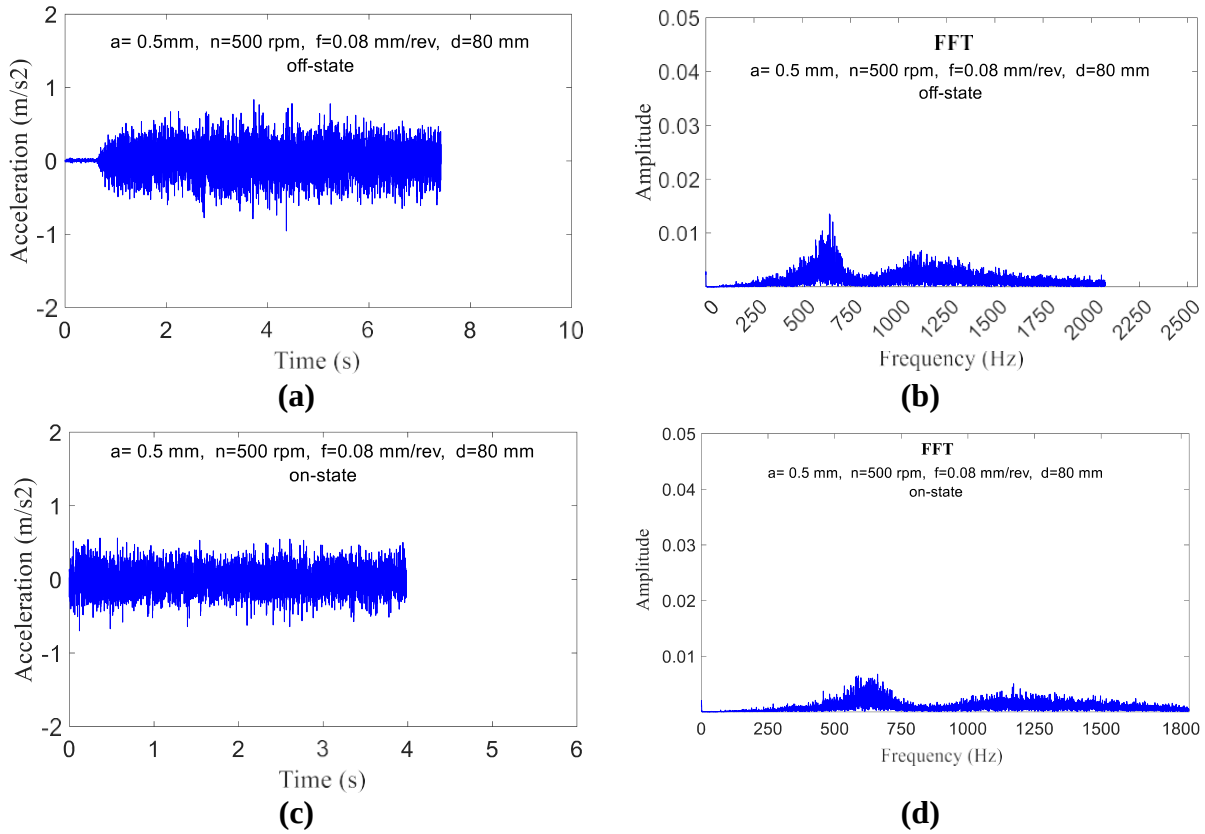

Fig. 11. Comparison of the tool acceleration signals and their corresponding FFT graphs obtained for two modes ”damper off” and “damper on”- (machining parameters a=0.5 mm, n=500 rpm, f= 0.08 mm/rev, d=80 mm).

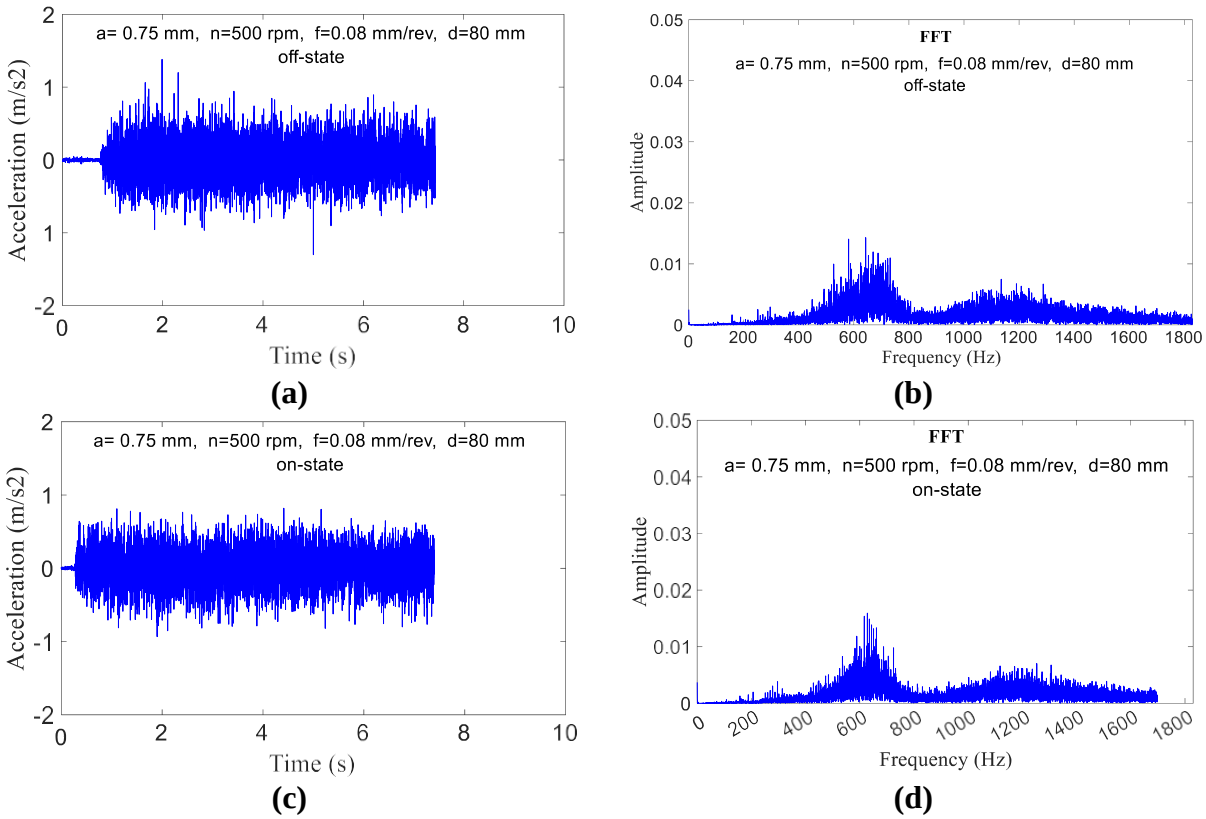

Fig. 12. Comparison of the tool acceleration signals and their corresponding FFT graphs obtained for two modes ”damper off” and “damper on”- (machining parameters a=0.75 mm, n=500 rpm, f= 0.08 mm/rev, d=80 mm).

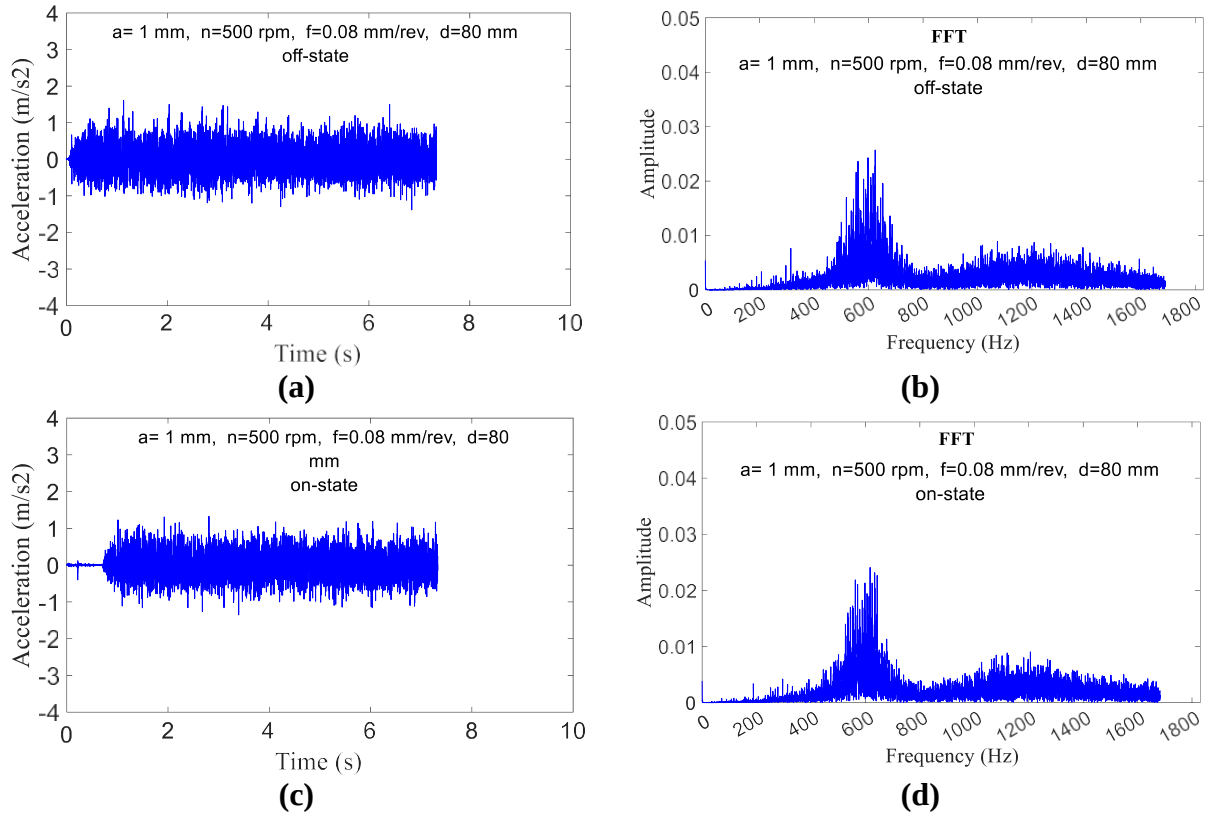

Fig. 13. Comparison of the tool acceleration signals and their corresponding FFT graphs obtained for two modes ”damper off” and “damper on” - (machining parameters a=1 mm, n=500 rpm, f= 0.08 mm/rev, d=80 mm).

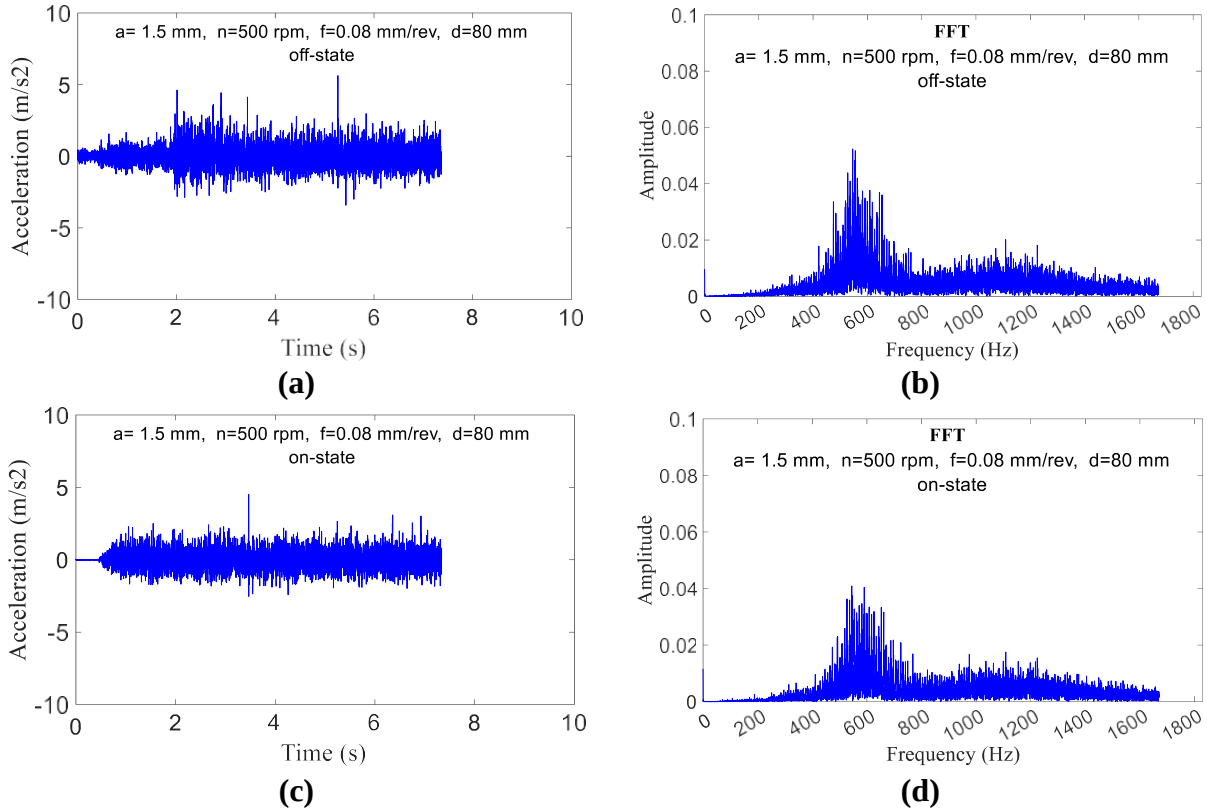

Fig. 14. Comparison of the tool acceleration signals and their corresponding FFT graphs obtained for two modes ”damper off” and “damper on” - (machining parameters a=1.5 mm, n=500 rpm, f= 0.08 mm/rev, d=80 mm).

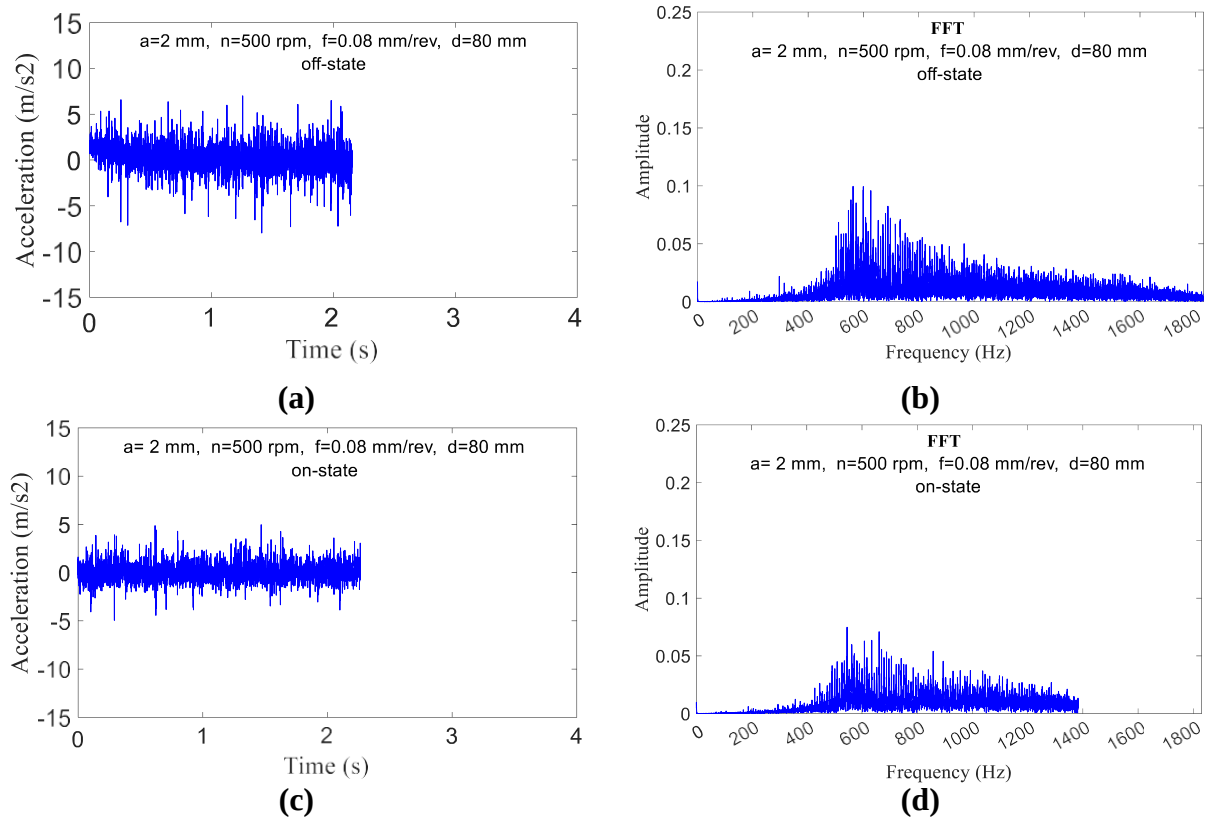

Fig. 15. Comparison of the tool acceleration signals and their corresponding FFT graphs obtained for two modes ”damper off” and “damper on”- (machining parameters a=2 mm, n=500 rpm, f= 0.08 mm/rev, d=80 mm).

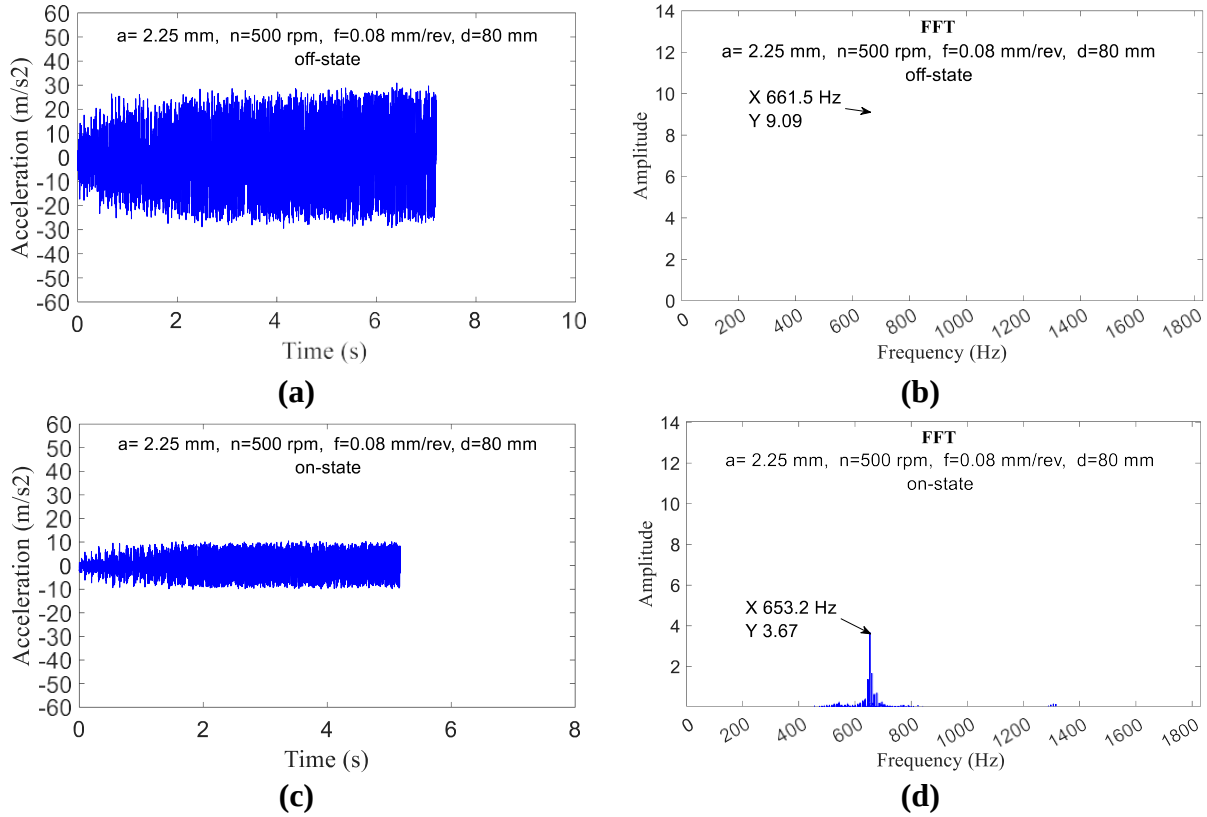

Fig. 16. Comparison of the tool acceleration signals and their corresponding FFT graphs obtained for two modes ” ”damper off” and “damper on”- (machining parameters a=2.25 mm, n=500 rpm, f= 0.08 mm/rev, d=80 mm).

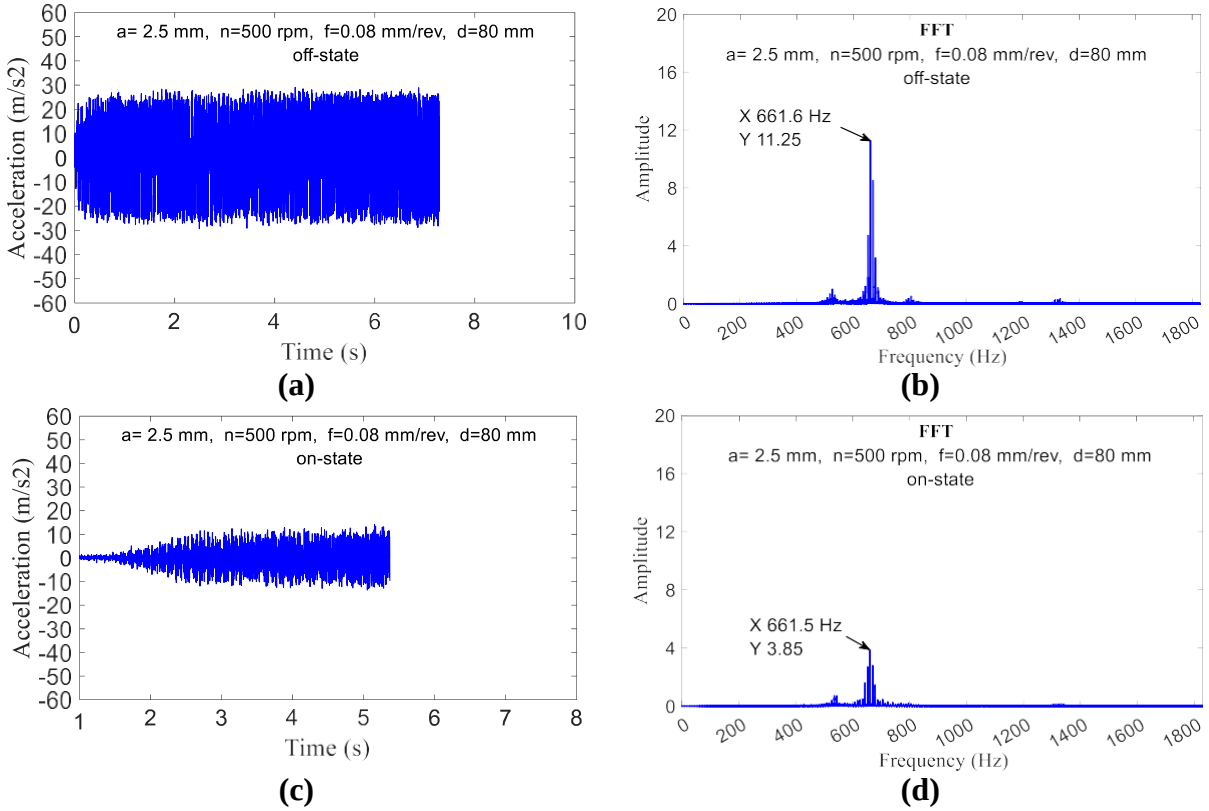

Fig. 17. Comparison of the tool acceleration signals and their corresponding FFT graphs obtained for two modes ”damper off” and “damper on”- (machining parameters a=2.5 mm, n=500 rpm, f= 0.08 mm/rev, d=80 mm).

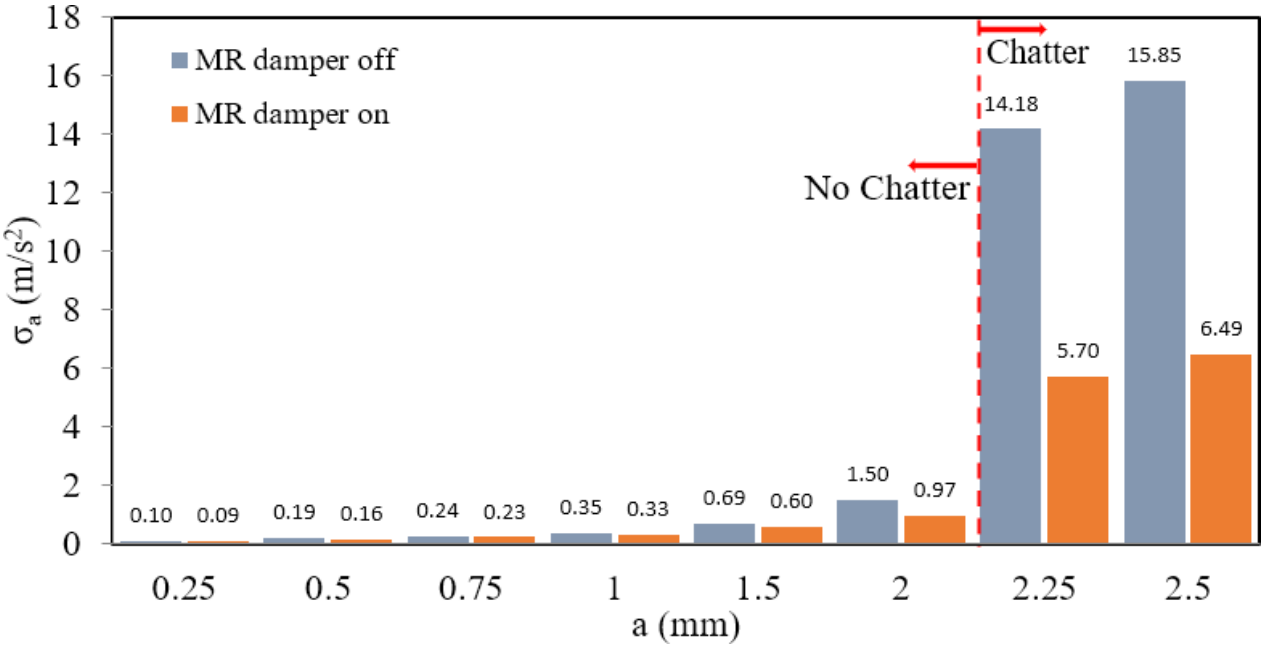

Fig. 18. Standard deviation values of the tool's acceleration data obtained from the machining test conducted with $n = 500$ rpm, $f = 0.08 \frac{\text{mm}}{\text{rev}}$, and $d = 80$ mm.

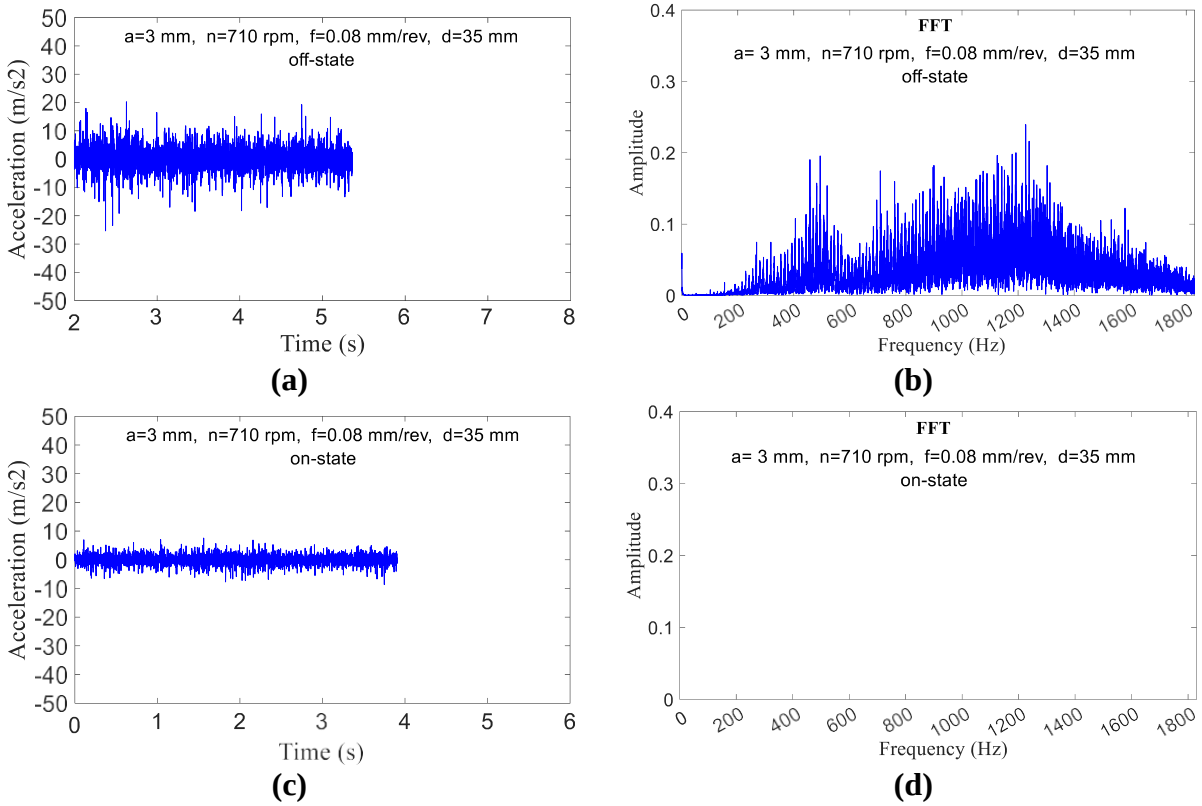

Fig. 19. Comparison of the tool acceleration signals and their corresponding FFT graphs obtained for two modes ” damper off” and “damper on”- (machining parameters a=3 mm, n=710 rpm, f= 0.08 mm/rev, d=35 mm).

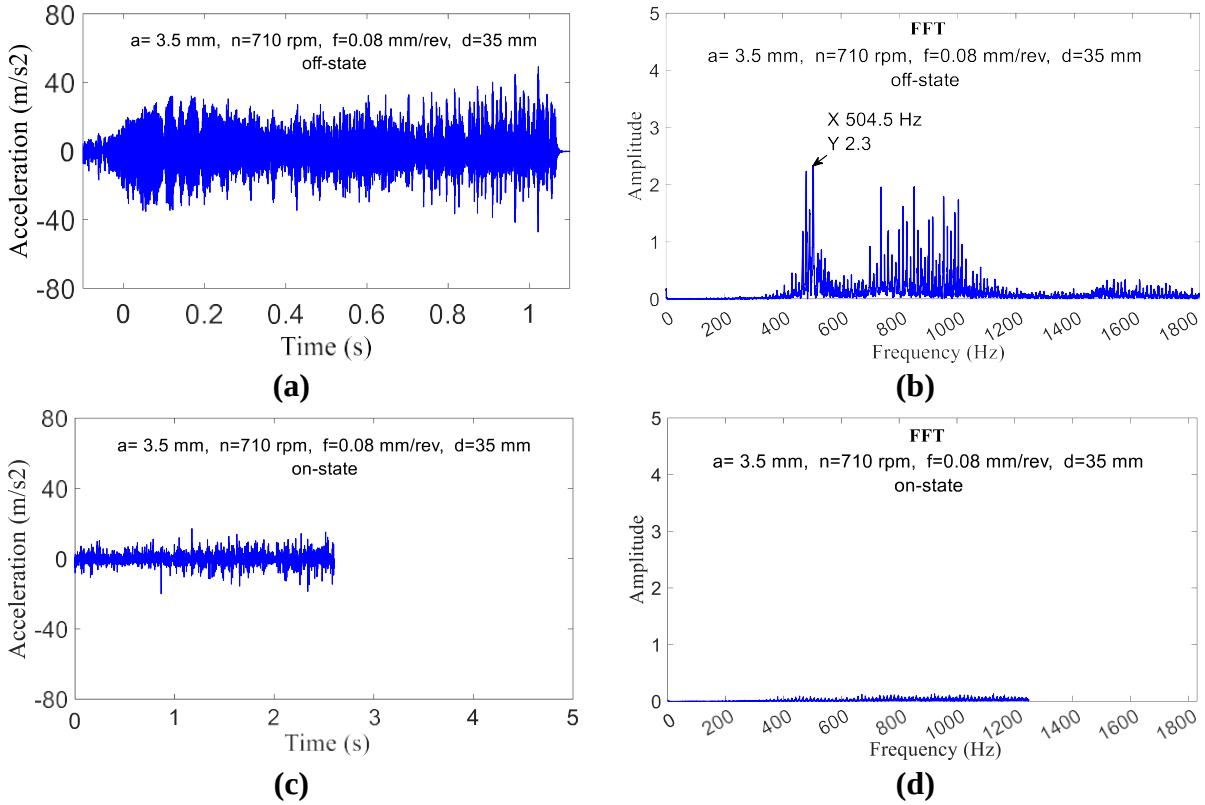

Fig. 20. Comparison of the tool acceleration signals and their corresponding FFT graphs obtained for two modes ”damper off” and “damper on” -(machining parameters a=3.5 mm, n=710 rpm, f= 0.08 mm/rev, d=35 mm).

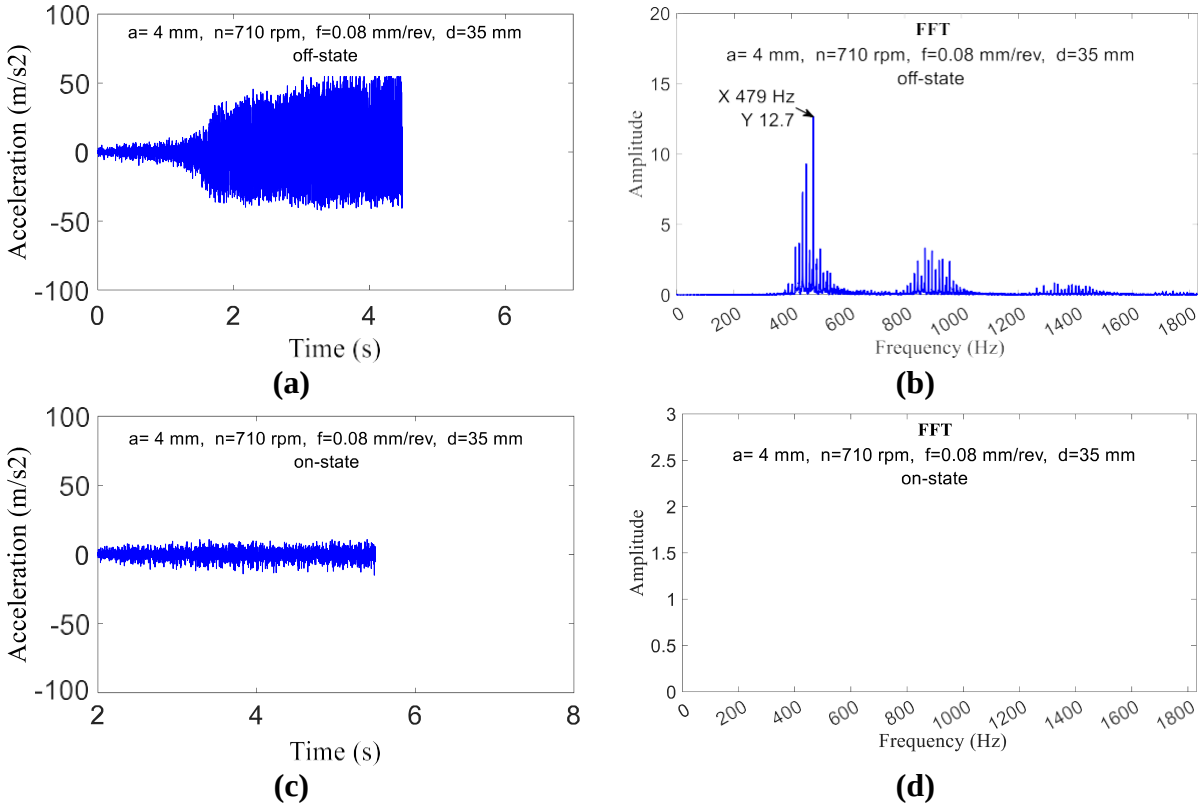

Fig. 21. Comparison of the tool acceleration signals and their corresponding FFT graphs obtained for two modes ”damper off” and “damper on” -(machining parameters a=4 mm, n=710 rpm, f= 0.08 mm/rev, d=35 mm).

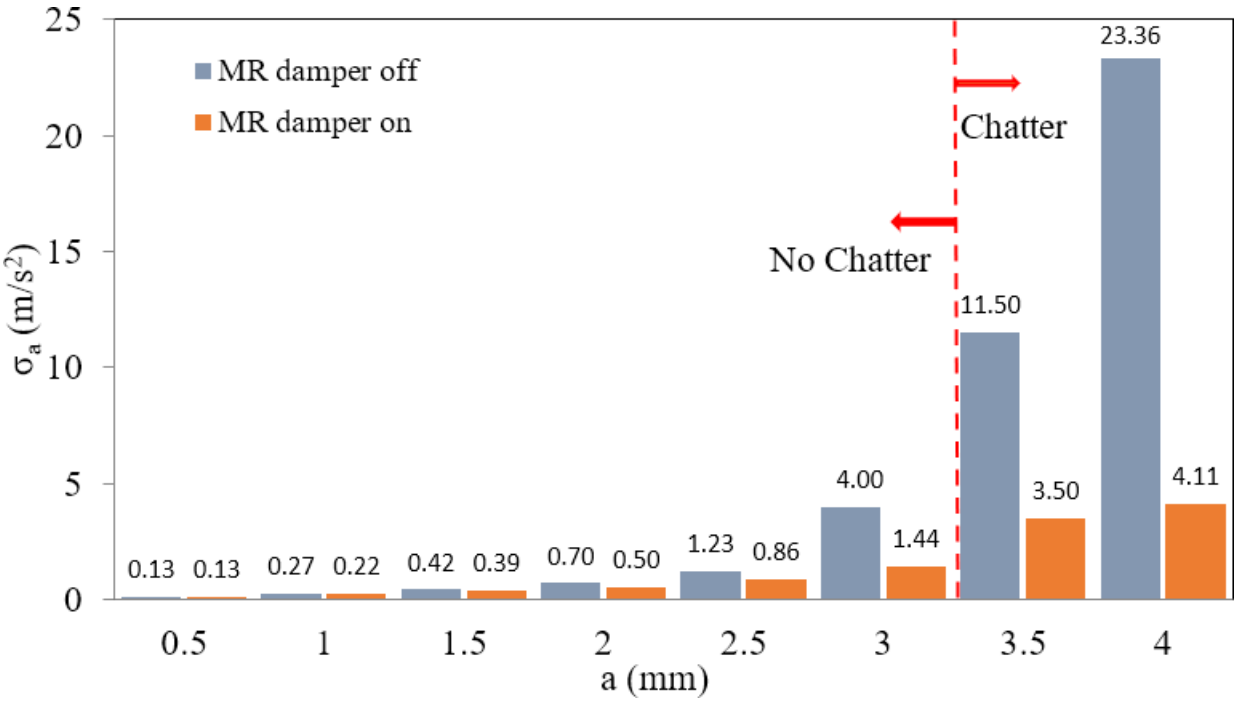

Fig. 22. Standard deviation values of the acceleration data obtained from the machining test conducted with $n = 710$ rpm, $f = 0.08 \frac{\text{mm}}{\text{rev}}$, and $d = 35$ mm.

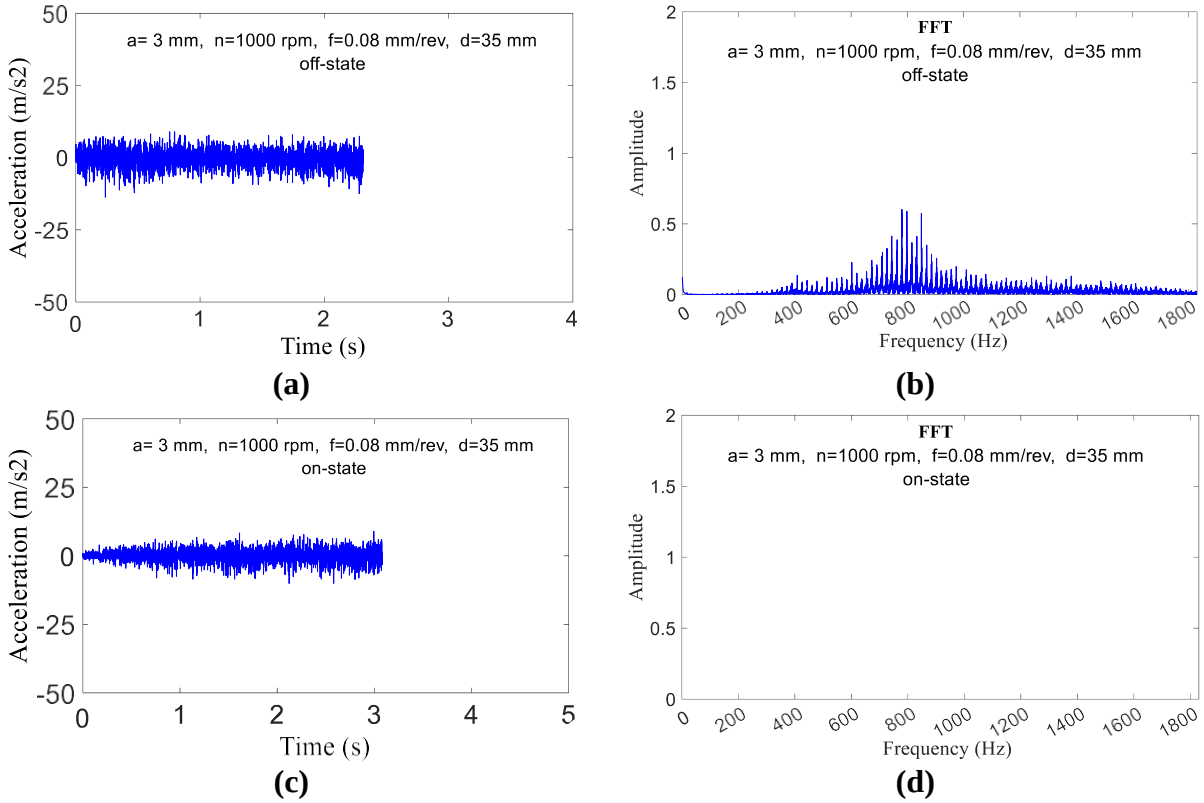

Fig. 23. Comparison of the tool acceleration signals and their corresponding FFT graphs obtained for two modes ”damper off” and “damper on”- (machining parameters a=3 mm, n=1000 rpm, f= 0.08 mm/rev, d=35 mm).

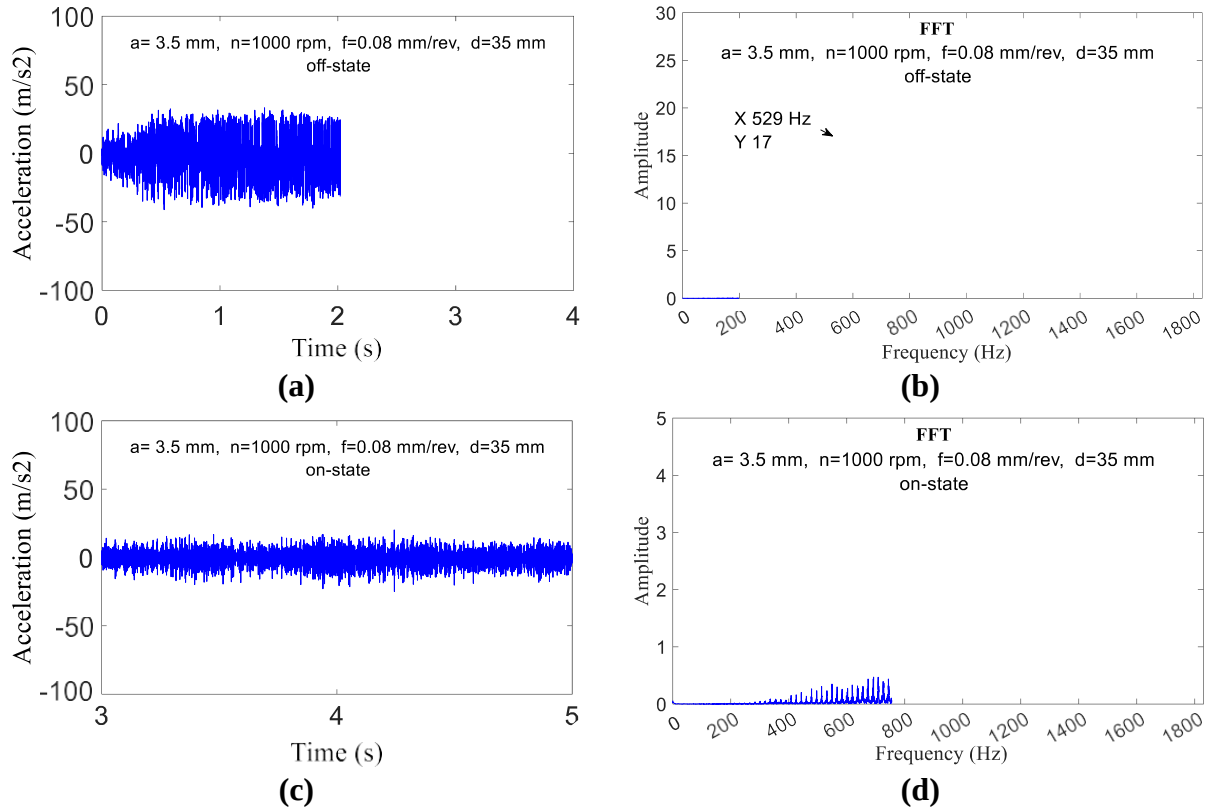

Fig. 24. Comparison of the tool acceleration signals and their corresponding FFT graphs obtained for two modes ”damper off” and “damper on” -(machining parameters a=3.5 mm, n=1000 rpm, f= 0.08 mm/rev, d=35 mm).

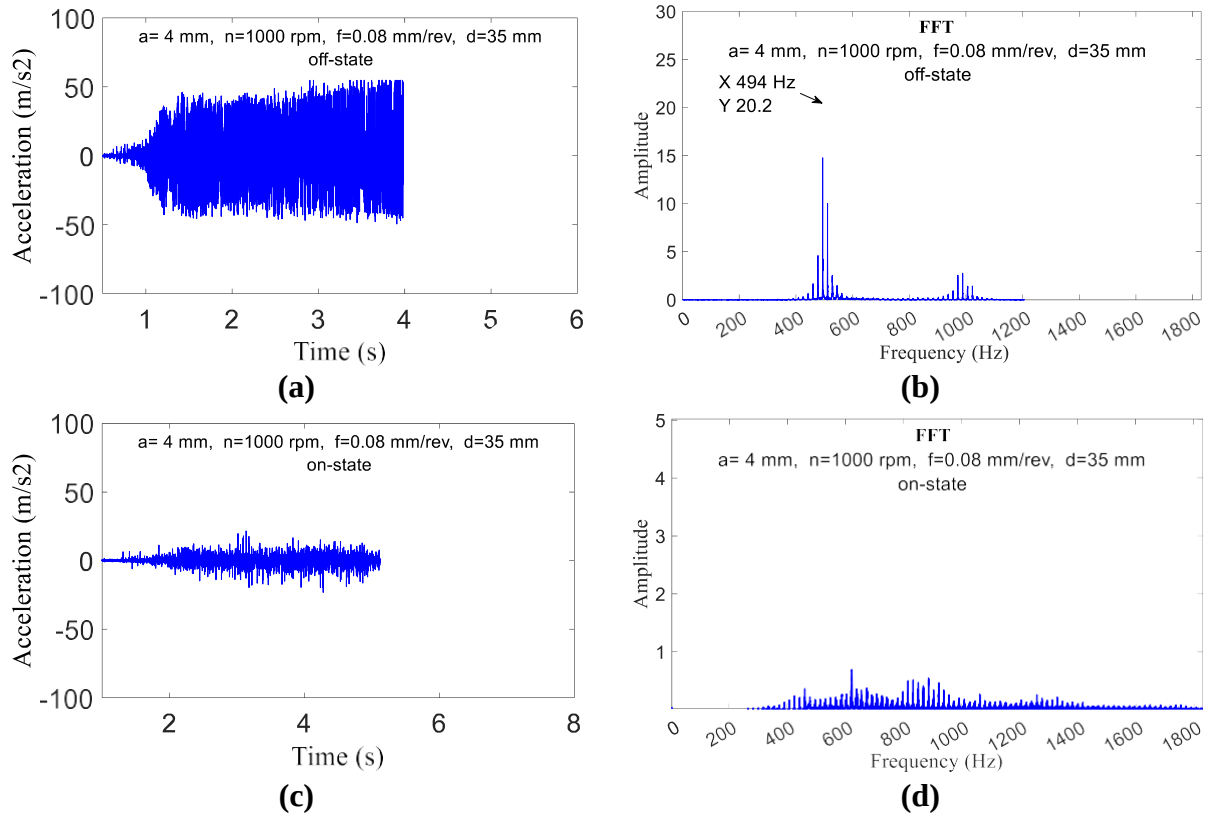

Fig. 25. Comparison of the tool acceleration signals and their corresponding FFT graphs obtained for two modes ”damper off” and “damper on”- (machining parameters a=4 mm, n=1000 rpm, f= 0.08 mm/rev, d=35 mm).

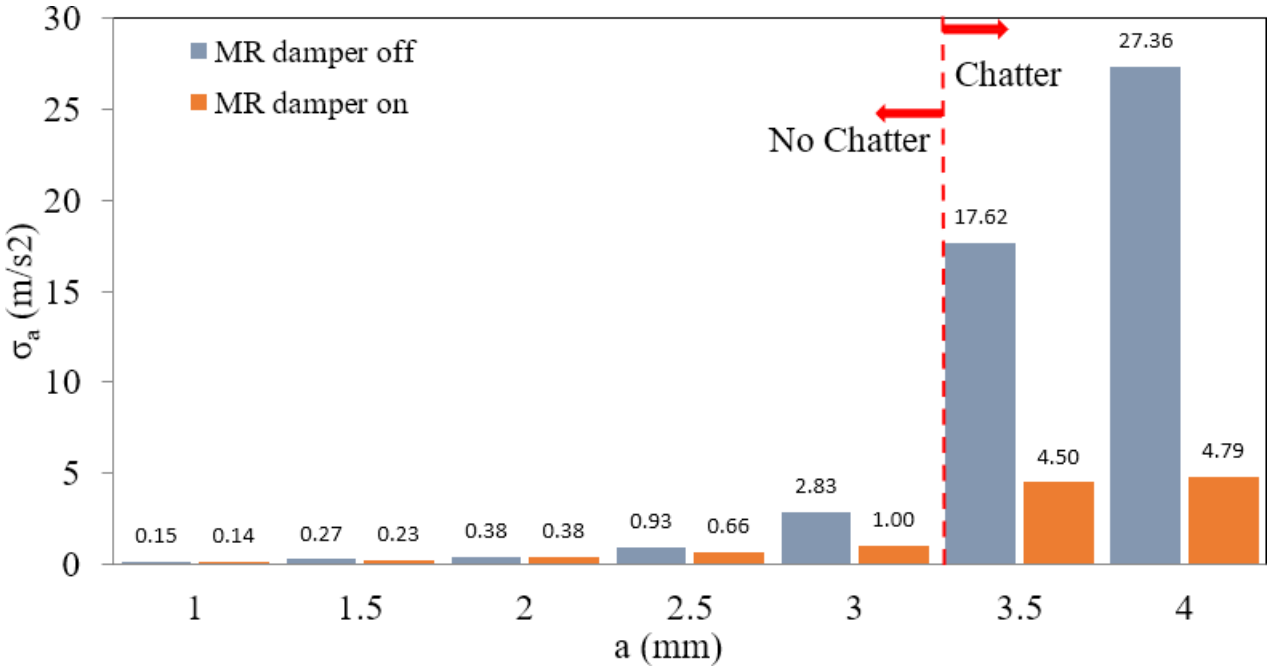

Fig. 26. STDV values of acceleration data obtained from the machining test conducted with $n = 1000$ rpm, $f = 0.08 \frac{\text{mm}}{\text{rev}}$, and $d = 35$ mm.

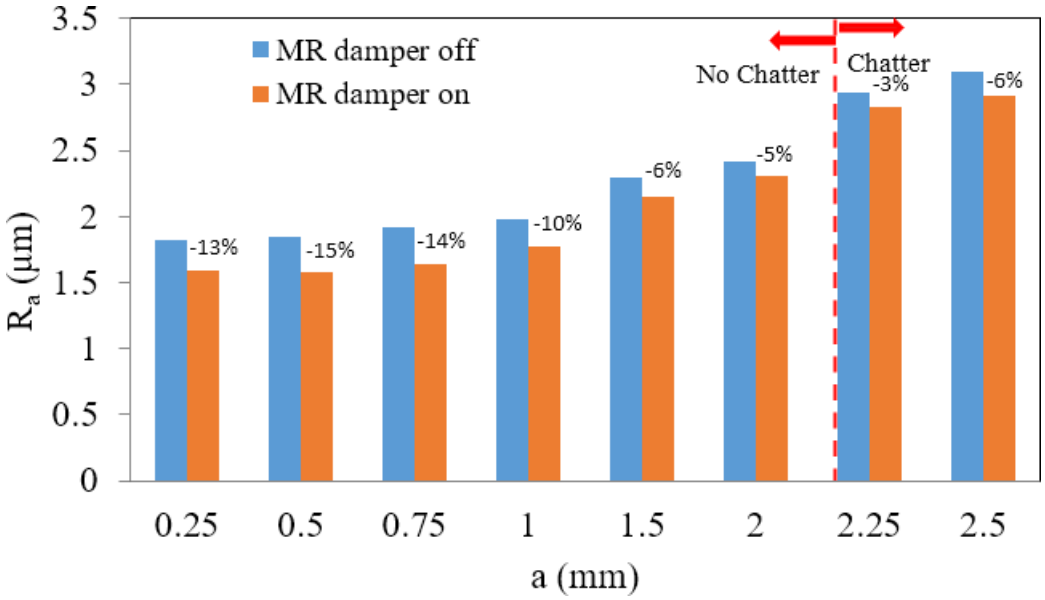

Fig. 27. Work Surface roughness values Ra obtained from the machining test conducted with $n = 500$ rpm, $f = 0.08 \frac{\text{mm}}{\text{rev}}$, and $d = 80$ mm.

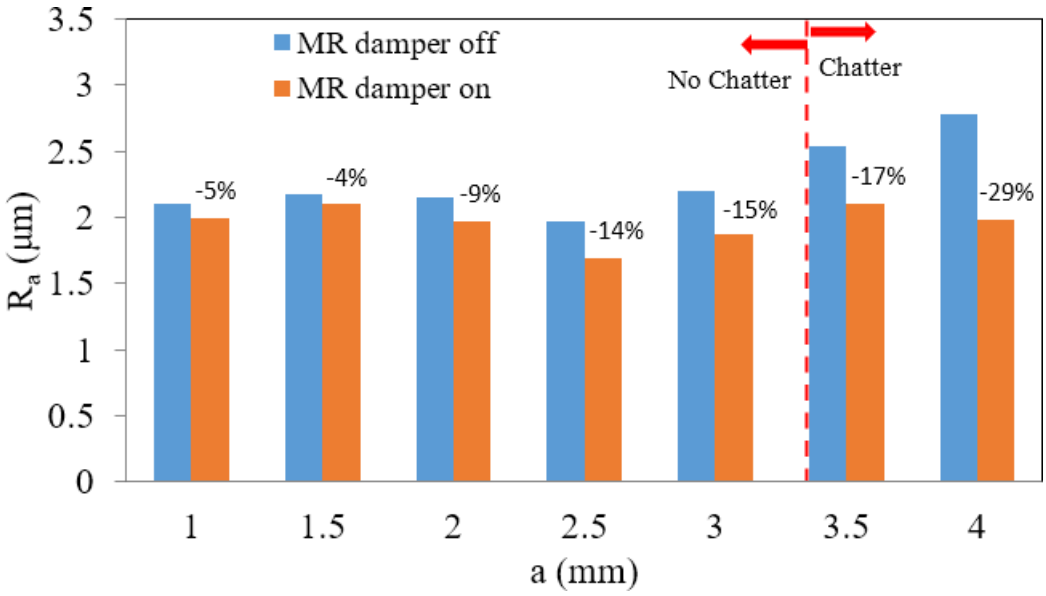

Fig. 28. Work Surface roughness values Ra obtained from the machining test conducted with $n = 1000$ rpm, $f = 0.08 \frac{\text{mm}}{\text{rev}}$, and $d = 35$ mm.

Table 1. MR fluid damper parts.

Part Number	Part Name	Description	Material	Manufacturing Method
1	External casing	External cover and retainer of internal parts	Polymer	Machining-Turning & Drilling
2	Flange	To close and seal the bottom of the fluid chamber	Stainless steel 316L	Machining-Turning & Drilling
3	Coil	Conductor of DC electric current to generate the magnetic field	Copper	Winding
4	Piston	MR fluid compressor to create damping force	Al 7075	Machining-Turning & Drilling
5	Cylinder	The fluid chamber in which the piston moves back and forth	AISI 1018	Machining-Turning
6, 9	Sealing washer	To seal and prevent fluid from escaping around the piston shaft	Polymer	Standard
7, 10	Circlip	Retaining ring of the sealing washer	Low alloy steel	Standard
8	Shaft guide and cap	Preventing the deviation of the piston shaft during reciprocating movement - top cap	Stainless steel 316L	Machining-Turning & Drilling
11	Shaft	The rod connecting the tool holder to the piston	Al 7075	Machining-Turning & Drilling

Table 2. MRF-132DG characteristics [29].

Base fluid	**Operating temperature**	**Density**	**Viscosity @ 40°C (no magnetic field applied)**	**K**	***β***
Hydrocarbon	-40 to 130˚C	3.09 g/cc	0.09 (±0.02) Pa.s	0.269 Pa.m/A	1

Table 3. Experimental Design.

	Damper parameters			
Test No.	**Depth of cut a (mm)**	**Spindle speed n (rpm)**	**Damper distance from toolup d (mm)**	**Damper's magnet condition**
1	0.25	500	80	Off
2	0.25	500	80	On
3	0.5	500	80	Off
4	0.5	500	80	On
5	0.75	500	80	Off
6	0.75	500	80	On
7	1	500	80	Off
8	1	500	80	On
9	1.5	500	80	Off
10	1.5	500	80	On
11	2	500	80	Off
12	2	500	80	On
13	2.25	500	80	Off
14	2.25	500	80	On
15	2.5	500	80	Off
16	2.5	500	80	On
17	0.5	710	35	Off
18	0.5	710	35	On
19	1	710	35	Off
20	1	710	35	On
21	1.5	710	35	Off
22	1.5	710	35	On
23	2	710	35	Off
24	2	710	35	On
25	2.5	710	35	Off
26	2.5	710	35	On
27	3	710	35	Off
28	3	710	35	On
29	3.5	710	35	Off
30	3.5	710	35	On
31	4	710	35	Off
32	4	710	35	On
33	0.5	1000	35	Off
34	0.5	1000	35	On
35	1	1000	35	Off
36	1	1000	35	On
37	1.5	1000	35	Off
38	1.5	1000	35	On
39	2	1000	35	Off
40	2	1000	35	On
41	2.5	1000	35	Off
42	2.5	1000	35	On
43	3	1000	35	Off
44	3	1000	35	On
45	3.5	1000	35	Off
46	3.5	1000	35	On
47	4	1000	35	Off
48	4	1000	35	On

Table 4. Comparison of stiffness and natural frequency of the tool-MR damper structure in two damper positions of "$d = 80$ mm" and "$d = 35$ mm".

Damper distance from the tooltip d (mm)	$\boldsymbol{G(0)}$	**Stiffness** $\boldsymbol{k}(\mathrm{N}/\boldsymbol{\mu m})$	**Natural Frequency** $\boldsymbol{f_n}(\mathbf{Hz})$
80	0.45	2.22	660
35	0.09	11.11	530

Table 5 Percentage reduction of the standard deviation of the tool's acceleration signal with $n = 500$ rpm, $f = 0.08 \frac{\text{mm}}{\text{rev}}$, and $d = 80$ mm.

Depth of cut	**0.25mm**	**0.5mm**	**0.75mm**	**1mm**	**1.5mm**	**2mm**	**2.25mm**	**2.5mm**
Percentage reduction of σ_a(vibration amplitude)	10%	15.79%	4.17%	5.71%	13.04%	35.33%	59.80%	59.05%

Table 6 Percentage reduction of the standard deviation of the tool's acceleration signal with $n = 710$ rpm, $f = 0.08 \frac{\text{mm}}{\text{rev}}$, and $d = 35$ mm.

Depth of cut (mm)	**0.5**	**1**	**1.5**	**2**	**2.5**	**3**	**3.5**	**4**
Percentage reduction of σ_a(vibration amplitude)	0	18.5%	7.14%	28.57%	30.08%	64%	69.56%	82.41%

Table 7 Percentage reduction of the standard deviation of the tool's acceleration signal with $n = 1000$ rpm, $f = 0.08 \frac{\text{mm}}{\text{rev}}$, and $d = 35$ mm

Depth of cut	**1mm**	**1.5mm**	**2mm**	**2.5mm**	**3mm**	**3.5mm**	**4mm**
Percentage reduction of σ_a(vibration amplitude)	6.67%	14.81%	0	29.03%	64.66%	74.46%	82.49%